A&A 465, 865–877 (2007)
DOI: 10.1051/0004-6361:20066280

Astronomy & Astrophysics

A survey of OH masers towards high mass protostellar objects⋆,⋆⋆

K. A. Edris[1,2], G. A. Fuller[1], and R. J. Cohen[3]

[1] The University of Manchester, School of Physics and Astronomy, Sackville Street Building, PO Box 88, Manchester M60 1QD, UK
e-mail: G.Fuller@manchester.ac.uk
[2] Al-Azhar University, Faculty of Science, Astronomy Department, PO Box 11884, Naser City, Cairo, Egypt
[3] The University of Manchester, Jodrell Bank Observatory, Macclesfield, Cheshire SK11 9DL, UK

Received 21 August 2006 / Accepted 18 December 2006

ABSTRACT

Context. Masers are important tracers of the early evolution of young high mass stars, but the relationship between different types of maser and the evolutionary state of the exciting source remains unclear.
Aims. To determine whether OH masers are common towards candidate high mass protostellar objects.
Methods. We present a survey of OH maser emission towards a sample of high mass protostellar objects made using the Nançay and GBT telescopes.
Results. OH maser emission was detected towards 63 objects with 36 new detections. There are 56 star-forming regions and 7 OH/IR candidates. Nearly half of the detected sources have OH flux densities $\lesssim$1 Jy. There is no evidence that sources with OH masers have a different range of luminosities from the non-maser sources. The results of this survey are compared with previous H_2O and class II CH_3OH maser observations of the same objects. Some of the detected sources are only associated with OH masers and some sources are only associated with the 1720 MHz OH maser line. The velocity range of the maser emission suggests that the water maser sources may be divided into two groups. The detection rates and velocity range of the OH and Class II CH_3OH masers support the idea that there is a spatial association of the OH and Class II CH_3OH masers. The sources span a wide range in R, the ratio of the methanol maser peak flux to OH 1665 MHz maser peak flux, however there are only a few sources with intermediate values of R, $8 < R < 32$, which has characterised previous samples. The majority of the sources are either methanol-favoured or OH-favoured. Sources which have masers of any species, OH, water or methanol, have redder [100 μm–12 μm] IRAS colours than those without masers. However, there is no evidence for different maser species tracing different stages in the evolution of these young high mass sources.
Conclusions. The detection of OH masers towards 26% of a sample of 217 sources should remove any doubt about the existence of OH maser emission towards these objects or this early evolutionary stage. Previous observations which have shown that the OH maser emission from similar sources traces the circumstellar disks around the objects. This combined with the sensitivity of the OH emission to the magnetic field, make the newly detected sources interesting candidates for future follow-up at high angular resolution.

Key words. masers – stars: formation – ISM: molecules – ISM: HII regions

1. Introduction

Compact HII regions, poorly collimated bipolar molecular outflows and circumstellar disks are signs of the existence of massive protostars (e.g. Garay & Lizano 1999; Churchwell 2002). Maser emission is also found to be associated with these objects (e.g. Garay & Lizano 1999; Edris et al. 2005) with OH, H_2O and CH_3OH the three most widespread types of maser associated with these regions. These species have been used as probes of star-forming regions as their maser emission provide unique information on these dense dusty regions (e.g. Cohen 1989, and references therein). Observations of H_2O and Class II CH_3OH masers have shown that both maser types are signposts of high mass star formation in very early evolutionary stages (Beuther et al. 2002a; Szymczak et al. 2000a, hereafter SHK2000; Palla et al. 1991, hereafter P91).

On the other hand OH masers are known to be associated with an advanced stage of the appearance of UCHII region (e.g. Garay & Lizano 1999, and references therein). Models of these OH masers assume that the maser arises in the compressed shell between the shock and ionisation fronts around the HII region (Elitzur & De Jong 1978). However in a survey, Caswell (1983) found a large proportion of OH masers have no closely related prominent HII regions. In some molecular outflow sources, OH masers have been mapped with high angular resolution and found to be associated with an earlier stage of molecular outflows and circumstellar disks (Cohen et al. 1984; Brebner 1988; Cohen et al. 2003; Edris et al. 2005). Since the masers can be observed with high spatial, and spectral, resolution they can probe the inner regions of these sources. OH masers also provide the possibility of measuring the magnetic fields in these regions.

With this in mind, and to form a more complete picture of the relationship between maser emission and the evolution of high mass protostars, 217 high mass protostellar object (HMPO) candidates have been surveyed for OH maser emission using the

⋆ Figures 17–20 and Appendix A are only available in electronic form at http://www.aanda.org

⋆⋆ Data files used for Figs. 19 and 20 are only available in electronic form at the CDS via anonymous ftp to
cdsarc.u-strasbg.fr (130.79.128.5) or via
http://cdsweb.u-strasbg.fr/cgi-bin/qcat?J/A+A/465/865

Table 1. IRAS colour index selection criteria proposed for different objects by different authors. $[x-y] \equiv \log(F_x)/\log(F_y)$. *References*: (1) Emerson (1987); (2) Wouterloot & Walmsley (1986); (3) Wood & Churchwell (1989); (4) Braz et al. (1989); (5) P91; CMC ≡ Compact Molecular Cloud; (6) Present work (Sect. 5.2).

Class of object	[25−12]	[60−25]	[100−60]	[60−12]	Ref.
Cores	0.4−1.0	0.4−1.3	0.1−0.7	–	1
H_2O maser	0.5−1.1	0.4−1.7	−0.1−0.5	–	2
UCHII regions	>0.6	–	–	>1.3	3
Bright IRAS	0.5−1.2	0.6−1.6	0.0−0.6	–	4
CMC+UCHII	≥0.57	0.61−1.74	0.087−0.52	≥1.3	5
OH maser	>1.2	–	–	>2.2	6

Nançay radio telescope[1] and the NRAO Green Bank Telescope[2] (GBT). The aims of this survey are:

- to determine whether OH masers are associated with these objects;
- to investigate the relationship between the OH and H_2O and/or CH_3OH maser emission and whether the masers are related to the evolutionary stage of these objects or represent different regions of the star formation core;
- to identify sources for further study at high angular resolution.

The description of the sample is given in Sect. 2 and the details of the observations are given in Sect. 3. In Sect. 4 we report the results of the survey while Sect. 5 presents some detection statistics. In Sect. 6 we discuss the interpretation while the conclusions are drawn in Sect. 7.

2. The sample

Different selection criteria have been proposed by many authors to use the IRAS point source catalogue to identify massive young sources (Table 1, and references therein). The sample of sources in this present survey is drawn from the sample of Sridharan et al. (2002, hereafter S02) and Molinari et al. (1996, hereafter M96). These two samples are believed to contain massive sources in a very early stage of evolution prior to the forming of UCHII regions. M 96 divided their sample into two subsamples, a *High* sample and a *Low* sample. The S02 sample and the *High* sub-sample of M 96 satisfy the colour selection criteria of Wood & Churchwell (1989, hereafter WC89) for UCHII regions. However the sources in these two samples (and also the M 96 *Low* sub-sample) are not known to be associated with detectable HII regions. M96 suggest that their *Low* sub-sample comprises objects which are in a different evolutionary stage from those in their *High* sub-sample, and therefore also from the S02 sample. The two samples (S02 and M 96) have sources with flux densities brighter than 90 Jy at 60 μm. Figure 1 shows the [25−12][3] versus [60−12] colour–colour diagram, indicating the location of the *High*, *Low* and S02 samples, for the whole sample observed here. Figure 1 also shows the results of this survey

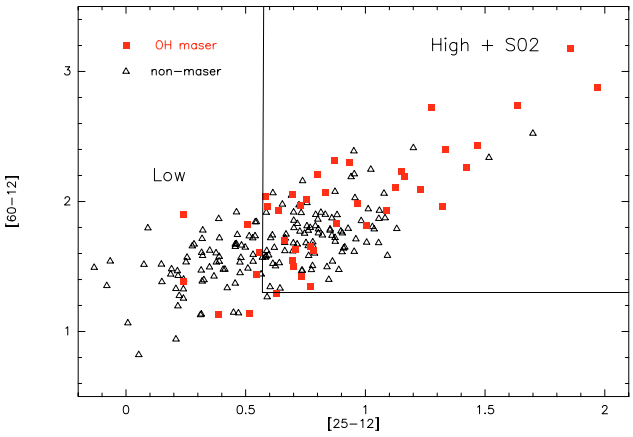

Fig. 1. The [60−12] vs. [25−12] two colour plot for the objects searched for OH maser emission (except the seven objects cataloged in Table 2 as offset sources). The box identifies the *High* and S02 samples which contain sources which agree with WC89 criteria to select UCHII region candidates. The sources of the *Low* sample are outside this box. OH maser sources are plotted as filled squares, while non−OH masers are shown as open triangles.

(Sect. 4); the detected sources of OH maser emission are marked with filled squares.

Observations show evidence of dense molecular gas associated with the majority of sources in the sample. The sources in the S02 sample have all been detected in CS $J = 2-1$ (S02) while ammonia was detected towards 80% and 45% of the *High* and *Low* sub-samples respectively of M 96. Further details about the sources and their selection criteria can be found in S02 and M 96 and references therein.

Combining the M 96 and S02 samples, and accounting for the 15 sources in common, results in a sample of 217 of HMPO candidates which have been observed here. The vast majority of the sources in the sample have luminosities in the range $\sim 10^3$ $L_\odot$ to $10^{5.5}$ $L_\odot$. However distance uncertainties affect the luminosity estimates of individual sources and are likely to explain a few sources with apparently with much lower luminosities. Although these objects have been previously systematically surveyed for water and methanol masers, only a handful have previously been searched for OH masers.

2.1. Water and methanol masers in the sample

S02 searched their sample for 22 GHz H_2O and 6.7 GHz CH_3OH masers using the Effelsberg 100 m telescope. The detected sources (29 H_2O and 26 CH_3OH masers) were mapped with the Very Large Array (VLA) by Beuther et al. (2002a). The M 96 sample had already been surveyed for H_2O maser by P91 with the Medicina 32 m telescope and most of the sources were searched for 6.7 GHz CH_3OH maser emission by Szymczak et al. (2000a) using the Toruń 32 m radio telescope. Towards the M 96 sample 40 H_2O and 26 CH_3OH maser sources have been reported. Therefore water and methanol masers were found towards 36% and 21%, respectively, of the 217 sources.

2.2. Outflows in the sample

Beuther et al. (2002b) searched 26 sources from the S02 sample at a spatial resolution of 11″ for bipolar molecular outflows. The signature of outflow was found towards 21 sources of them. The other five sources showed confusing morphology but have

[1] The Nançay Radio Observatory is the Unité scientifique de Nançay of the Observatoire de Paris, associated as Unité de Service et de Recherche (USR) No. 704 to the French Centre National de la Recherche Scientifique (CNRS). The Nançay Observatory also gratefully acknowledges the financial support of the Conseil Régional de la Région Centre in France.

[2] The National Radio Astronomy Observatory (NRAO) is a facility of the National Science Foundation operated under cooperative agreement by Associated Universities, Inc.

[3] $[x-y]$ indicates $\log(F_x)/\log(F_y)$.

strong line wings. More recently, Zhang et al. (2005) studied this phenomenon towards 69 sources of the M 96 sample. Mapping in the CO $J = 2-1$ line, they identified 39 molecular outflows. Therefore, among 95 sources systematically searched out of the total of 217 objects, 60 sources show clear evidence of bipolar molecular outflows. This gives a 63% detection rate which indicates that molecular outflows are very common in these regions.

3. Observations

3.1. Nançay observations

Observations using the Nançay radio telescope were performed between July 2002 and June 2003. At 18 cm the telescope has a beamsize of $3.5' \times 19'$ (RA × Dec). We simultaneously observed the four OH transitions at 1665, 1667, 1612 and 1720 MHz in both left and right circular polarizations. The 8192 channel autocorrelator was configured into eight banks of 1024 channels. Each bank had a total bandwidth of 1.5625 MHz yielding velocity resolutions of 0.284, 0.275, 0.274 and 0.266 km s^{-1} at 1612, 1665, 1667 and 1720 MHz, respectively. Inband frequency−switching was used during these observations. The total integration time per sources was 18 min, giving a typical noise level in a single polarisation of about 50 mJy. A total useable velocity range of about ±160 km s^{-1} was covered towards each source. The radial velocities were measured with respect to the local standard of rest (LSR). The spectral bandwidth was centred at the molecular gas velocity of the observed source, as given by M 96 and S02. The NAnçay Preprocessing Software (NAPS) program was used for the initial data processing and eliminating bad integrations, and integrating the whole cycles of each scan. The data were then imported into *CLASS* for further processing. In *CLASS*, the spectra were FOLDed to remove ripples coming from the frequency−switching technique and finally the spectral plots were produced.

3.2. GBT observations

The Green Bank Telescope (GBT) was used to re-observe the sources detected by Nançay in order to: (1) observe them with higher spectral resolution; (2) decrease the contamination due to Nançay's large beam size ($3.5' \times 19'$, comparing to ∼$8'$ of GBT); and (3) make small maps to determine whether the masers were associated with these IRAS sources or offset from them. The GBT was also used to observe a small set of sources we did not have enough time to observe with Nançay. The observations were carried out from 18 to 23 May 2003. The 12.5 MHz, 9 level, 8 sampler correlator setting was used to observe all four OH lines (1665, 1667, 1612 and 1720 MHz) in both senses of circular polarizations. After confirming the presence of an OH maser towards the IRAS position of a source, most of the sources were mapped with small 3 arcmin sampled maps, typically 3 × 3 pixels in size, to determine the position of the peak emission. For the majority of sources, where the position of the OH masers was consistent with the IRAS position, a higher resolution spectrum (with a velocity channel width of ∼0.07 km s^{-1}) was then obtained towards the IRAS position. The typical noise level in these high resolution spectra as about 0.1 Jy. For the high resolution spectra, the 12.5 MHz, 3 level, 8 sampler mode was used to obtain four times higher resolution and covering all four OH lines in both senses of circular polarizations. Frequency switching was used during these observation. The typical system temperature was ∼20 K resulting in a typical noise level of 50 mJy and 150 mJy in the low and high resolution spectrum respectively. Note that sources observed at Nançay but not detected were not reobserved at GBT.

4. Results

Combining the results from both Nançay and GBT, a total of 63 sources show OH maser emission, defined as bright and narrow polarized lines, in one or more of the OH transitions. Of these 36 have not been reported before.

The nature of the OH maser emission provides the opportunity to distinguish between sources which have same colours as HMPOs but are in fact late type stars around which OH masers are also known to occur (e.g. Cohen 1989). Towards evolved stars the 1612 MHz line spectrum usually shows double-peaked profile with sharp external edges and smooth internal ones with the two peaks separated by 15 to 40 km s^{-1} (Cohen 1989). Of the sources detected here 7 have 1612 MHz masers which indicate that they are OH/IR candidates.

The 63 sources detected include 57 detected at both Nançay and GBT, and 6 which were detected at Nançay but not observed at the GBT. We categorize these 6 sources as *not confirmed*, and do not consider them in our subsequent analysis.

The association of the maser emission and the IRAS source that we searched towards is confirmed by GBT maps for the first 46 sources in the table. Only these 46 objects are considered in the IRAS-related statistical analysis that follows. Thirty nine of these IRAS-associated sources are typical star-forming regions with masers strong in the main lines, 1665 and 1667 MHz. One source, IRAS 18463+0052, is associated with an OH/IR star. The remaining 6 sources have OH masers which are not typical of star-forming regions; they show maser emission in one of the satellite lines only (see Sect. 6.4). There are remaining 11 confirmed sources with OH maser emission offset by $>2'$ from the IRAS position are cataloged as *offset* sources in Table 2. They include 4 OH/IR candidates and 7 sources with OH spectra characteristic of star-forming regions.

The 57 confirmed maser sources and their OH line parameters are listed in Table 2. Column 1 gives the IRAS name of the source, Cols. 2 and 3 the maser position, where measured, with the uncertainties, Col. 4 the frequency and circular polarization of the maser line, with either L or R referring to lefthand or righthand circular polarisation respectively, Col. 5 the feature central velocity (relative to the LSR), Cols. 6 and 7 the velocity interval at zero intensity, Col. 8 the peak flux density in Jy, Col. 9 rms noise, Col. 10 the ratio of the CH_3OH peak flux density to the OH peak flux density, R, as defined by Caswell (1998), and Col. 11 some comments.

Figure 2 shows an example set of OH maser spectra and map from the GBT (IRAS 18144–1723, left panels). The figure also shows an example of one of the sources cataloged as *offset* because their map reveal that the emission is not consistent with the IRAS position (IRAS 18540+0220, right panels). Many of the sources with maser emission, for example IRAS 17527–2339 (Fig. 19), show "conjugate" behaviour with one of the satellite lines in emission while the other is in absorption (Elitzur 1976). The maps and spectra of all the OH detected sources are shown in Figs. 17 and 19 respectively. The maps and spectra of the sources with maser emission offset from the IRAS position by $>2'$ are separated in to Figs. 18 and 20 respectively.

A further 79 sources were detected in thermal emission and/or absorption. They are listed in Table 3 along with the 75 sources which were not detected in our observations. Table 3 also list the 6 sources categorized as *not confirmed* maser

Table 2. The detected OH maser lines and their parameters. The *offset* star forming region and OH/IR candidates are separated at the end of this table. The listed positions are measured from GBT observations except some positions taken from higher resolution observations of Argon et al. (2000) and Edris et al. (2005) (Refs. 1 and 2 in the table respectively).

IRAS Name	Position		Frequency	Velocity at			Flux at	rms	R	Ref./Notes
	RA(J2000)	Dec(J2000)		V_{peak}	V_{min}	V_{max}	S_{peak}			
	h m s	° ′ ″		km s^{-1}			Jy	Jy		
05137+3919	05 17 12.8 ± 2.2	39 22 05 ± 38	1665R	−21.58	−24.5	−21.2	2.20	0.40		
05274+3345	05 31 06.4 ± 1.4	33 47 27 ± 19	1665R	−3.61	−5	0.6	1.34	0.18	70	
			1667L	−4.93			0.14	0.04		
			1612L	−3.87			0.13	0.05		
05358+3543	05 39 13.0 ± 0.1	35 45 51 ± 01	1665L	−10.88	−16.5	−8.5	2.82	0.47	91	1
			1667L	−10.53			0.93	0.17		
05382+3547	05 41 12.9 ± 1.3	35 54 06 ± 20	1665R	−26.83	−27.0	−26.5	0.50	0.13	15	
06056+2131	06 08 52.4 ± 1.6	21 34 06 ± 23	1665L	10.14	3.0	11.0	3.23	0.51	6	
			1667R	9.44			0.22	0.05		off source
			1720R	3.37			0.60	0.10		
17527−2439	17 55 28.3 ± 1.9	−24 36 36 ± 27	1665R	11.53	8.2	12.2	0.40	0.14		
18018−2426	18 04 53.1 ± 0.1	−24 26 41 ± 01	1665R	10.84	10.0	12.0	8.10	1.83		
			1667L	11.05			0.98	0.20		1
18024−2119	18 05 25.6 ± 2.3	−21 14 59 ± 19	1665R	−4.05	−9.0	31.0	0.69	0.17	145	
			1667R	−3.75			0.38	0.10		
18048−2019	18 07 44.6 ± 2.2	−20 18 41 ± 38	1665R	44.36	40.0	44.7	0.34	0.08	104	
			1667L	40.28			0.27	0.09		
18089−1732	18 11 51.4 ± 0.1	−17 31 29 ± 01	1665L	32.92	31.0	36.0	10.30	1.86	6	1
			1667L	33.36			2.00	0.32		
18090−1832	18 11 47.4 ± 1.5	−18 29 47 ± 26	1665R	108.9	103.0	110.0	0.70	0.08	110	
			1667R	106.6			0.49	0.08		
18102−1800	18 13 04.4 ± 1.5	−18 00 23 ± 16	1665R	24.40	24.0	25.0	0.42	0.10	31	
18144−1723	18 17 26.5 ± 1.1	−17 22 29 ± 16	1665L	48.33	48.0	64.0	35.9	3.45	1	
			1667L	61.75			4.80	0.62		
18182−1433	18 21 11.0 ± 1.0	−14 31 23 ± 14	1665L	61.55	58.0	64.0	0.72	0.16	33	
			1667L	62.45			0.40	0.12		
18236−1205	18 26 36.2 ± 1.0	−12 04 54 ± 14	1665R	31.09	20.0	32.0	0.80	0.16	8	
	18 26 31.7 ± 1.0	−12 03 26 ± 14	1667L	62.45			0.28	0.06		
18264−1152	18 29 19.2 ± 1.1	−11 50 05 ± 17	1720L	39.31	37.5	43.5	2.30	0.55		
18278−1009	18 30 37.9 ± 1.1	−10 07 25 ± 17	1665R	119.7	118.0	121.0	0.42	0.09	33	
18290−0924	18 31 46.4 ± 1.1	−09 22 14 ± 15	1665R	78.33	76.0	84.0	2.30	0.41	5	
			1667R	78.45			0.34	0.90		
18310−0825	18 33 36.0 ± 0.8	−08 19 46 ± 13	1667L	88.74	88.0	89.0	1.40	0.21		
18316−0602	18 34 25.9 ± 1.1	−06 00 01 ± 16	1665R	39.90	36.0	46.0	6.00	0.87	30	
			1667L	40.41			3.38	0.48		
18345−0641	18 47 08.0 ± 2.8	−02 19 05 ± 40	1612R	93.52	92.0	96.0	0.43	0.07	23	
18360−0537	18 38 42.2 ± 1.1	−05 36 25 ± 16	1665R	102.9	102.0	106.0	0.54	0.05		
	18 38 47.2 ± 1.2	−05 35 40 ± 17	1667L	105.3			0.74	0.05		
18385−0512	18 41 18.2 ± 1.0	−05 08 57 ± 14	1665R	24.87	21.0	30.0	1.01	0.04		
18440−0148	18 46 37.8 ± 1.0	−01 44 27 ± 13	1665R	101.4	99.0	110.0	6.00	0.08	0.5	
			1667R	102.6			2.00	0.10		
18454−0158	18 48 01.3 ± 1.0	−01 54 34 ± 15	1665L	39.6	30.0	44.0	0.35	0.10		
18463+0052	18 48 46.8 ± 2.2	00 56 55 ± 24	1612R	67.32	67.0	70.0	2.26	0.09		OH/IR
18488+0000	18 51 30.5 ± 1.0	00 03 21 ± 16	1665R	79.57	79.0	87.0	4.52	0.07	6	
			1667R	77.90			2.66	0.05		
18507+0121	18 53 18.2 ± 1.2	01 24 30 ± 18	1665L	55.78	53.0	56.0	2.00	0.08	14	
			1667L	53.88			1.10	0.09		
18527+0301	18 54 46.5 ± 2.5	03 05 07 ± 40	1665R	74.44	72.0	75.0	0.21	0.02	48	
			1667L	73.30			0.16	0.02		
18553+0414	18 57 50.7 ± 1.2	04 18 36 ± 18	1720L	6.63	4.0	8.0	0.67	0.03		
18566+0408	18 59 08.7 ± 1.1	04 10 21 ± 17	1665L	83.41	52.0	92.0	1.00	0.12	7	
	18 59 10.4 ± 1.0	04 13 21 ± 14	1667L	81.52			0.50	0.14		
19035+0641	19 06 01.6 ± 0.0	06 46 35 ± 01	1665L	32.44	24.2	36.2	90.00	0.61	0.2	1
			1667R	27.33			22.30	0.27		
19092+0841	19 11 45.9 ± 0.4	08 46 49 ± 06	1665R	57.87	54.0	62.0	3.45	0.04	3	
	19 11 46.6 ± 0.4	08 46 19 ± 10	1667L	60.51			1.75	0.04		
19118+0945	19 14 29.7 ± 1.6	09 51 47 ± 46	1665R	61.25	61.0	71.0	0.35	0.05		
			1667L	58.90			0.22	0.05		
19217+1651	19 23 57.9 ± 0.9	16 56 42 ± 13	1665L	0.21	−2.0	10.0	1.35	0.05	1	
			1667L	6.69			1.22	0.05		
19220+1432	19 24 19.7 ± 1.5	14 37 23 ± 30	1720R	60.67	59.5	61.0	0.44	0.08		

Table 2. continued.

IRAS Name	Position		Frequency	Velocity at			Flux at	rms	R	Ref./Notes
	RA(J2000)	Dec(J2000)		V_{peak}	V_{min}	V_{max}	S_{peak}			
	h m s	° ′ ″		km s^{-1}			Jy	Jy		
19374+2352	19 39 37.4 ± 4.0	23 59 53 ± 109	1665R	37.06	35.0	40.0	0.46	0.06		
			1667R	37.00			0.13	0.02		
			1720R	37.05			0.17	0.03		
19388+2357	19 41 10.2 ± 2.2	24 03 44 ± 25	1665L	35.81	34.0	39.0	0.32	0.04	77	
19410+2336	19 43 12.2 ± 1.1	23 44 03 ± 12	1665L	20.67	20.0	23.0	0.71	0.03	48	
20062+3550	20 08 12.7 ± 1.2	35 59 20 ± 20	1665R	0.77	−1.0	2.2	0.17	0.03	59	
20126+4104	20 14 26.06 ± 0.002	41 13 32.63 ± 0.02	1665R	−12.27	−16.0	2.0	2.37	0.11	16	2
20188+3928	20 20 41.8 ± 1.0	39 37 42 ± 12	1720L	−1.03	−3.0	4.0	4.18	0.14		
20227+4154	20 24 34.6 ± 1.3	42 06 12 ± 22	1665L	24.29	10.0	25.0	0.80	0.07		
22198+6336	22 21 00.7 ± 1.3	63 51 57 ± 16	1665L	−12.14	−23.0	−10.0	2.00	0.08		
	22 21 37.6 ± 0.4	63 51 47 ± 08	1667L	−13.00			3.50	0.17		
22272+6358	22 28 58.5 ± 0.8	64 15 52 ± 14	1665L	−12.12	−12.0	−8.0	1.10	0.06	83	
			1667L	−11.96			1.68	0.07		
23139+5939	23 16 06.8 ± 1.0	59 58 52 ± 13	1612R	−72.93	−74.0	−68.0	0.63	0.11		
Masers sources offset										
04579+4703			1720R	−17.70	−18.1	−16.8	0.22	0.05		
06382+0939			1665R	11.48	9.2	13.0	0.80	0.16		
18408−0348			1665R	89.60	88.0	113.0	1.00	0.10		
18511+0146			1665R	47.91	47.0	49.0	0.38	0.04		
18540+0220			1665R	49.13	48.0	53.5	53.73	0.19		
			1667L	50.38			10.57	0.09		
18586+0106			1665L	42.00	38.5	46.0	0.50	0.18		
			1667L	42.50			0.70	0.17		
			1720R	38.81			3.00	0.31		
20099+3640			1665R	−42.74	−43.0	−42.0	0.30	0.04		
OH/IR sources offset										
18258−0737			1612R	93.00	63.0	95.0	2.00	0.10		OH/IR
18348−0616			1612L	70.00	25.0	73.0	1.50	0.18		OH/IR
18424−0329			1612L	40.00	38.0	82.0	0.50	0.13		OH/IR
18565+0349			1612L	27.00	25.0	62.0	1.50	0.11		OH/IR

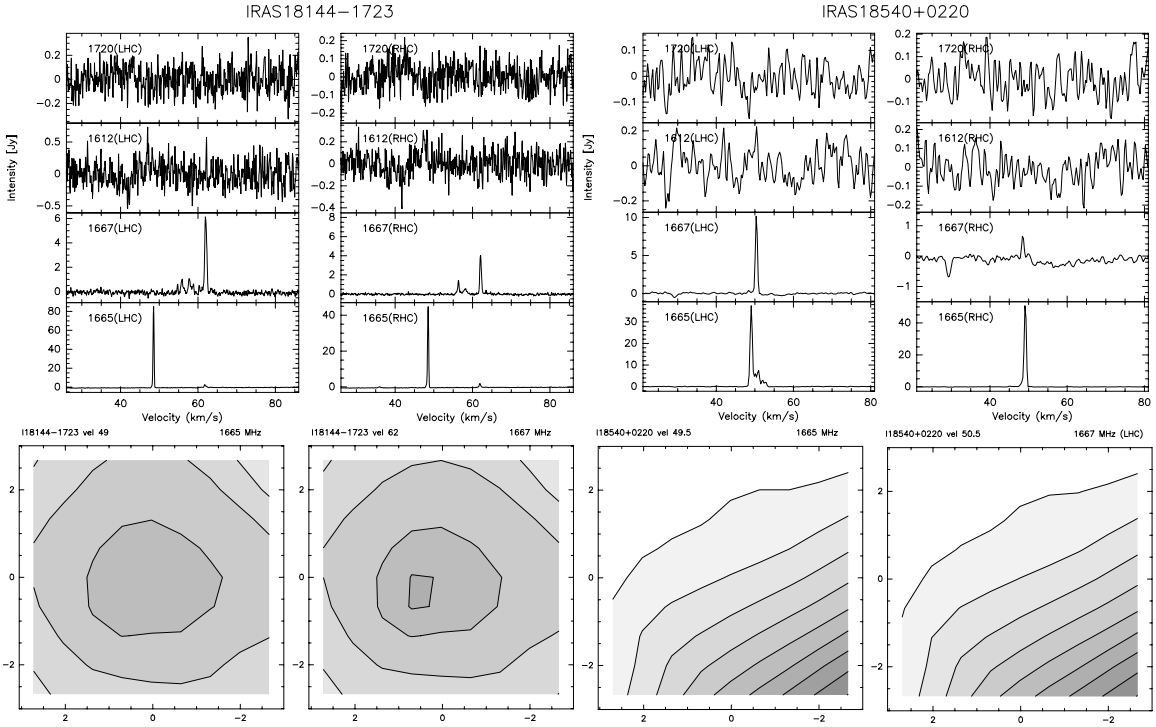

Fig. 2. Examples spectra and maps of OH masers detected with the GBT. The maps shows if the OH maser emission is consistent with the IRAS position (as for IRAS 18144−1723, *left panels*) or offset from it (as for IRAS 18540+0220, *right panels*). The maps are 9-points maps of the integrated intensities over the velocity range of each maser component. The contours range from 10% to 90% of the peak flux given in Table 2 in steps of 10%. The axes show RA and Dec offset from the IRAS position in arcminutes.

Table 3. Non-OH maser sources cataloged as: sources with thermal emission and/or absorption in one or more of the OH maser lines, sources with no detectable features, not confirmed maser sources (sources detected with Nançay only), not confirmed OH/IR sources.

IRAS sources with thermal absorption and/or thermal emission			
00420+5530	18167−1614	18551+0302	20081+2720
05168+3634	18172−1548	18567+0700	20180+3558
05345+3157	18212−1320	18571+0326	20205+3948
05373+2349	18223−1243	18571+0349	20216+4107
06061+2151	18256−0742	18596+0536	20217+3947
06063+2040	18288−0158	19001+0402	20220+3728
06105+1756	18306−0835	19002+0454	20293+3952
06299+1011	18337−0743	19012+0505	20293+4007
06303+1021	18363−0554	19012+0536	20319+3958
17417−2851	18396−0431	19023+0538	20332+4124
17450−2742	18426−0204	19045+0518	20333+4102
17495−2624	18437−0216	19088+0902	20343+4129
17582−2234	18445−0222	19175+1357	21078+5211
18024−2231	18447−0229	19198+1423	21548+5747
18039−2052	18454−0136	19295+1637	22551+6221
18134−1942	18517+0437	19332+2028	23026+5948
18156−1343	18530+0215	19343+2026	23033+5951
18159−1550	18532+0047	19368+2239	23140+6121
18159−1648	18537+0145	20050+2720	23545+6508
18162−1612	18544+0112	20051+3435	
IRAS sources with no detected absorption or emission			
00117+6412	18272−1217	19542+3004	22187+5559
01420+6401	18317−0513	20028+2903	22267+6244
03211+5446	18355−0550	20056+3350	22305+5803
04034+5116	18372−0541	20106+3545	22344+5909
05490+2658	18470−0044	20278+3521	22457+5751
05553+1631	18472−0022	20286+4105	22506+5944
06068+2030	18521+0134	20321+4112	22570+5912
06103+1523	19043+0726	20406+4555	23146+5954
06104+1524	19077+0839	20444+4629	23151+5912
06155+2319	19094+0944	21046+5110	23152+6034
06291+0421	19183+1556	21080+4758	23314+6033
06308+0402	19045+0813	21202+5157	23330+6437
06584−0852	19213+1723	21307+5049	23385+6053
17571−2328	19266+1745	21336+5333	23448+6010
17504−2519	19282+1814	21391+5802	23507+6230
18014−2428	19403+2258	21519+5613	
18123−1203	19411+2306	21526+5728	
18151−1208	19413+2332	22134+5834	
18197−1351	19458+2442	22147+5948	
18247−1147	19471+2641	22172+5549	
Maser sources not confirmed			
00070+6503	18311−0701	18431−0312	19074+0752
OH/IR sources not confirmed			
18308−0841	18460−0307		

sources. A brief description and discussion of each of the OH maser sources is given in Appendix A.

5. Detection statistics and analysis

The survey observations detected 63 OH maser sources out of 217 IRAS sources. For 46 of these the association with the IRAS source is confirmed by maps made with the GBT. Of these 36 are new detections. That gives a detection rate of 29% (including unconfirmed and not associated with IRAS position sources) or 21% if only the confirmed IRAS associated sources are considered. This is very similar to the 22% detection rate of Cohen et al. (1988) although the Cohen et al. sample contained only sources with $F_{60} > 1000$ Jy. Cohen et al. also found that higher F_{60} was correlated with a higher probability of the presence of OH masers. There is little evidence for such a correlation in the objects observed in this survey, although the small number of high flux sources in this sample makes it difficult draw any firm conclusion.

Figure 3 summarises the detection statistics for OH, H_2O and 6.7 GHz, Class II, CH_3OH masers towards the sample. OH and CH_3OH masers show very similar percentages of detections. Indeed, among the detected OH masers sources, the two types of maser have 67% of sources in common. The number of detections of the three maser types towards the sub-samples is also shown. The S02 and *High* samples show similarly higher detection rates than the *Low* sample for which 70% of its sources have no maser emission. Not only are masers of any type relatively rare towards the *Low* sub-sample, sources with all three types of maser are particularly uncommon. In the *Low* sub-sample there are only three such sources, namely IRAS 19092+0841, IRAS 18024−2119 and IRAS 18144−1723. Water masers show the highest detection rates towards the *High* sample (46%), while CH_3OH masers show high detection rate towards S02 sample (42%). Perhaps surprisingly there is a significant difference in the detection rates of S02 and *High* sample for CH_3OH maser, 42% and 25% respectively. OH masers have similar detection rates towards the *High* and S02 samples, ∼26%. The sources which show only OH maser emission are mostly from the *Low* sample. This point is discussed in Sect. 6.3.

5.1. OH maser flux densities

Figure 4 shows the distribution of 1665 MHz peak flux densities towards the three sub-samples, *High* sample (solid line), *Low* sample (dashed line) and S02 sample (dotted line). The right panel of Fig. 4 shows an expanded view for sources with 1665 MHz flux density weaker than 4.5 Jy. These figures show that nearly half of the detected sources have peak flux densities $\lesssim$1 Jy. The significance of this result is discussed in Sect. 6.2. Figure 4 also shows a further difference between the different sub-samples. Most of the *Low* sample have 1665 MHz flux densities between 0.25 and 0.75 Jy while most of those of the S02 sample between 0.75 and 1.25 Jy and the *High* sample shows a wider spread of 1665 MHz flux densities.

5.2. IRAS flux densities and colour analysis

The correlation of maser emission and IR flux has been studied by many authors to examine if masers are pumped by IR photons or not. A correlation of OH maser flux and IR flux has been clearly seen at 60 and 100 μm by several authors (Cohen et al. 1988; Moore et al. 1988; Slysh et al. 1997). Figure 5 plots the 1665 MHz peak flux densities against the IRAS flux densities at 12, 25, 60 and 100 μm for the sample observed here. The top-left panel of F_{60} vs. F_{1665} also shows the results of previous studies: the Slysh et al. (1997) data upper limit (dashed line) corresponds to $F_{\rm OH} = 0.024\ F_{60}$ and the dotted line is the upper limit line of Moore et al. (1988) data (corresponding to $F_{\rm OH} = 0.1\ F_{60}$). The solid line corresponds to equal flux densities. Although the sources searched here have flux densities similar to Slysh et al. (1997), the survey results are more consistent with the Moore et al. (1988) line and appear to be consistent with an extension of Moore et al. sample to lower IR flux densities. The distribution at 60 and 100 μm flux densities confirm previous conclusions that, at these wavelengths, a minimum IR flux density is required for a given maser line strength (Cohen et al. 1988; Moore et al. 1988; Slysh et al. 1997).

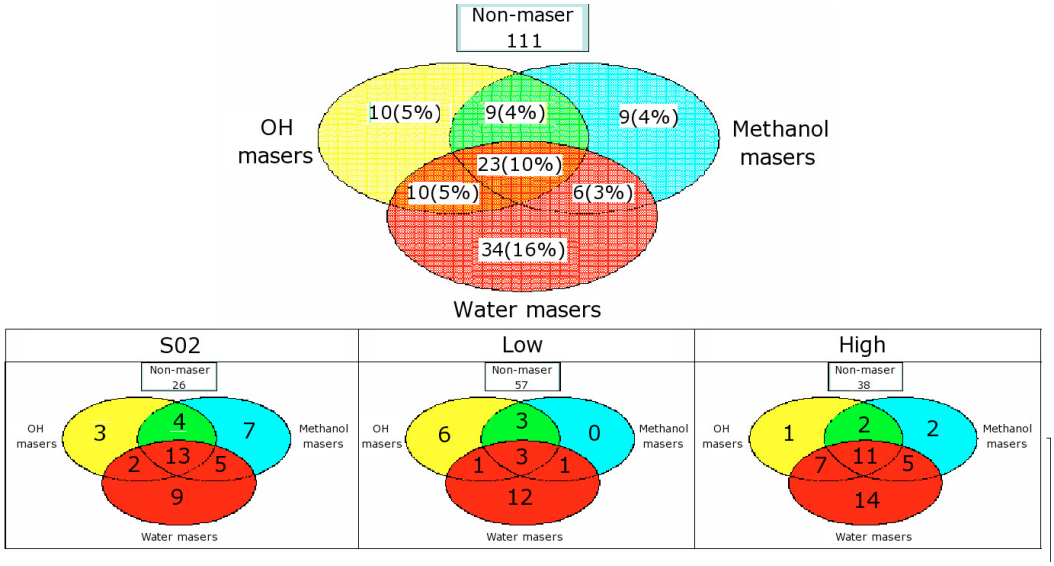

Fig. 3. *Upper panel*: number (and percentage of sample) of detected sources of the 217 HMPOs sample based on which masers are present. Note that the 7 offset star forming region candidates in Table 2 are considered here while the 5 OH/IR candidates detected are excluded. More than half of the sample do not show maser emission. *Bottom panels*: same as *upper panel* but divided by subsamples. For the whole sample there are 100 sources associated one or more types of maser, while there are 43, 26 and 42 maser sources in the S02, *Low* and *High* subsamples respectively. Note that some sources are common in the S02 and *High* subsamples.

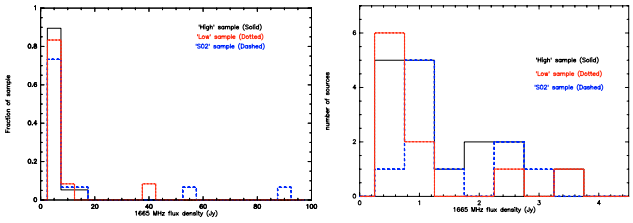

Fig. 4. The flux densities at 1665 MHz line towards the three subsamples, *high* sample (solid line), *low* sample (dashed line) and S02 sample (dotted line). An expanded view for the 1665 MHz flux densities weaker than 4.5 Jy is re-plotted in the righthand panel.

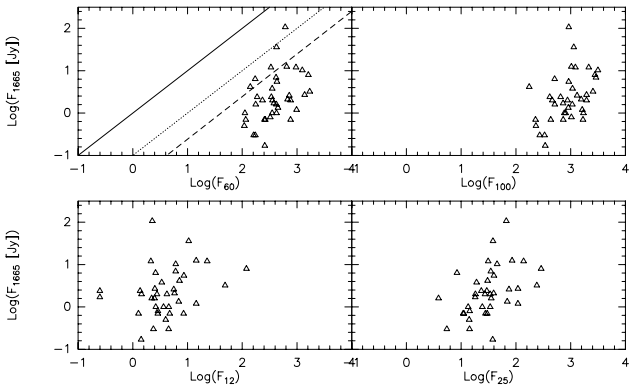

Fig. 5. OH 1665 MHz peak flux densities of the detected masers are plotted against IRAS flux densities at 12, 25, 60 and 100 μm. The solid line, in the top-left panel, corresponds to equal flux densities, the dashed line is the line of Slysh et al. (1997) data (corresponding to $F_{\rm OH}$ = 0.024 F_{60}) and the dotted line is the line of Moore et al. (1988) data (corresponding to $F_{\rm OH}$ = 0.1 F_{60}).

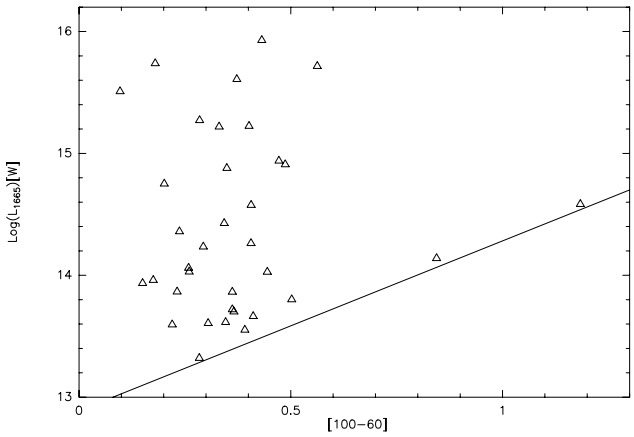

Fig. 6. The 1665 MHz OH luminosities of the detected masers are plotted against the [100–60] colour index. There may be a suggestion of a lower envelope to the distribution at about Log L_{1665} ~ 0.7 × [100–60] (solid line). Three sources with suspect distances (IRAS 18024−2119, 20062+3550 and 20227+4154) are not shown on the plot.

Figure 6 plots the [100−60] colour index vs. OH 1665 MHz maser luminosity, L_{1665}. There may be a suggestion of a lower envelope to the distribution at $\log L_{1665}$ ~ 0.7 [100–60] indicating masers are found prefentially towards sources with warmer radiation temperatures.

To see if there is a difference in IR flux densities or colours between maser and non-maser sources, IRAS sources associated with one or more type of maser were compared with the rest of the sources. Table 4 gives the results of Kolmogorov-Smirnov (KS) test for the probability D, that the flux density or colour distribution between maser and non-maser source are different. The table shows that in general, the maser sources do show different flux densities and colours from non-maser ones. The difference between maser sources and non-maser sources is most evident in the [60−12] and [100−12] colours for all types of masers where $D \equiv 100\%$ and in the [25−12] colour for H_2O and CH_3OH masers where $D \geq 99.9\%$. Figure 7 plots the distribution of these three colour indices for the OH maser and non-maser sources to demonstrate the last points. It can also be seen

Table 4. Results of KS test for the maser and non-maser population being drawn from the same populations. The table shows the probability D that the maser and non-maser sources are drawn from different populations. Clearly the most consistent difference is in [60−12] and [100−12] for which maser sources of all types have consistently different colours than the non-maser sources. Values greater than 99.9% shown as 100%. For comparison a 3σ result would correspond to $D = 99.87\%$.

Maser type/s	[25−12] %	[60−12] %	[60−25] %	[100−60] %	[100−12] %	F_{12} %	F_{25} %	F_{60} %	F_{100} %
OH	96.5	100	53.6	19.7	100	98.8	84.8	92.4	96.5
H_2O	100	100	61.3	12.4	100	83.1	99.2	99.7	99.5
CH_3OH	99.9	100	91.7	98	100	100	41.1	99.6	100
OH, H_2O & CH_3OH	96.5	100	81.5	74.5	100	99.9	81.5	99.4	99.4

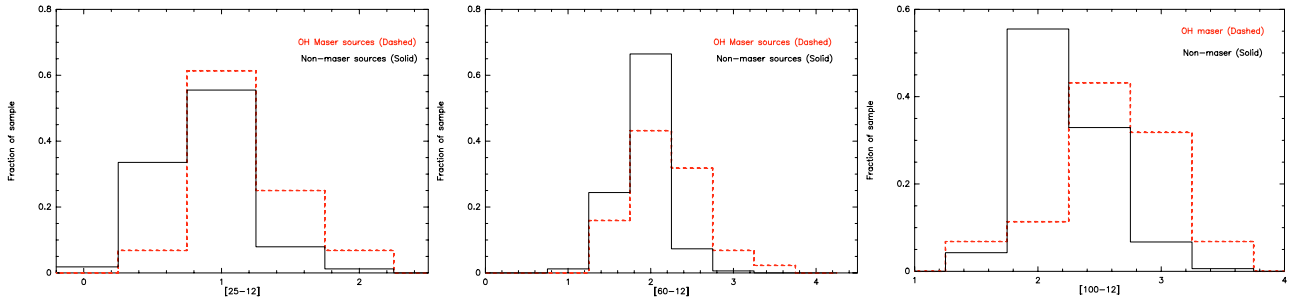

Fig. 7. The [25−12] (*left panel*), [60−12] (*middle panel*) and [100−12] (*right panel*) colour indices for OH maser sources (dashed lines) and non-OH-maser sources (solid lines). In each case OH maser sources have on average redder colours than the non-maser sources and objects with colours [25−12] > 1.2, [60−12] > 2.2 and [100−12] > 2.7 are dominated by sources with OH masers.

in Fig. 1, where it is clear that sources with OH masers dominate over non-maser sources in the regions [25–12] > 1.2 and [60–12] > 2.2. Even for colours ∼0.2 smaller than these values, the maser sources make up ∼50% of the population, a higher fractor than for sources with smaller colours and for the sample overall. The redder colours of the maser sources is unlikely to be affected by the uncertainties in the colours of the sources unless the uncertainties preferentially affect maser sources and non-maser sources in different senses.

The [25−12] and [60−12] colour indices are the ones used by WC89 to identify UCHII regions. These results show that maser sources tend to be relatively faint at 12 μm compared to their fluxes at longer wavelengths. Figure 8 shows the four IRAS flux densities against each other for maser sources (squares) and non-maser sources (dots). The difference between maser sources and non-maser sources is obvious in the lower panels which include the 12 μm flux densities. On the other hand, as Table 4 also shows, sources with only OH or H_2O masers have [60−25] and [100−60] colours indistinguishable from non-maser sources.

Given the differences in [60−12] and [100−12] colours of sources with any type of maser, it is interesting to ask whether there is any systematic difference in source colour as a function of maser type. Figure 9 compares these colours for sources with each type of maser showing that there is no significant difference in the distribution of these colours as a function of maser type. For this sample there appears to be no evidence in their IRAS colours that different types of maser trace sources in significantly different evolutionary states.

Regarding the 100, 60, 25 and 12 μm flux densities, the probabilities, D in Table 4 are relatively large for all flux densities, except the CH_3OH only sources at 25 μm. However only for few maser-flux combinations are the individual D probabilities statistically significant at a 3σ level. Although methanol masers are believed to be excited by mid-IR photons (Cragg et al. 2005), Fig. 10 shows that there is no clear correlation between CH_3OH maser and 12 μm flux densities.

Figure 11 compares the luminosity of maser sources and non-maser sources. The distributions are statistically indistinguishable, indicating that masers are not preferentially associated with only the more luminous sources.

Comparing the IRAS colour indices to the ratio of CH_3OH and OH maser flux densities, Fig. 12 plots the ratio of the OH peak flux density to the CH_3OH peak flux density, R, versus the IRAS colours of a source. According to Caswell (1998) the spread in the ratio R reflects the range in evolutionary stage of the sources, but this figure does not show any evidence that R depends on the colour of a source which might also be expected to evolve as a source evolves. In considering this result, it should be noted that the IRAS colours may suffer from confusion because of the poor spatial resolution of IRAS and maser observations combined with the tendency of massive stars to form in clusters (cf. Bourke et al. 2005).

5.3. Velocity range of masers

The range of velocities over which maser emission is observed can be used to investigate whether the emission from different masers arises from different material associated with the sources. Figure 13 shows the distribution of the range of velocity for each OH maser source detected (Table 2). For comparison the figure also shows the velocity range of the H_2O and CH_3OH masers from SHK2000, P91, S02 (and references therein) and Han et al. (1998). The righthand panel of Fig. 13 shows an expanded view of the sources with velocity range ≤20 km s^{-1}.

For all three species the velocity range peaks at less than 10 km s^{-1}. The CH_3OH masers and OH masers extend up to velocity ranges of 17.5 and 22.5 km s^{-1} respectively. Overall the figures show that the OH and CH_3OH agree very well in their distribution of velocity range, peaking at ∼5 km s^{-1}, suggesting that these masers may originate in similar material around the sources. On the other hand the H_2O masers show a quite different distribution. In some sources emission covering up to 65 km s^{-1} has been observed. However the distribution actually peaks at

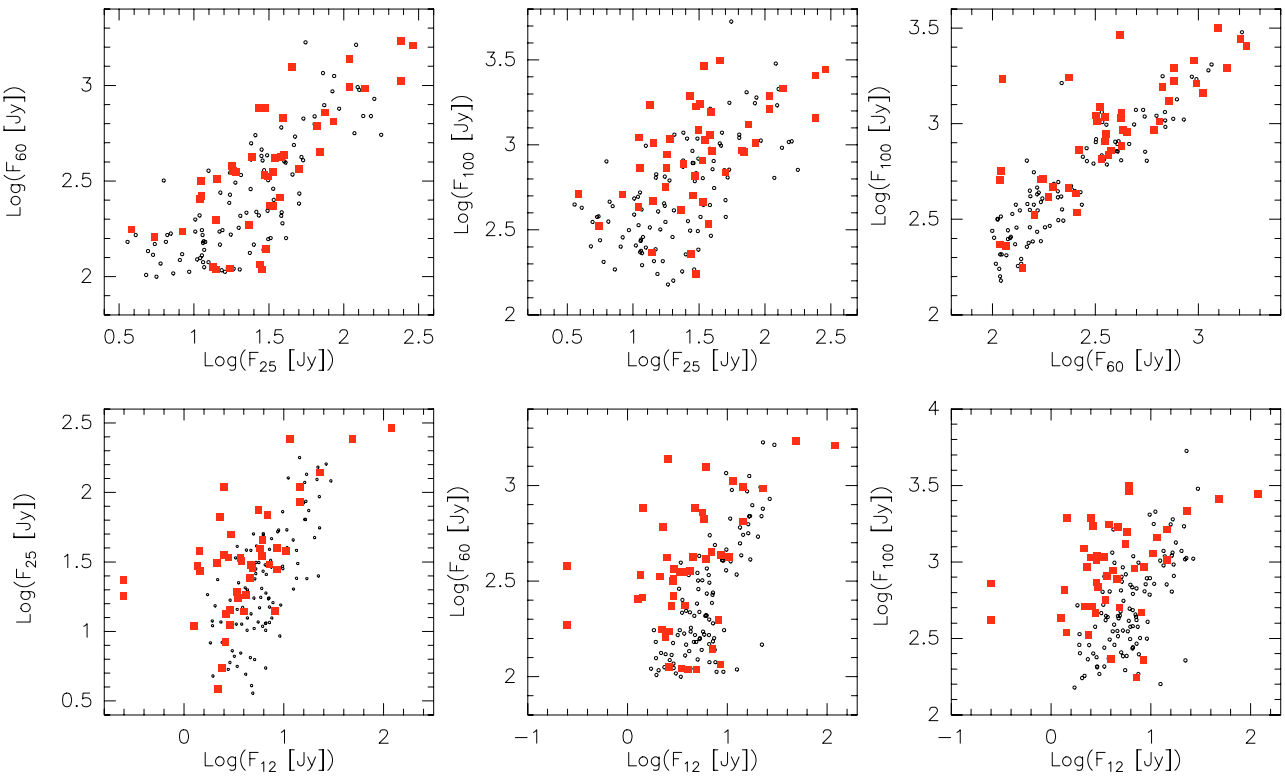

Fig. 8. Comparison of the IRAS flux densities for sources with OH masers (red squares) and those without OH masers (black dots). The difference between flux densities of maser source and non-maser ones is apparent in the lower panels where the effect of the 12 μm is obvious, while there is no apparent difference in the upper panels.

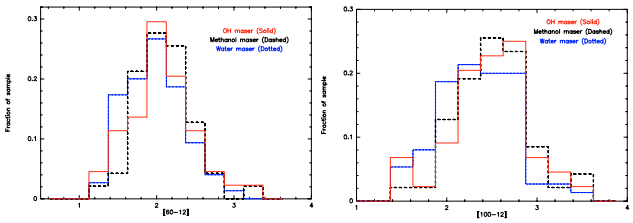

Fig. 9. [60−12] and [100−12] colours of sources with any type of maser, water (dotted lines), methanol (dashed lines) and OH (solid lines). There is no significant difference in the distribution of these colours as a function of maser type.

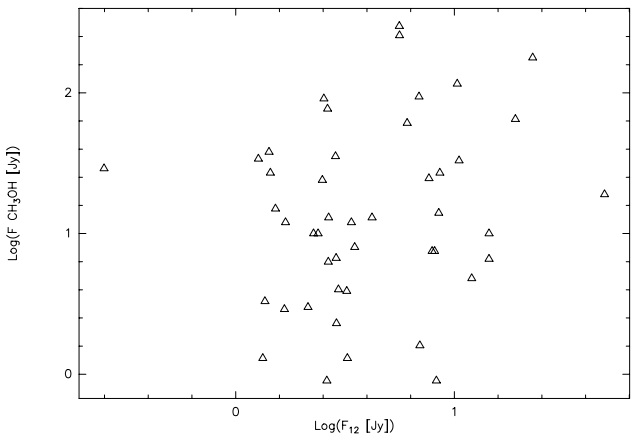

Fig. 10. Methanol maser peak flux densities are plotted against IRAS flux densities at 12 μ. No correlation is apparent.

spreads <4 km s^{-1}, smaller than for the OH and CH_3OH. This suggests a two population structure, with one group of sources with velocity ranges between ~1 km s^{-1} and ~4−5 km s^{-1} and a second with velocity ranges >5 km s^{-1}.

The offset between the OH maser velocity and the velocity of the dense gas towards each source (M 96 and S02) is shown in Fig. 14 (left). Overall the OH maser velocities are distributed around the gas velocity, as they are also for some particular sources. On the other hand there are exceptions with some sources where the OH masers are offset by up to ~20 km s^{-1} from the gas velocity. Comparing the velocity offset between different maser type and dense gas for sources with all three types of masers (Fig. 14, right), it is difficult to identify any global trend. However inspection of the observations shows 8 out of the 23 sources with all three masers have $\Delta V(\mathrm{OH}) > \Delta V(\mathrm{CH_3OH}) > \Delta V(\mathrm{H_2O})$.

6. Discussion

6.1. Comparison of OH masers with 6668 MHz methanol masers

The similarity in detection rates and velocity ranges suggest an association between OH and Class II CH_3OH masers in these sources as first suggested by Caswell et al. (1995) and modelled by Cragg et al. (2002). A similar result has also been found by Szymczak & Gérard (2004) who searched a sample of 100 CH_3OH maser sources for OH masers. They found that 55% of CH_3OH maser sources also have OH maser emission. Their results also show that OH and CH_3OH masers cover similar velocity ranges.

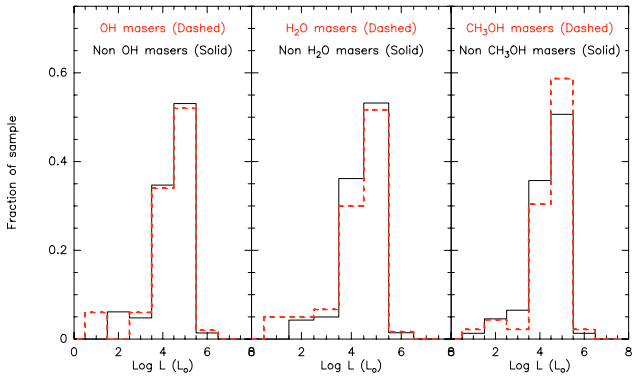

Fig. 11. Comparison of the luminosity of maser sources and non-maser sources. Note that the panels show sources with a specific maser type with sources are not associated with this type but may be associated with other types of masers.

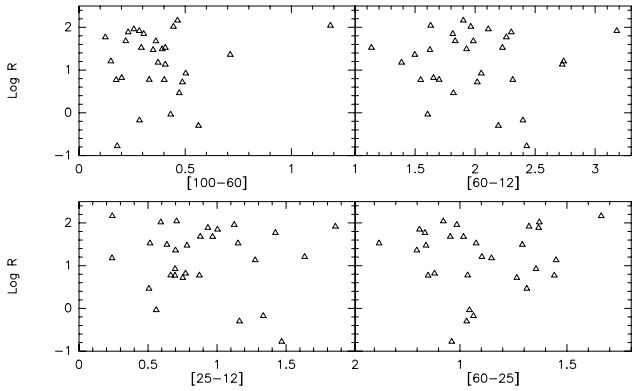

Fig. 12. Ratio of the 6668 MHz CH_3OH peak flux density to the 1665 MHz OH peak flux density, log$R$, versus IRAS colours.

We applied the suggestion of Caswell (1996) for characterizing the maser sites where methanol and OH masers occur using the ratio of peak methanol intensity to peak 1665-MHz OH intensity. Figure 15 shows the distribution of the OH to CH_3OH intensity ratio, $R = \frac{F(6668)}{F(1665)}$ (Table 2). For the 29 sources which show both 1665 MHz OH masers and 6668 MHz masers, 12 sources have values of $R > 32$ which places them in methanol-favoured region and 10 sources in OH-favoured region ($R \leq 8$).

There are an additional 12 sources which do not have OH maser emission but do have methanol masers and 20 sources with OH masers but no methanol masers. Limits on R for these sources were obtained by adopting a three sigma limit on the presence of OH masers of 150 mJy (typical of this survey) and a limit of 1500 mJy for the presence of methanol masers (Pestalozzi et al. 2005). The resulting 3-sigma limits are also shown in Fig. 15. All the methanol non-detections are consistent with the sources being OH favoured. For the OH non-detections, one source with a lower limit on R of 3 could be OH favoured, 8 sources are definitely methanol favoured and the remaining 3 have lower limits on R between 8 and 32.

The sources observed here have a very wide range in R, with measured values from ranging from 0.2 to 145 and three lower limits on R in excess of 400. The distribution of these values is in marked contrast to the results of Caswell (1996), who found most sources to have R in the range 8 to 32, with a typical value of 16. Over our whole sample, including the limits, 25 sources (41%) are OH-favoured. A similar fraction of the sample, 26 sources (43%), are CH_3OH favoured, which

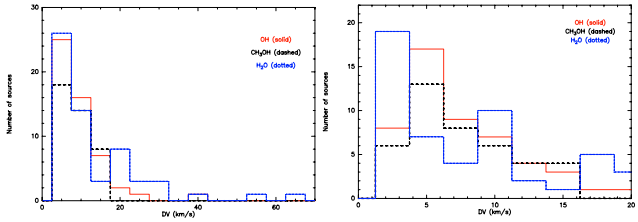

Fig. 13. The velocity spread of the masers associated with the whole sample: OH (solid line), CH_3OH (dashed line) and H_2O (dotted line). The righthand panel is an expanded view for velocities spreads $\leq$20 km s^{-1}.

Caswell (1996) suggested are sources in an earlier evolutionary stage than OH-favoured sources. Only 7 sources (11%) have measured values of R between 8 and 32 plus there are a further 3 lower limits (corresponding to a further 5% of the sample) which could place these sources in this range of R. If R does indeed trace the evolutionary status of sources as Caswell has suggested, then these results suggest that the sample observed here represent a particular mix of sources in different evolutionary stages distinct from that in the sample observed by Caswell. The high fraction of methanol favoured sources here suggesting that this sample contains a higher portion of younger objects.

6.2. OH maser flux densities

Figure 4 shows that nearly half of the detected sources show OH flux densities $\lesssim$1 Jy, which indicates two points. First it demonstrates how less sensitive observations (with detection limits of $\gtrsim$1 Jy, e.g. Cohen et al. 1988) could be missing a significant population of OH maser sources. More importantly it indicates that the sources observed here, which are believed to be in an early stage of formation with no observable UCHII regions, have lower OH flux densities than sources in more evolved objects associated with HII regions, where typical OH masers have flux densities $\geq$1 Jy.

Figure 6 shows that most of the OH maser sources prefer warmer radiation fields. This is probably because most of the FIR transitions which pump the OH maser are at wavelengths between ~60 μm and 100 μm (Gray et al. 1992). The luminosity of the 1665 MHz line spans a factor of about 300 across the sample, but the origin of this scatter is unclear. However it is likely that individual maser spots are saturated, so for a given source luminosity (especially in the spectral region ~60 μm $\leq$ $\lambda \leq$ 100 μm) the maser luminosity may reflect the number of maser sites or volume of masing gas (Gray priv. comm.).

Models of OH maser emission show different physical conditions give rise to different combinations of OH maser lines. For example the Cragg et al. (2002) models show that 1665 MHz masers trace a wider range of conditions that 1667 MHz masers. In particular, gas kinetic temperatures >75 K, and gas number densities $\gtrsim 10^7$ cm^{-3} more strongly quench the emission at 1667 MHz than the emission at 1665 MHz suggesting that ratio of these lines fluxes may be a probe of the conditions in the gas, with masers seen in only the 1665 MHz line tracing warmer, denser gas.

For the sample observed here 28 sources were detected in both the 1665 MHz and 1667 MHz lines. For all except four of these objects the 1665 MHz line was stronger that the 1667 MHz line. The ratio of the flux density at 1665 MHz to that at 1667 MHz for these objects is shown in Fig. 16. A further 16 objects were detected in only the 1665 MHz line. The

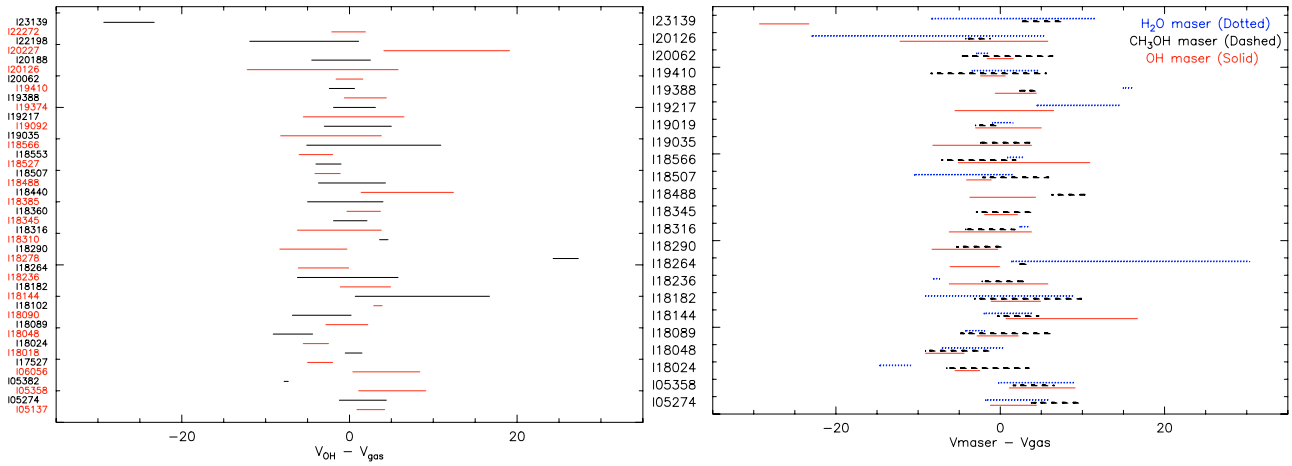

Fig. 14. *Left hand panel*: the velocity range relative to cloud gas velocity for OH maser sources. *Right hand panel*: the same as left hand panel but for the 23 sources showing three maser types. Note that some sources, although detected in H_2O and/or CH_3OH, do not have published information on their velocity extent.

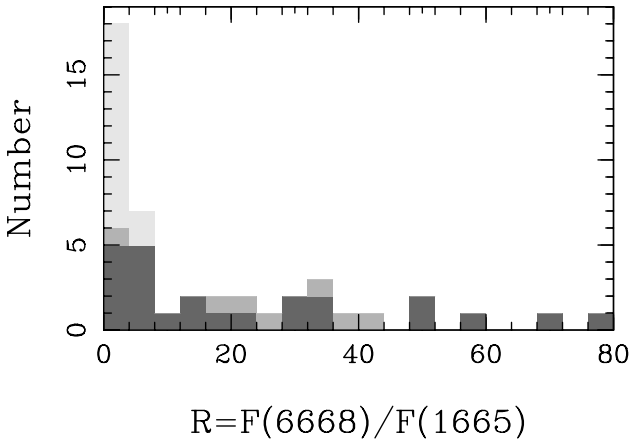

Fig. 15. Distribution of number of sources as a function of $R = \frac{F(6668)}{F(1665)}$, the ratio of the peak CH_3OH maser intensity to the peak OH maser intensity. The darkest bars show measured values. The lightest bars show upper limits on R for sources with no detected methanol masers and the mid-grey bars show the lower limits on R for sources with no detected OH masers. There are 5 sources with measured values of $R > 82$ and 5 lower limits with $R > 82$ which are not shown on the plot. Caswell (1997) identified sources with $R \leq 8$ as OH-favoured and those with $R \geq 32$ as methanol-favoured.

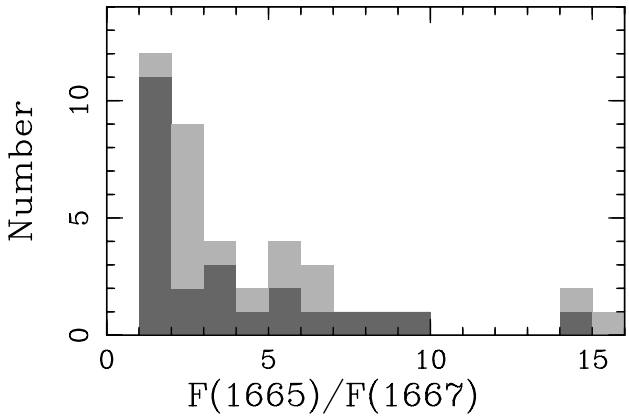

Fig. 16. The distribution of the ratio of peak 1665 MHz flux density to peak 1667 MHz flux density for the sources. The dark coloured bars show the measured ratios. There are four sources for which the 1667 MHz line is stronger than the 1665 MHz which are not shown. The light coloured bars show the 3 sigma lower limits for the sources which were detected at 1665 MHz but not 1667 MHz. There is one source detected at 1667 MHz but not 1665 MHz which is also not shown. Sources where the masers are offset from the IRAS position are included in the distributions.

3-sigma lower limits on the 1665 MHz to 1667 MHz ratio for these sources are also shown the figure. The majority of sources have ratios of less ∼3, but there is a tail of sources (and limits) up to ratios as large as ∼15. Whether this range of intensity ratios reflects different physical conditions in these sources requires more detailed follow-up observations of the sources, particularly at higher angular resolution.

6.3. OH maser only sources

There is a group of newly detected sources associated with only OH maser emission; namely IRAS 06382+0939, 18408−0348, 18540+0220, 18454−0158, 18511+0146, 18586+0106, 19118+0945, 19220+1432 and 20099+3640. The already known OH maser source IRAS 18018−2426 may also be in this group, although there has been no search for CH_3OH maser emission towards it. However for only four of these objects, IRAS 18018−2426, 18454−0158, 19118+0945 and 19220+1432 are the OH masers positionally associated with the IRAS source. The OH masers towards the other sources are offset from the IRAS position and so it is possible that previous searches for other types of maser may have missed masers which are also offset from the IRAS position.

Interestingly, six of the ten OH-only objects, including IRAS 18018–2426 and IRAS 19118+0945, are from the *Low* sub-sample of M 96 which contains sources which do not have UCHII region IRAS colours (WC89). However, four of these sources are associated with radio continuum emission and no equivalent observations has been carried out towards the other two sources, IRAS 06382+0939 and 19118+0945. M96 found a lower incidence of ammonia emission towards their *Low* sample than the *High* one and suggested that the *Low* sample contains sources in two different evolutionary stages. Some sources are in a stage before the existence of an UCHII region and others are in a stage after the HII region has evolved.

The sources with evolved HII regions were suggested to be a very late HMPO stage and are expected to be associated with relatively small amounts of neutral gas. The absence of detectable ammonia towards IRAS 18408−0348, 19118+0945 (M 96), 18454−0158 and 18540+0220 (S02) but the presence of only OH masers suggest that these objects could be relatively evolved.

6.4. 1720 MHz only sources

There are five sources, IRAS 04579+4703[4], 18264−1152, 18553+0414, 19220+1432 and 20188+3928, which have OH maser emission, but only in the 1720 MHz transition. These sources, apart from IRAS 19220+1432, are associated with other maser types. They are, apart from IRAS 04579+4703, also associated with, at most, weak radio continuum emission (<1 to 11 mJy). Isolated 1720-MHz masers are sometimes observed in star-forming regions in association with 6668-MHz methanol masers (e.g. Etoka et al. 2005), an association which can be understood in terms of common pumping conditions (Cragg et al. 2002). Other objects associated with only 1720-MHz OH maser emission are believed to be supernova remnants. Elitzur (1976) suggests that the level inversion of these 1720 MHz masers is due to collisional excitation. Models suggest that the masers originate in the post-shock molecular gas behind C-type shocks (e.g. Lockett et al. 1999). However, these 4 sources appear to be star-forming regions. If the Elitzur (1976) model is correct, the masers may be tracing post-shock gas towards these sources. Confirmation of this interpretation will require detailed follow-up of these objects.

7. Conclusions

The results of this survey confirm that OH masers are common, not only towards HII and UCHII regions as previously known, but also towards less evolved high mass young stars which, although luminous, have not yet significantly ionised their surroundings. Indeed towards these young sources OH masers are as common as the H_2O and Class II CH_3OH masers which have often been been cited as evidence of the youth of these sources. Compared to the OH masers associated with HII/UCHII regions, the OH masers towards these younger sources are weaker, suggesting that the OH maser flux density could be a crude evolutionary indicator.

There is no evidence within the observed sample for a luminosity difference between those sources with OH masers and those without masers. However, on average the sources with OH masers have significantly redder [100–12] and [60–12] IRAS colours than those which do not have OH masers, suggesting that the OH maser sources are more deeply embedded and hence younger. Similar colour differences are also seen for sources with H_2O and CH_3OH masers. However intercomparing the distribution of these colours for sources with each type maser shows them to be indistinguishable. For the sources in this study at least, there is no evidence that one or other of the types of maser in particular traces younger (or older) sources.

The velocity range of the maser emission suggests that the water maser sources may be divided into two groups, one of which shows narrow velocity spread of less than 4−5 km s^{-1}, while the other shows a much wider one, with sources which have H_2O maser velocities spread over up to ~65 km s^{-1}. This division may well reflect the suggestion by Torrelles et al. (1997, 1998) that H_2O masers can trace both molecular outflows and accretion disks perpendicular to the molecular outflow.

Comparing the OH and methanol maser peak fluxes, the majority of the sources are either methanol-favoured or OH-favoured with over 40% of the sources in each of these categories. Both the detection rate and velocity coverage of the maser emission suggests a close association between OH and CH_3OH masers, which has also been reported by other authors (e.g. Caswell 1998, and references therein; Szymczak & Kus 2000; Szymczak & Gérard 2004). However understanding the exact origin of the OH masers and the detailed connection between the OH and CH_3OH masers requires higher spatial resolution follow-up studies such as that of IRAS 20126+4104 by Edris et al. (2005). High resolution observations of some molecular outflow sources have shown that towards HMPOs the OH masers often arise from a circumstellar disc around the central source (Hutawarakorn & Cohen 1999; Hutawarakorn et al. 2002; Hutawarakorn et al. 2003; Edris et al. 2005). Such high resolution follow-up of the sources in this survey may therefore identify additional HMPOs with circumstellar disks and making use of the Zeeman sensitivity of the OH emission, measure the magnetic field within them.

Acknowledgements. We would like to thank the staff at both Nançay and Green Bank for their invaluable help in obtaining the data presented here. We would also like to thank Malcolm Gray for helpful discussions. K.A.E and G.A.F would like to dedicate this paper to the memory of R.J. Cohen who passed away on 1 November 2006.

[4] Note that the masers towards IRAS 04579+4703 are offset from the IRAS source.

References

Argon, A. L., Reid, M. J., & Menten, K. M. 2000, ApJS, 129, 159
Benson, J. M., & Johnston, K. J. 1984, ApJ, 277, 181
Beuther, H., Walsh, A., Schilke, P., et al. 2002a, A&A, 390, 289
Beuther, H., Sridharan, T. K., Schilke, P., et al. 2002b, A&A, 383, 892
Beuther, H., Schilke, P., Menten, K. M., et al. 2002c, ApJ, 566, 945
Beuther, H., Schilke, P., Gueth, F., et al. 2002d, A&A, 387, 931
Beuther, H., Schilke, P., & Gueth, F. 2004, ApJ, 608, 330
Beuther, H., Zhang, Q., Sridharan, T. K., & Chen, J. 2005, ApJ, 628, 800
Bourke, T. L., Hyland, A. R., & Robinson, G. 2005, ApJ, 625, 883
Braz, M. A., Lepine, L. R. D., Sivagnanam, P., & Le Squeren, A. M. 1990, A&A, 236, 479
Brebner, G. C. 1988, Ph.D. Thesis University of Manchester
Bronfman, L., Nyman, L. A., & May, J. 1996, A&AS, 115, 81
Caswell, J. L. 1996, MNRAS, 279, 79
Caswell, J. L. 1997, MNRAS, 289, 203
Caswell, J. L. 1998, MNRAS, 297, 215
Caswell, J. L., & Haynes, R. F. 1983, Aust. J. Phys., 36, 361
Caswell, J. L., Vaile, R. A., & Forster, J. R. 1995, MNRAS, 277, 210
Cesaroni, R., Felli, M., Testi, L., Walmsley, C. M., & Olmi, L. 1997, A&A, 325, 725 (C97)
Churchwell, E. 2002, ARA&A, 40, 27
Cohen, R. J. 1989, Rep. Prog. Phys., 52, 881
Cohen, R. J., Rowland, P. R., & Blair, M. M. 1984, MNRAS, 210, 425
Cohen, R. J., Baart, E. E., & Jonas, J. L. 1988, MNRAS, 231, 205
Cohen, R. J., Brebner, G. C., Hutawarakorn, B., & Gasiprong, N. 2003, IAU General Assembly, 2003 IAUS, 221P, 168C
Cragg, D. M., Sobolev, A. M., & Godfrey, P. D. 2002, MNRAS, 331, 521
Cragg, D. M., Sobolev, A. M., & Godfrey, P. D. 2005, MNRAS, 360, 533
Edris, K. A., Fuller, G. A., Cohen, R. J., & Sandra, E. 2005, A&A, 343, 213
Elitzur, M. 1976, ApJ, 203, 124
Elitzur, M., & de Jong, T. 1978, A&A, 67, 323
Etoka, S., Cohen, R. J., & Gray, M. D. 2005, MNRAS, 360, 1162
Foster, J. R., & Caswell, J. L. 2000, ApJ, 530, 371
Galt, J. 2004, AJ, 127, 3479
Garay, G., & Lizano, S. 1999, PASP, 111, 1049
Genzel, R., & Downes, D. 1977, A&AS, 30, 145
Gray, M. D., Field, D., & Doel, R. C. 1992, A&A, 262, 555
Haynes, R. F., Caswell, J. L., & Simons, L. W. J. 1979, Aust. J. Phys. Astrophys. Suppl., 48, 1

Hofner, P., Cesaroni, R., Rodríguez, L. F., & Marti, J. 1999, A&A, 345, 43
Hughes, V. A., & Macleod, G. C. 1993, AJ, 105, 1495
Hutawarakorn, B., & Cohen, R. J. 1999, MNRAS, 303, 845
Hutawarakorn, B., & Cohen, R. J. 2003, MNRAS, 345, 175
Hutawarakorn, B., Cohen, R. J., & Brebner, G. C. 2002, MNRAS, 330, 349
Jenness, T., Scott, P. F., & Padman, R. 1995, MNRAS, 276, 1024
Lada, C. J. 1976, ApJS, 32, 603
Lockett, P., Gauthier, E., & Elitzur, M. 1999, ApJ, 447, 211
Minier, V., Conway, J. E., & Booth, R. S. 2001, A&A, 369, 278
Minier, V., Burton, M. G., Hill, T., et al. 2005, A&A, 429, 945
Miralles, M. P., Rodríguez, L. F., & Scalise, E. 1994, ApJS, 92, 173
Molinari, S., Brand, J., Cesaroni, R., & Palla, F. 1996, A&A, 308, 573
Molinari, S., Brand, J., Cesaroni, R., Palla, F., & Palumbo, G. G. C. 1998, A&A, 336, 339
Molinari, S., Testi, L., Rodríguez, L., & Zhang, Q. 2002, ApJ, 570, 758
Moore, T. J. T., Mountain, C. M., Yamashita, T., & Selby, M. J. 1988, MNRAS, 234, 95
Moscadelli, L., Cesaroni, R., & Rioja, M. J. 2000, A&A, 360, 663 (MCR)
Palla, F., Brand, J., Cesaroni, R., Comoretto, G., & Felli, M. 1991, A&A, 246, 249 (P91)
Pestalozzi, M. R., Minier, V., & Booth, R. S. 2005, A&A, 432, 737
Schutte, A. J., Van der Walt, D. J., Gaylard, M. J., & Macleod, G. C. 1993, MNRAS, 261, 783
Shepherd, D. S., Nürnberger, D. E. A., & Bronfman, L. 2004, ApJ, 602, 850
Simon, M., Cassar, L., Felli, M., et al. 1984, ApJ, 278, 170
Slysh, V. I., Dzura, A. M., Val'tts, I. E., & Gérard, E. 1994, A&AS, 106, 87
Slysh, V. I., Dzura, A. M., Val'tts, I. E., & Gérard, E. 1997, A&AS, 124, 85
Slysh, V. I., Val'tts, I. E., Kalenskii, S. V., et al. 1999, A&AS, 134, 115
Sridharan, T. K., Beuther, H., Schilke, P., Menten, K. M., & Wyrowski, F. 2002, ApJ, 566, 931
Szymczak, M., & Gérard, E. 2004, A&A, 414, 235
Szymczak, M., & Kus, A. J. 2000, A&AS, 147, 181
Szymczak, M., Hrynek, G., & Kus, A. J. 2000a, A&AS, 143, 269 (SHK2000)
Szymczak, M., Kus, A. J., & Hrynek, G. 2000b, MNRAS, 312, 211
Tofani, G., Felli, M., Taylor, G. B., & Hunter, T. R. 1995, A&AS, 112, 299
Torrelles, J. M., Gómez, J. F., Rodríguez, L. F., et al. 1997, ApJ, 489, 744
Torrelles, J. M., Gómez, J. F., Rodríguez, L. F., et al. 1998, ApJ, 505, 756
Verdes-Montenegro, L., Torelles, J. M., Rodriguez, L. F., et al. 1989, ApJ, 346, 193
Walsh, A. J., Burton, M. G., Hyland, A. R., & Robinson, G. 1998, MNRAS, 301, 640
Williams, S. J., Fuller, G. A., & Sridharan, T. K. 2004, A&A, 417, 115
Wood, D. O. S., & Churchwell, E. 1989, ApJS, 83, 119 (WC89)
Wu, Y., Wei, Y., Zhao, M., et al. 2004, A&A, 426, 503
Zhang, Q., Hunter, T. R., & Sridharan, T. K. 1998, ApJ, 505, 151
Zhang, Q., Hunter, T. R., Brand, J., et al. 2005, ApJ, 625, 864

Online Material

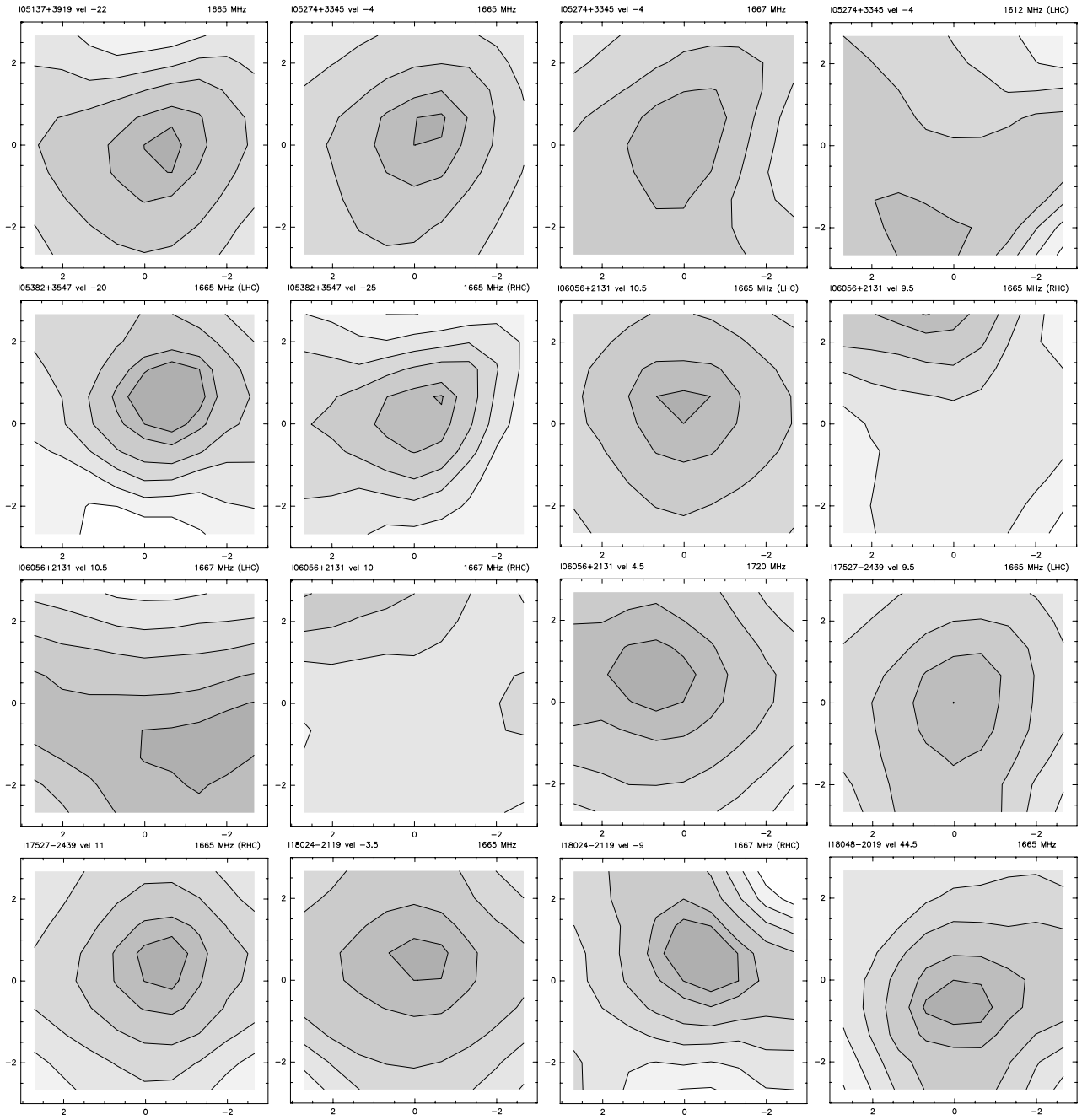

Fig. 17. The 9-point maps of the maser intensity integrated over the velocity range of each maser component detected by the GBT observations. The axes show RA and Dec offset in arcminutes from the IRAS position. The contours levels run from 10% to 90% (in 20% steps) of the peak flux given in Table 2.

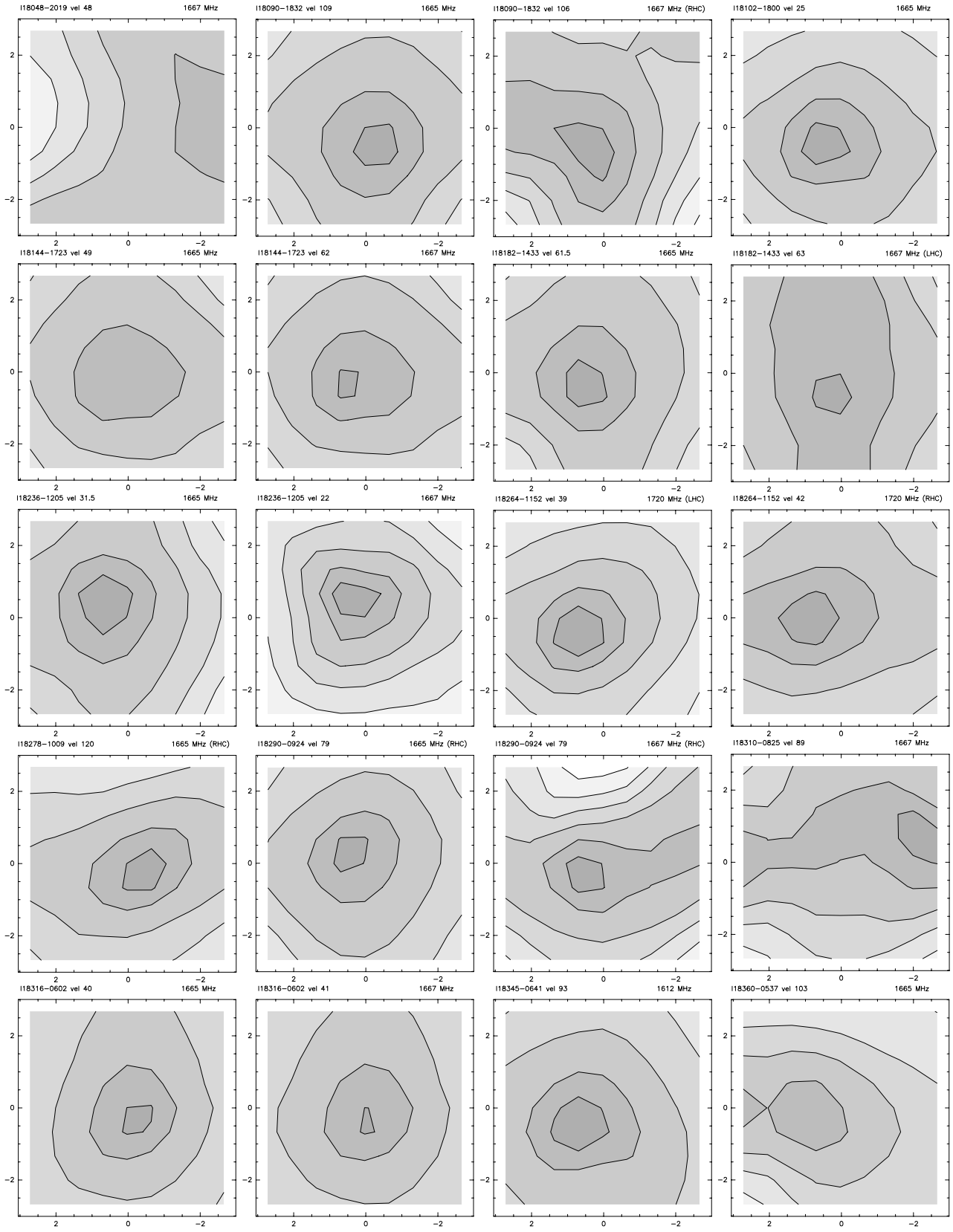

Fig. 17. continued.

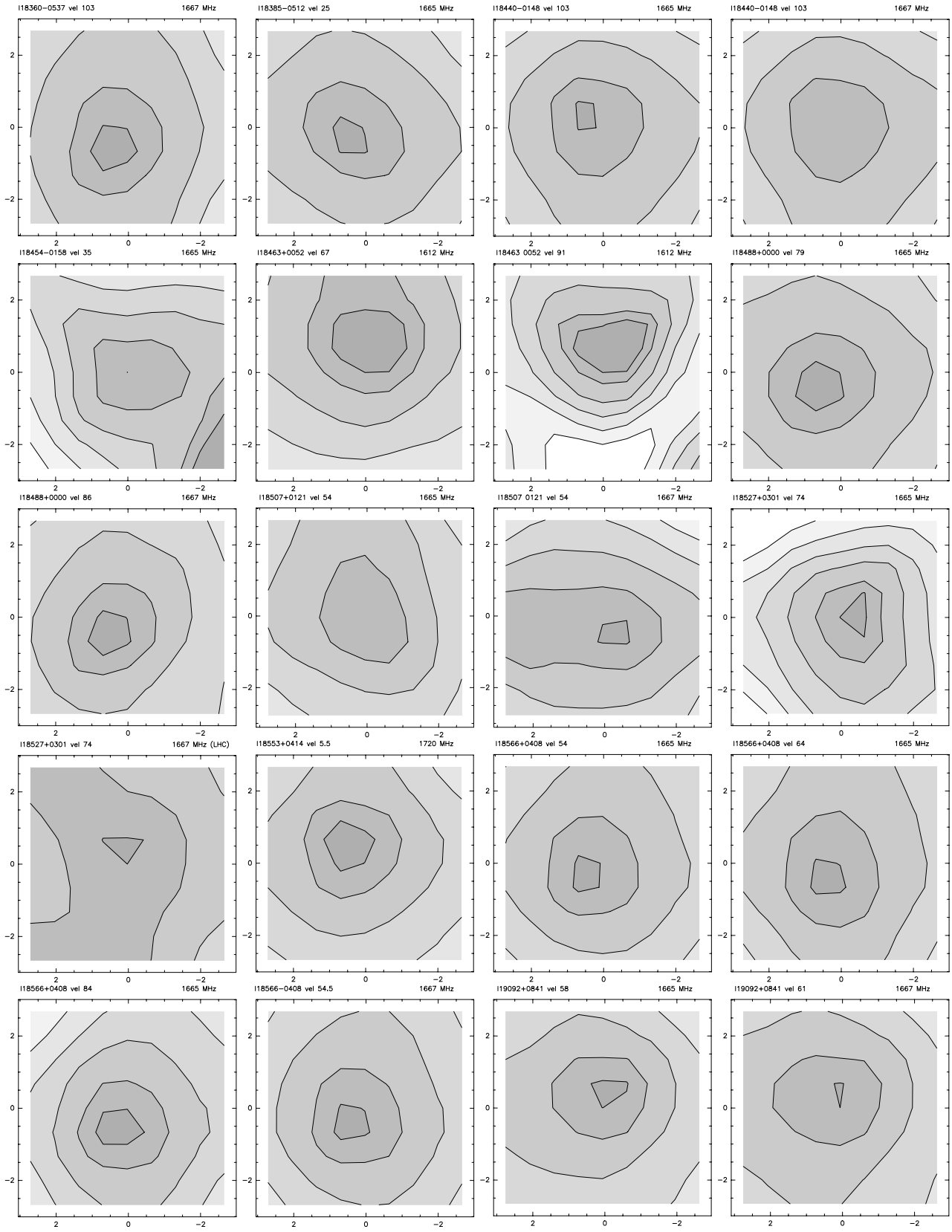

Fig. 17. continued.

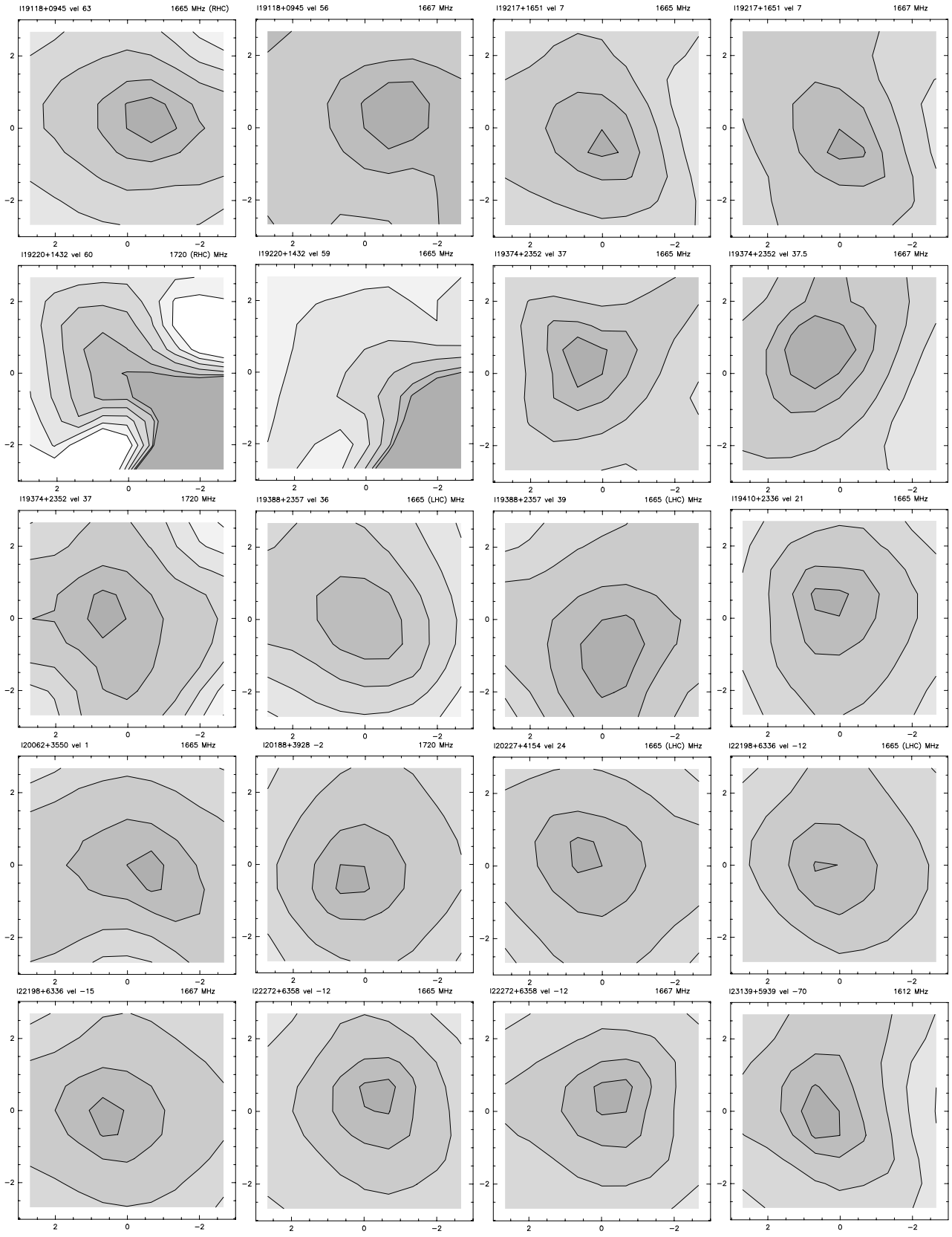

Fig. 17. continued.

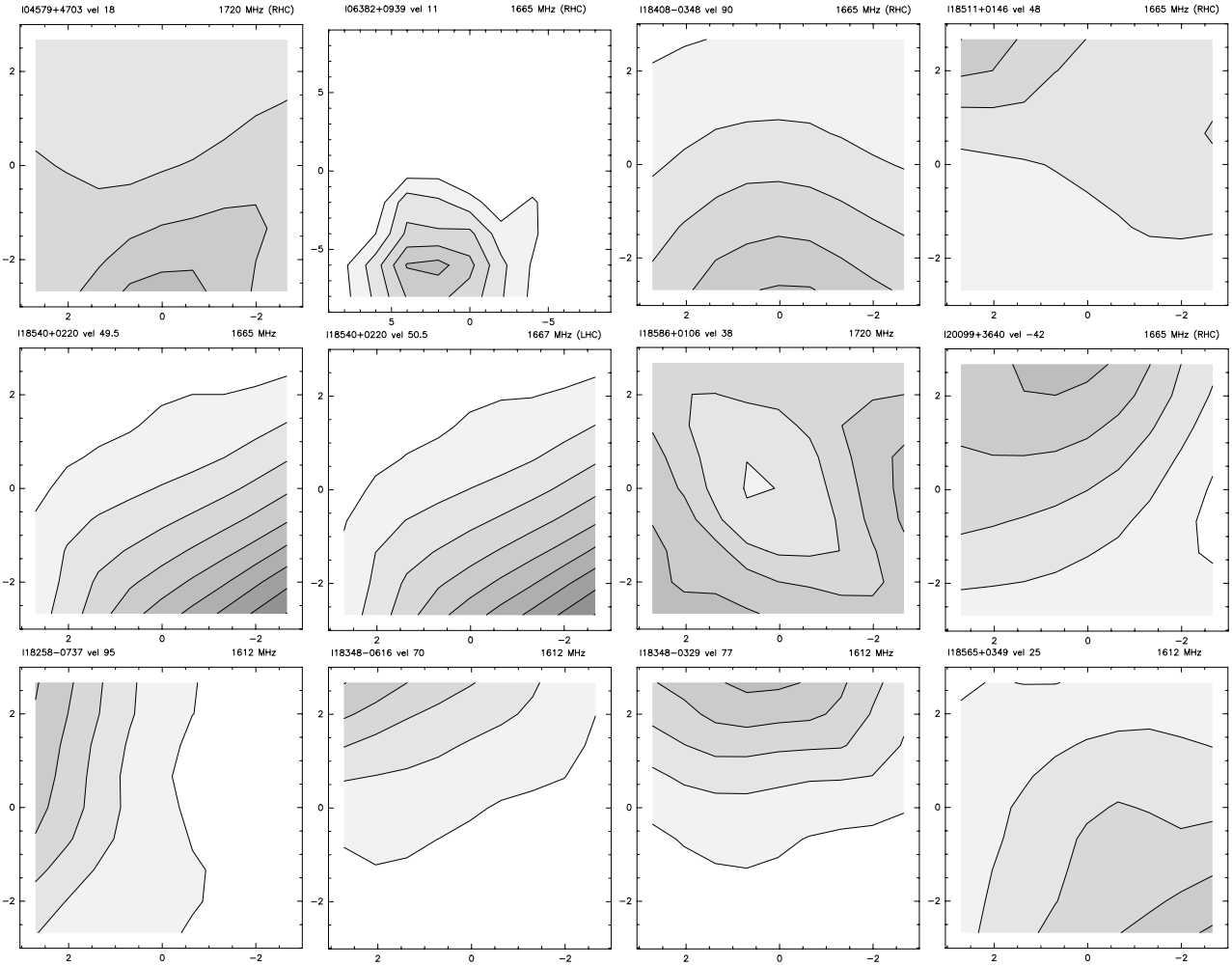

Fig. 18. Same as Fig. 17 but for OH maser sources offset from the IRAS position by >2′.

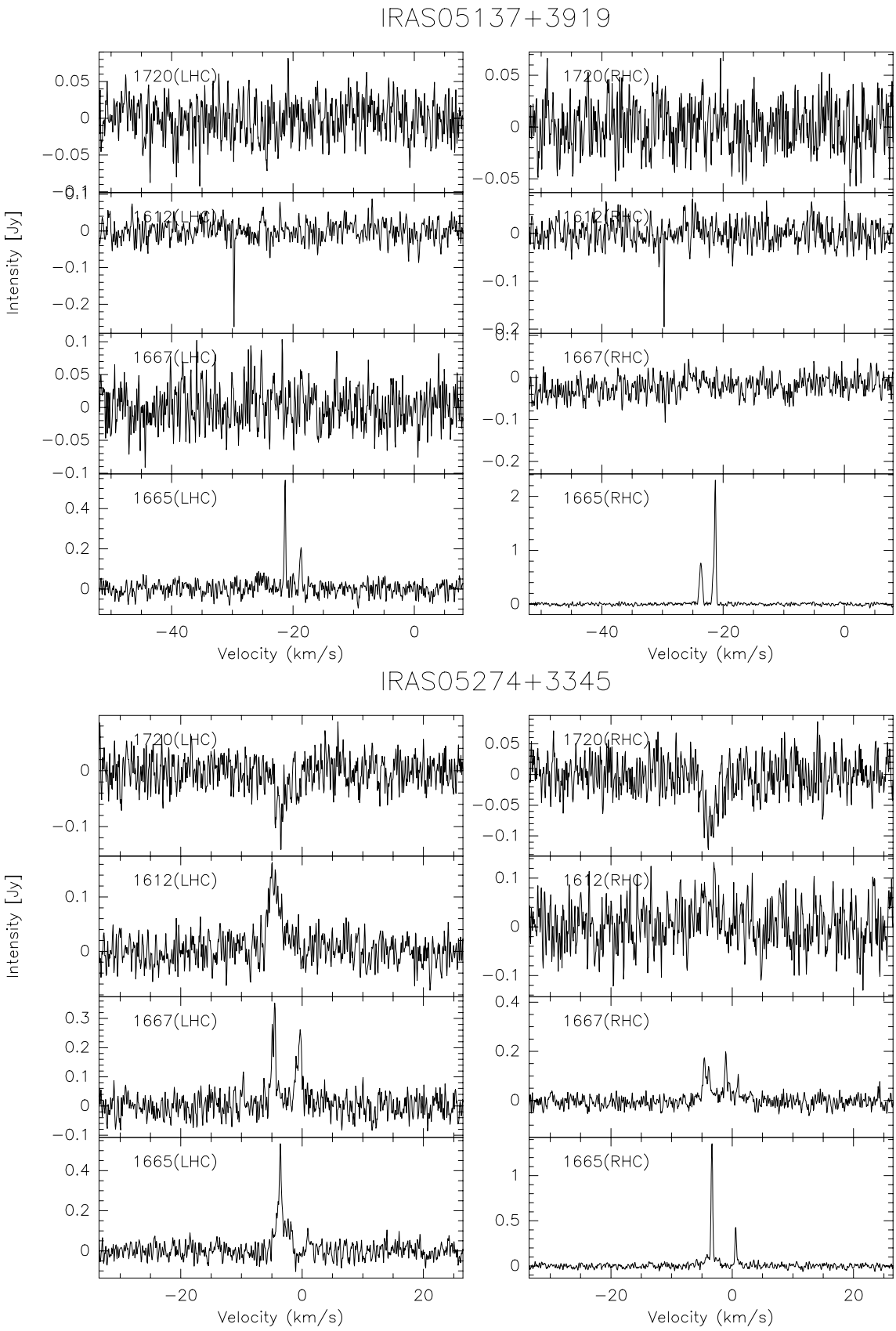

Fig. 19. The spectra of each OH maser line detected by GBT and Nançay observations. The sources names are given at the top of each group of spectra. The intensities are in Jy.

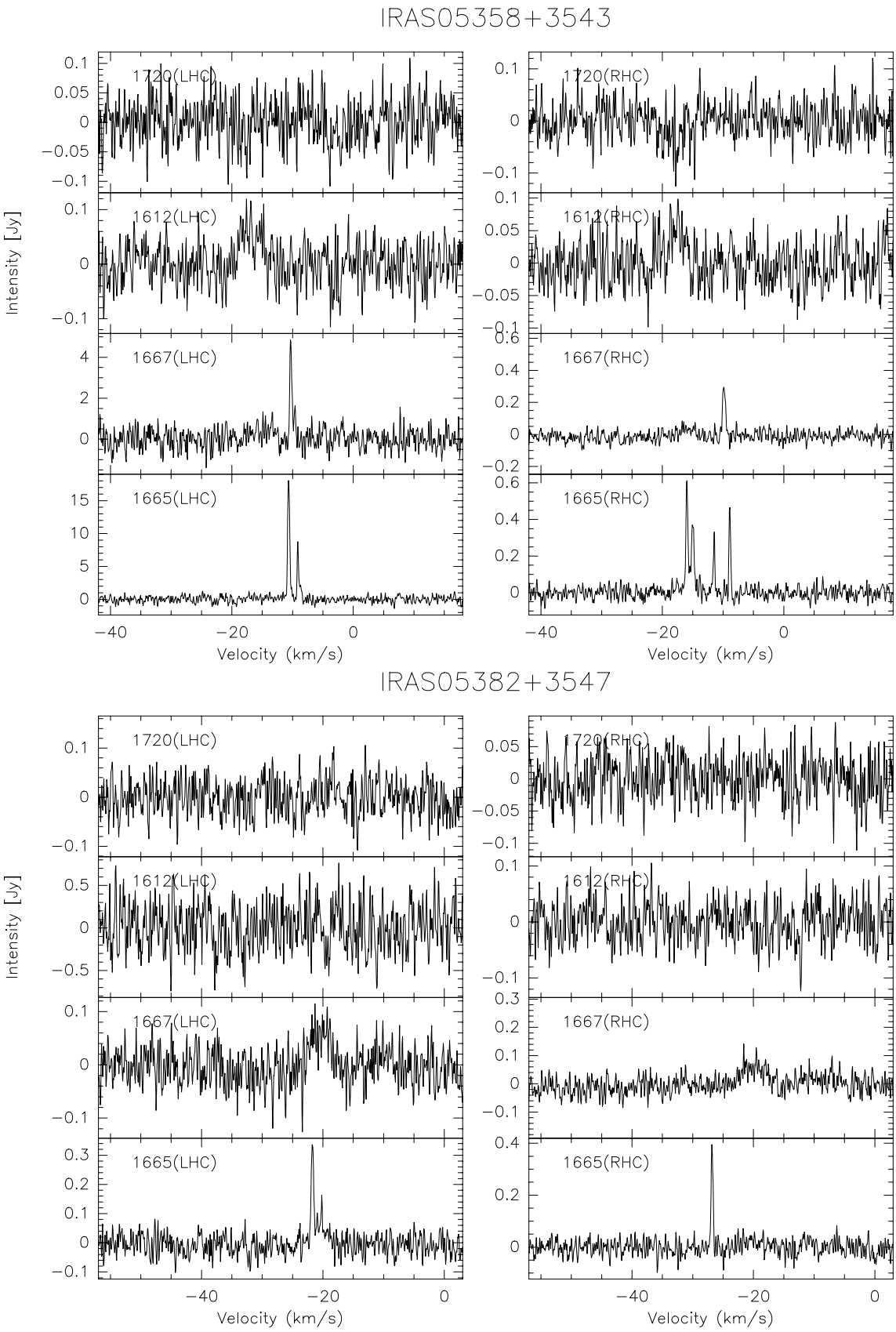

Fig. 19. continued.

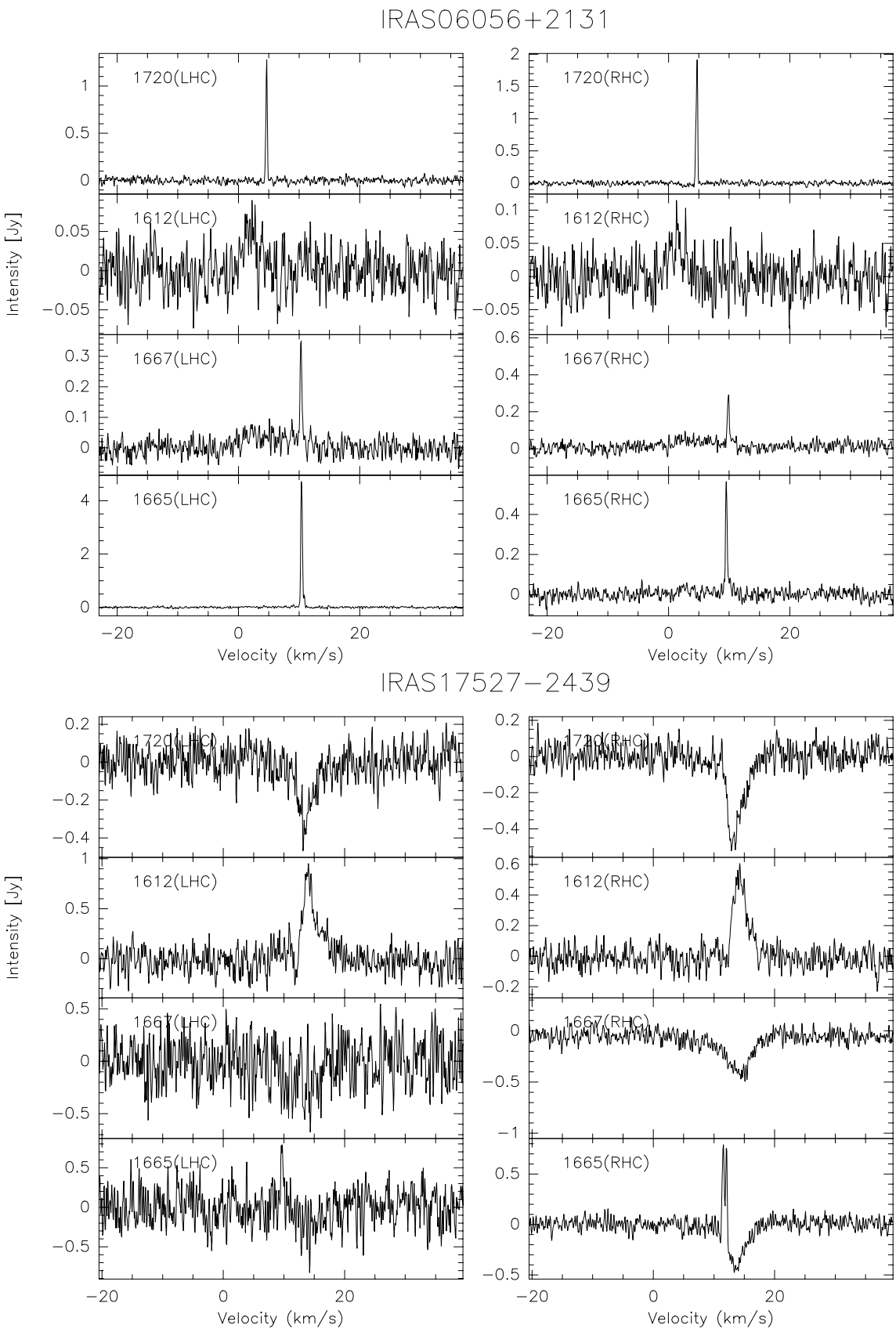

Fig. 19. continued.

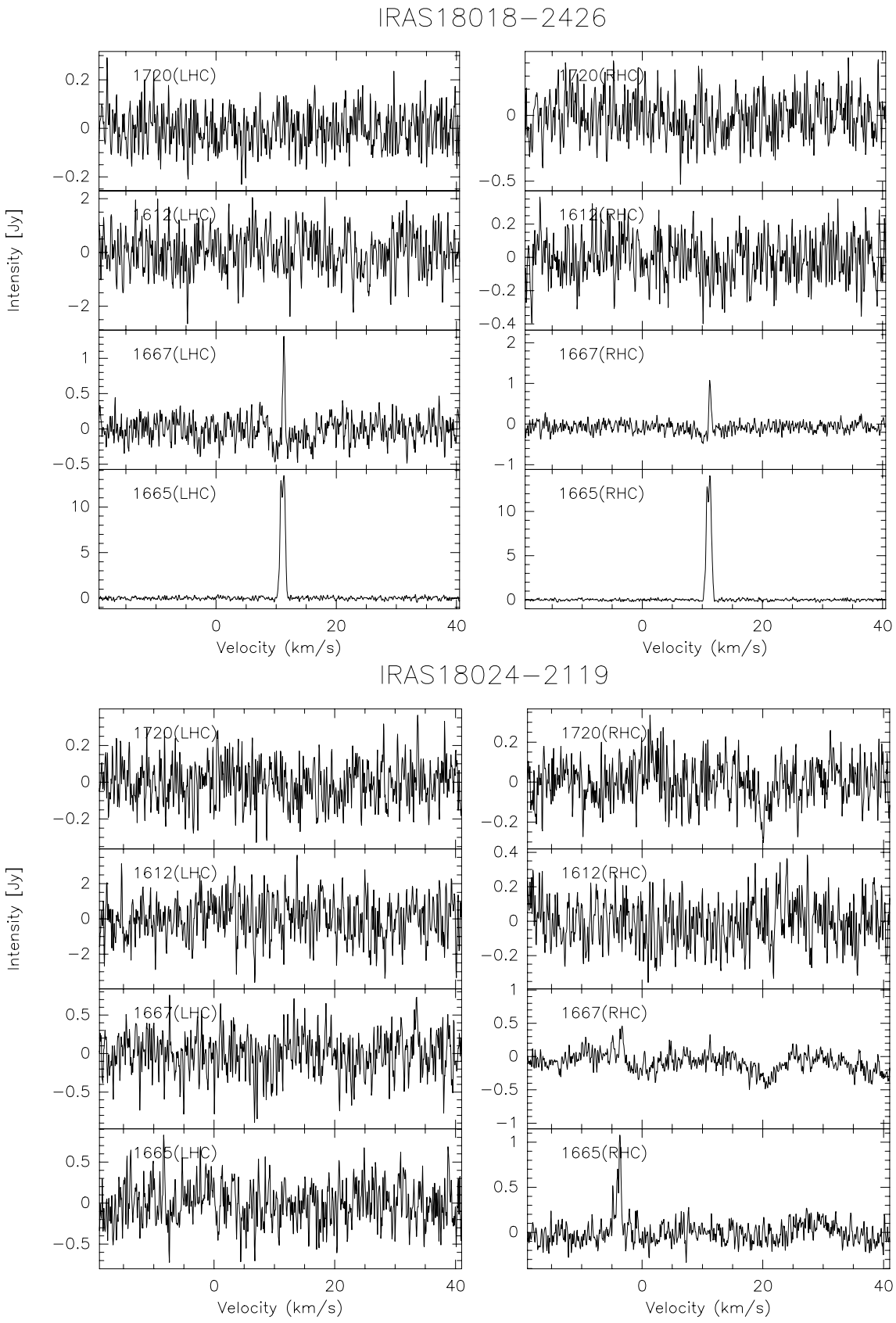

Fig. 19. continued.

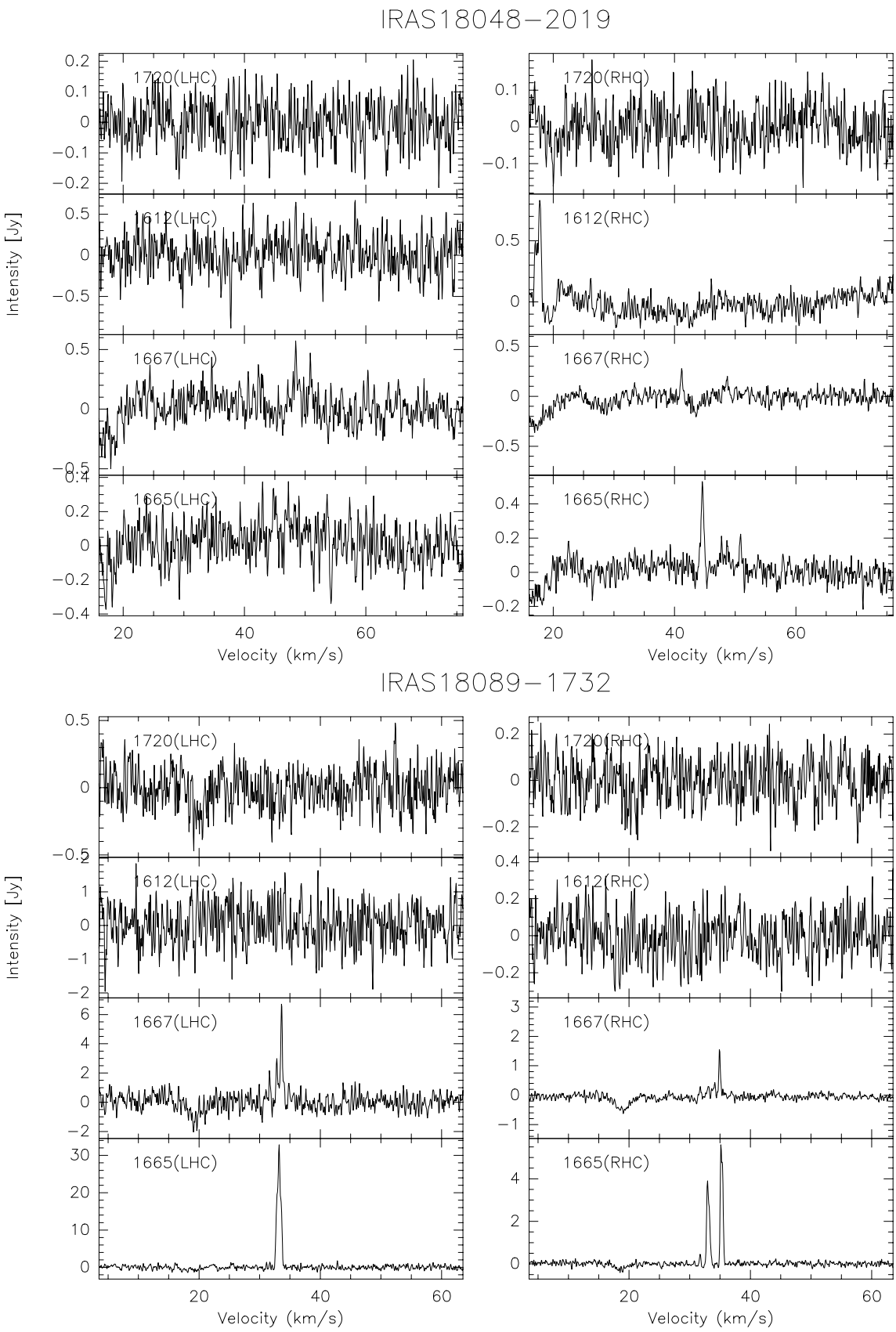

Fig. 19. continued.

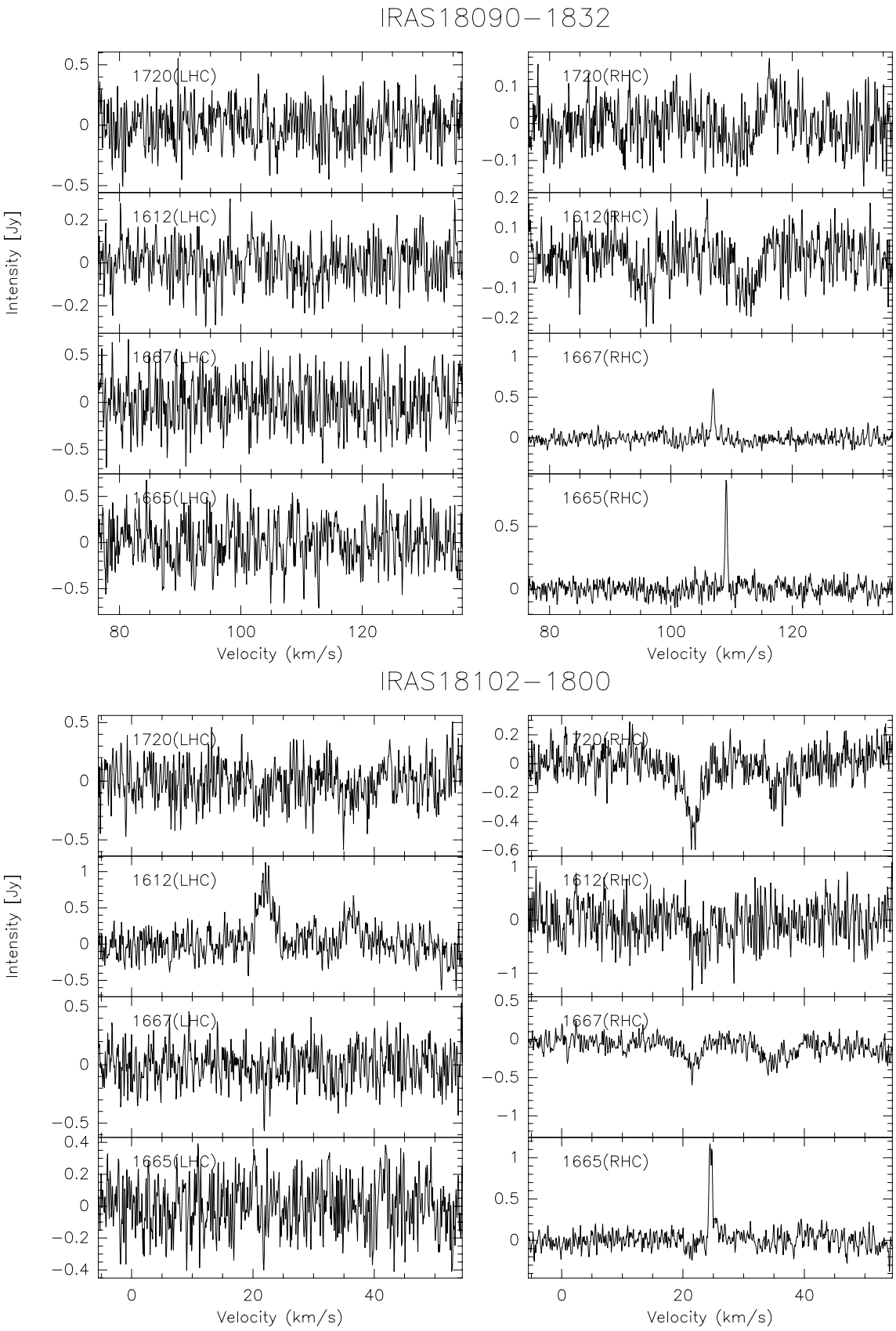

Fig. 19. continued.

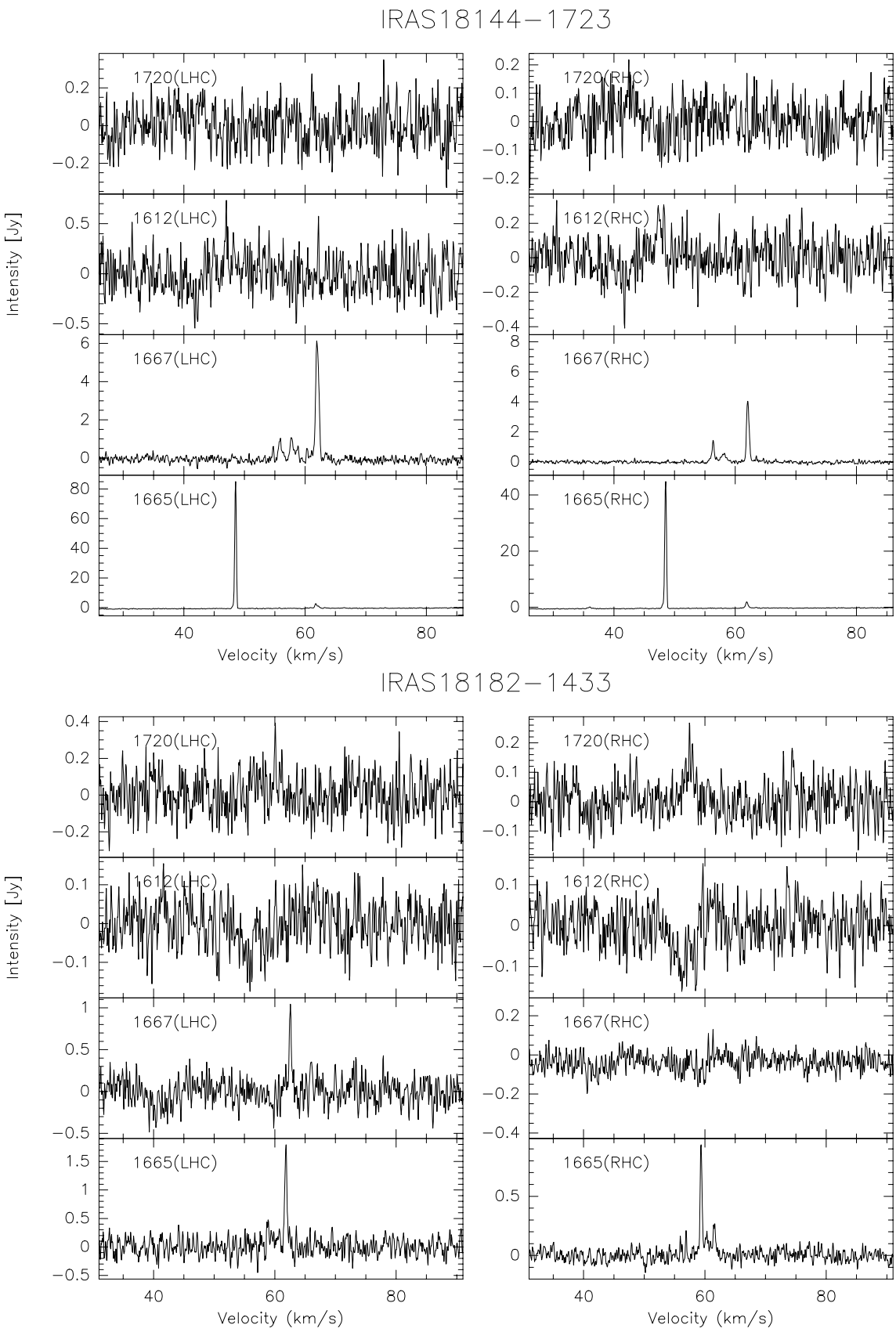

Fig. 19. continued.

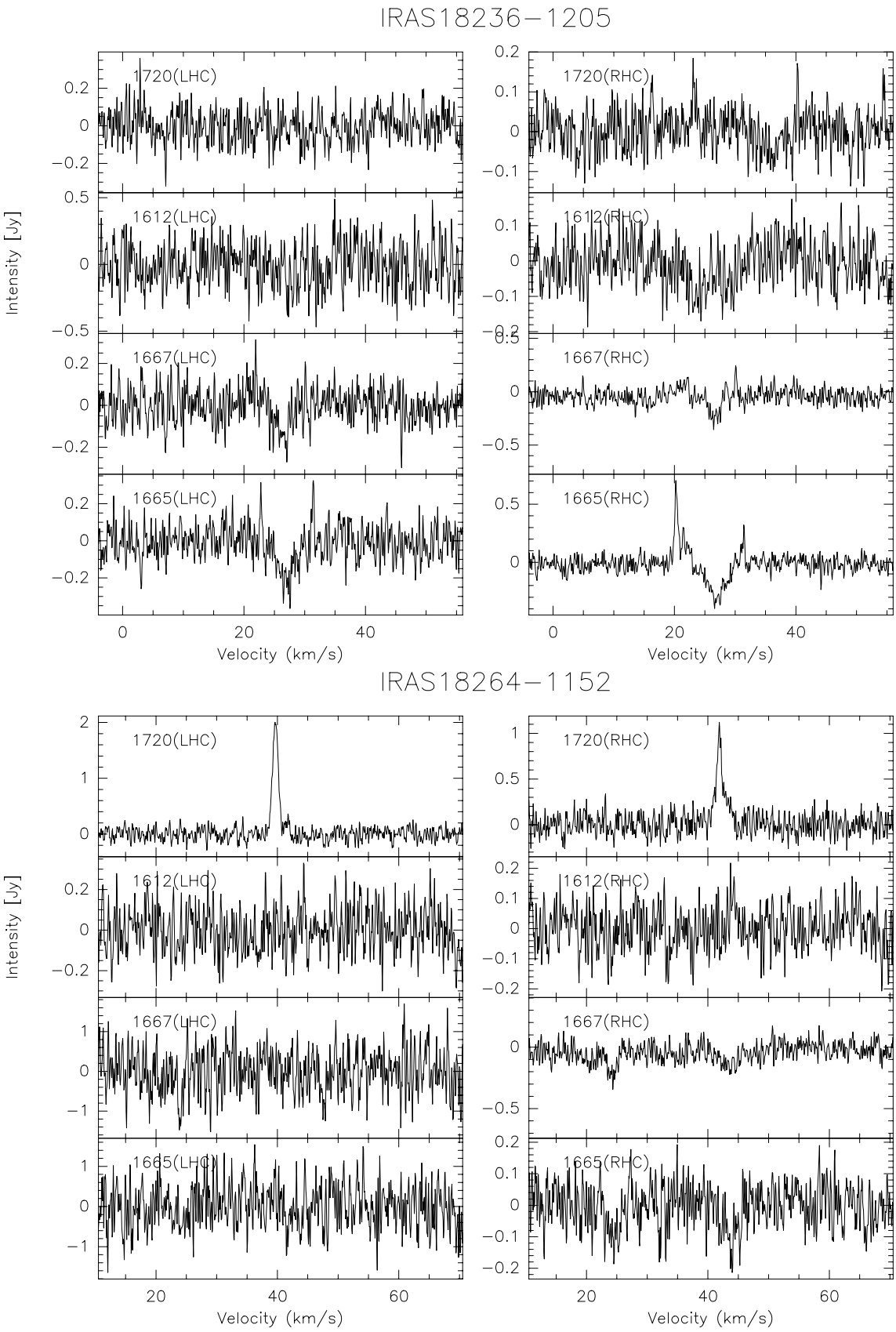

Fig. 19. continued.

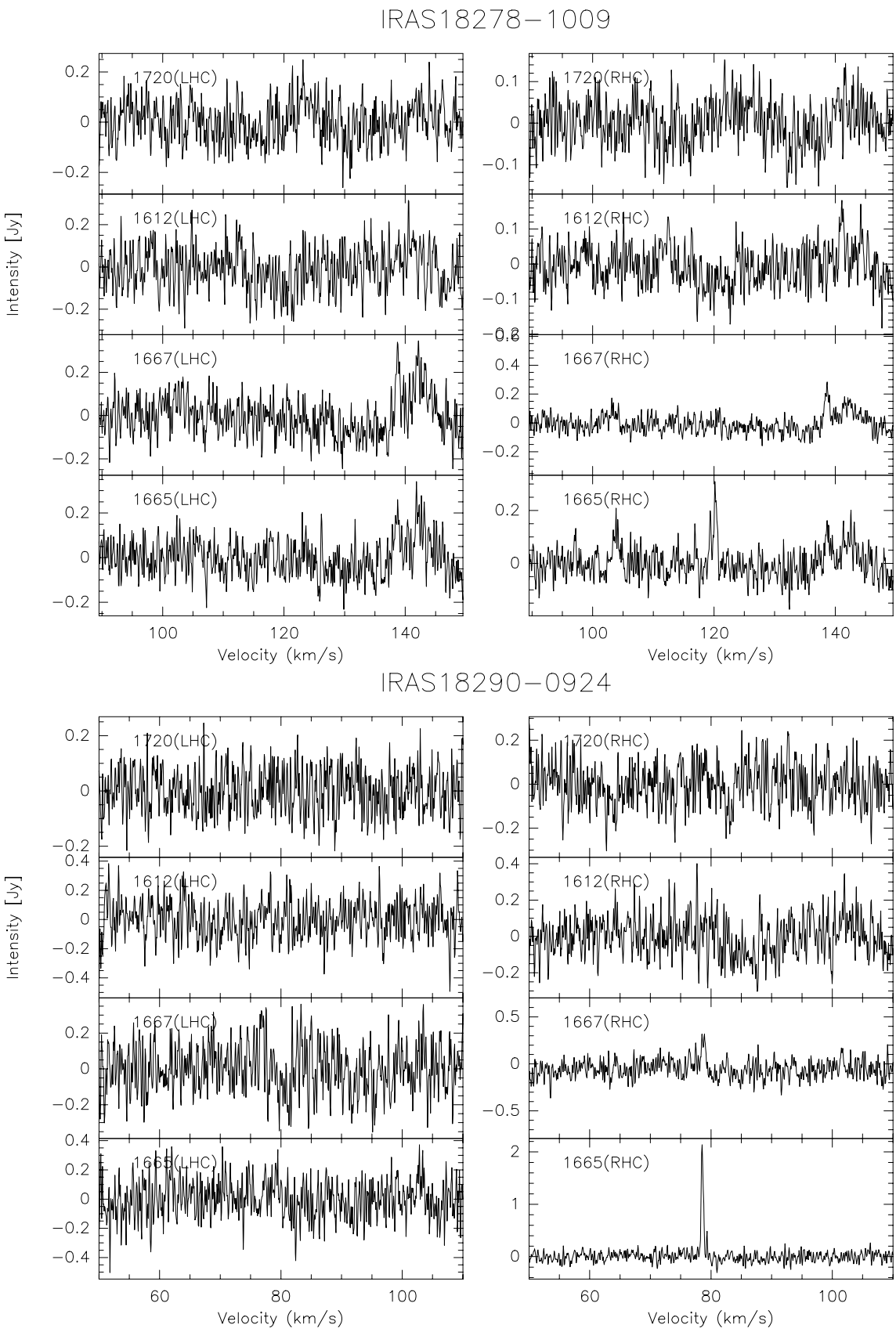

Fig. 19. continued.

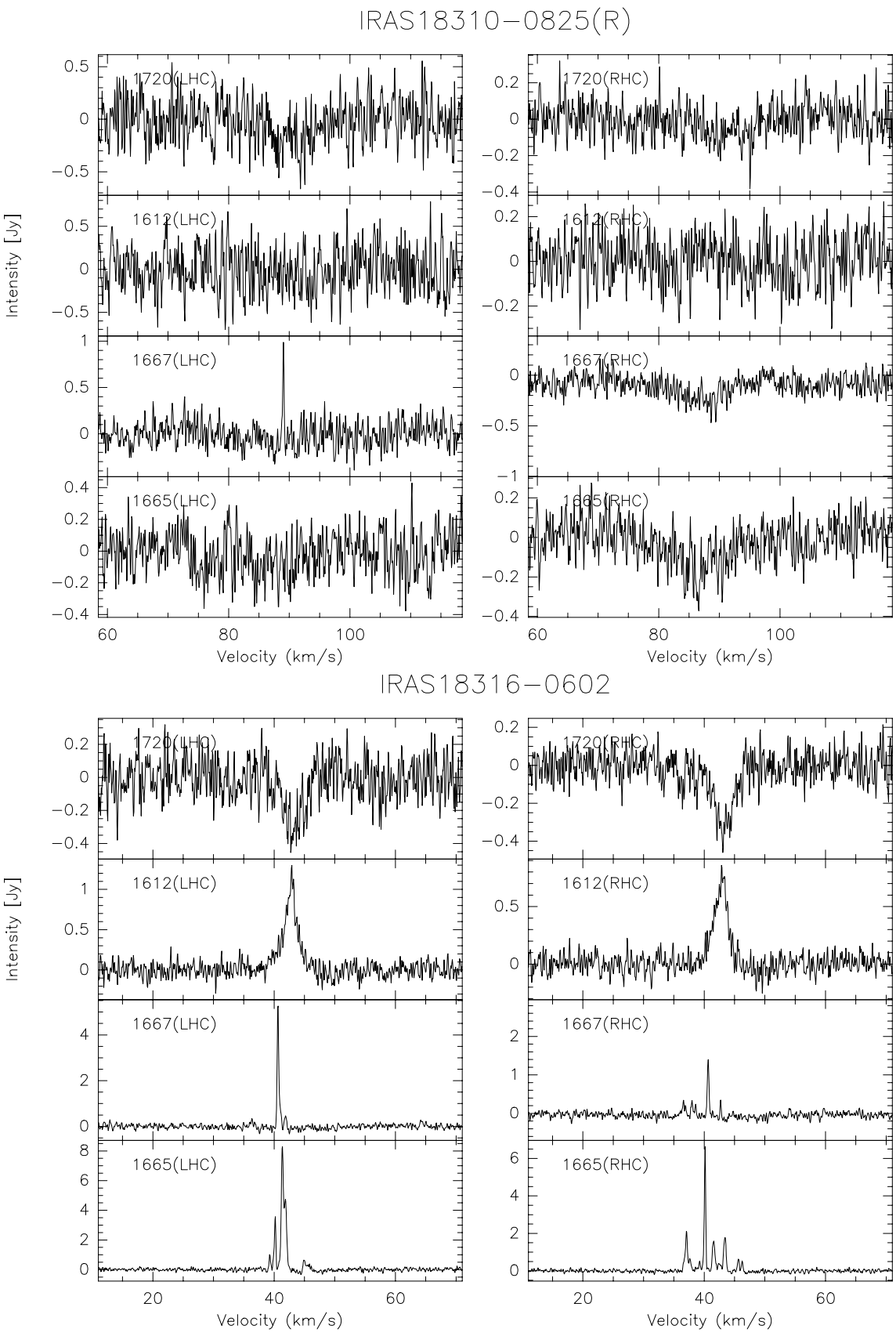

Fig. 19. continued.

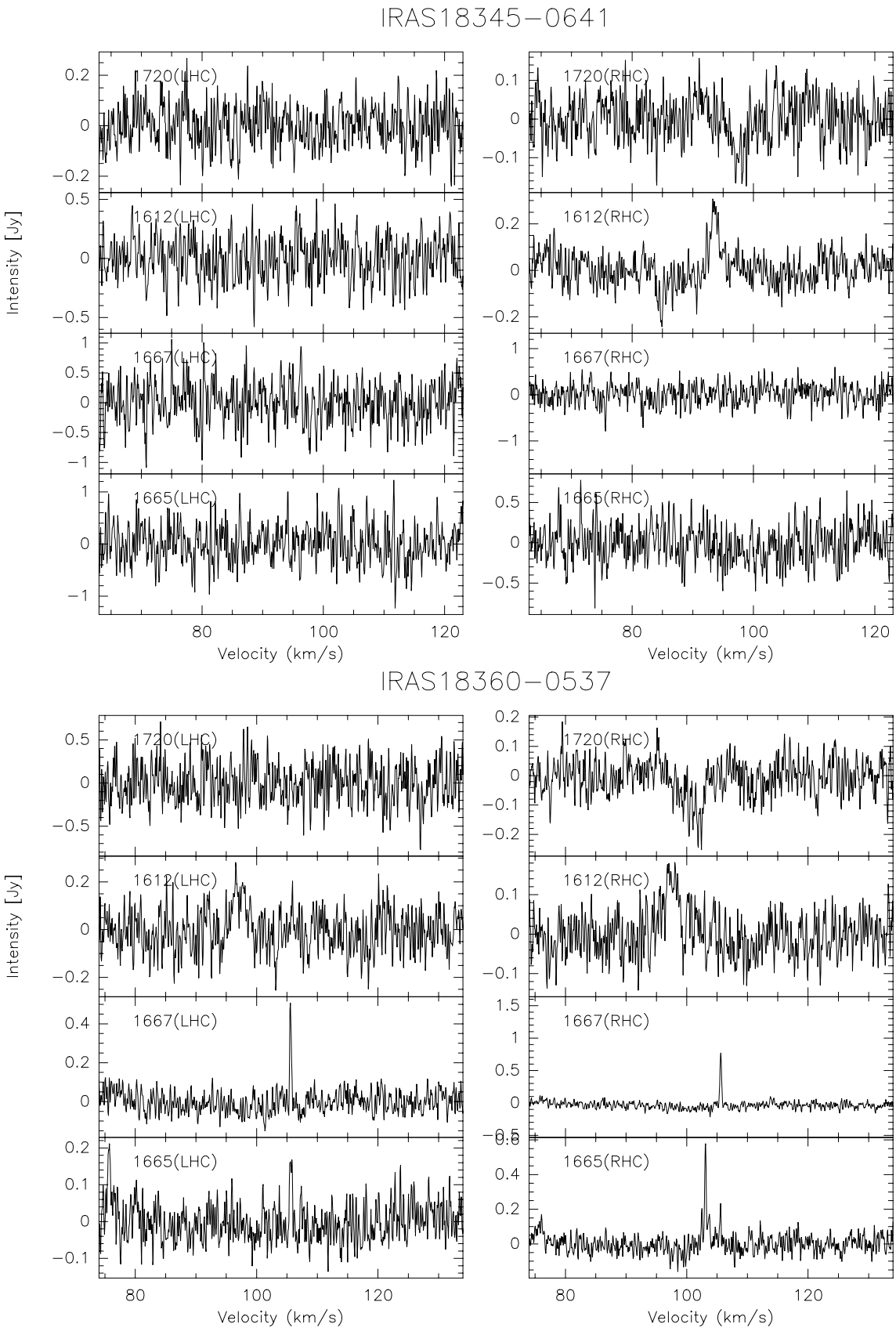

Fig. 19. continued.

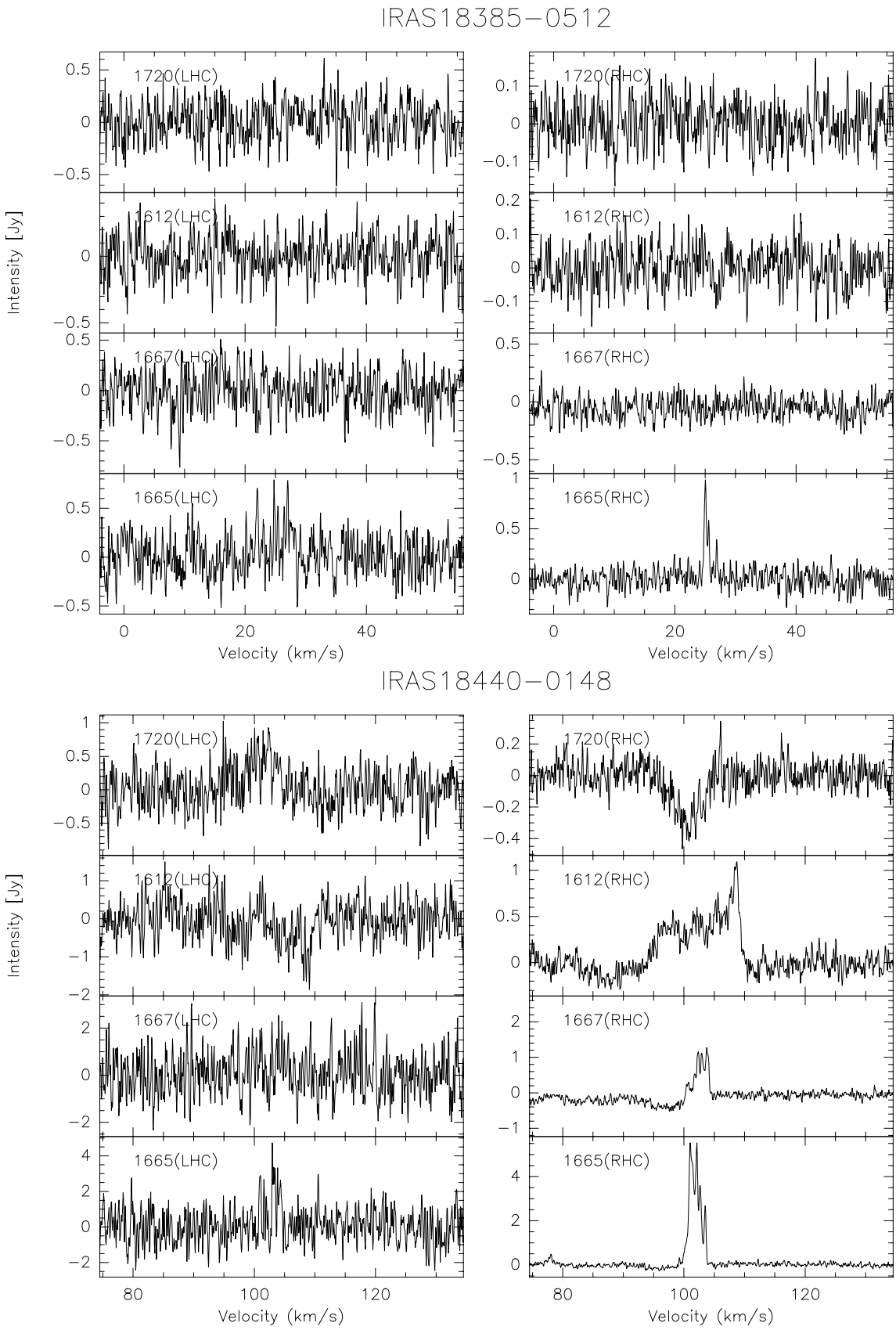

Fig. 19. continued.

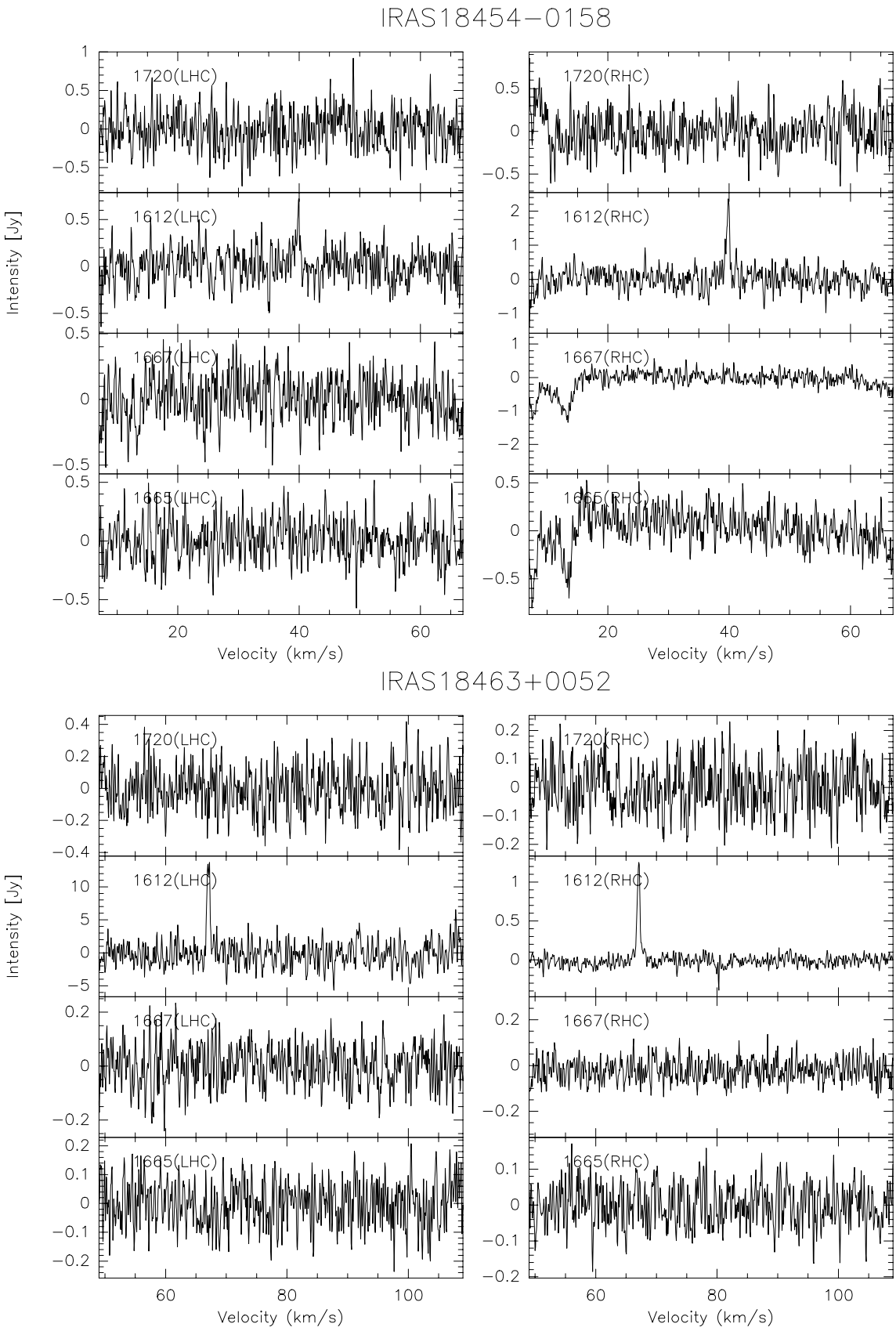

Fig. 19. continued.

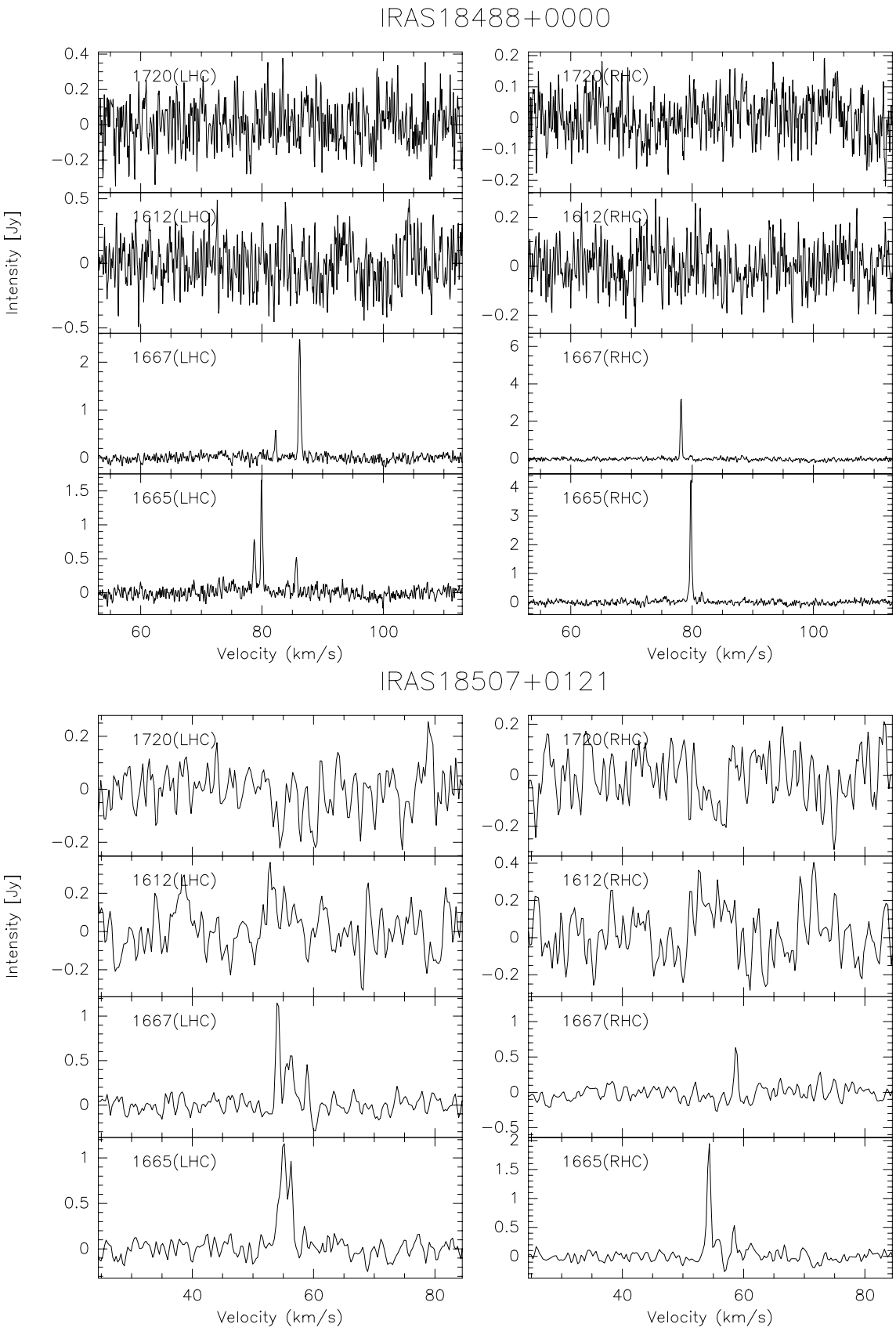

Fig. 19. continued.

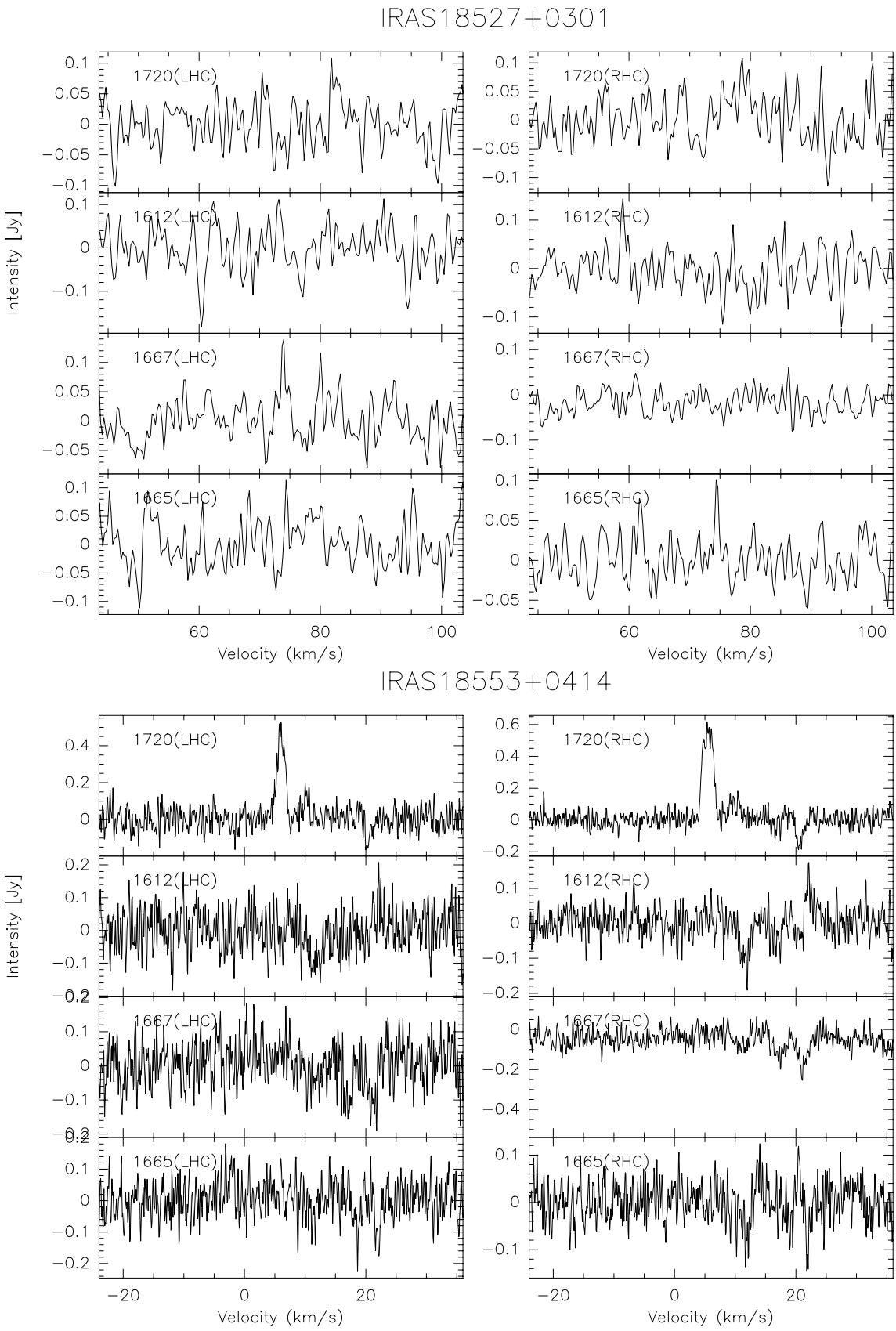

Fig. 19. continued.

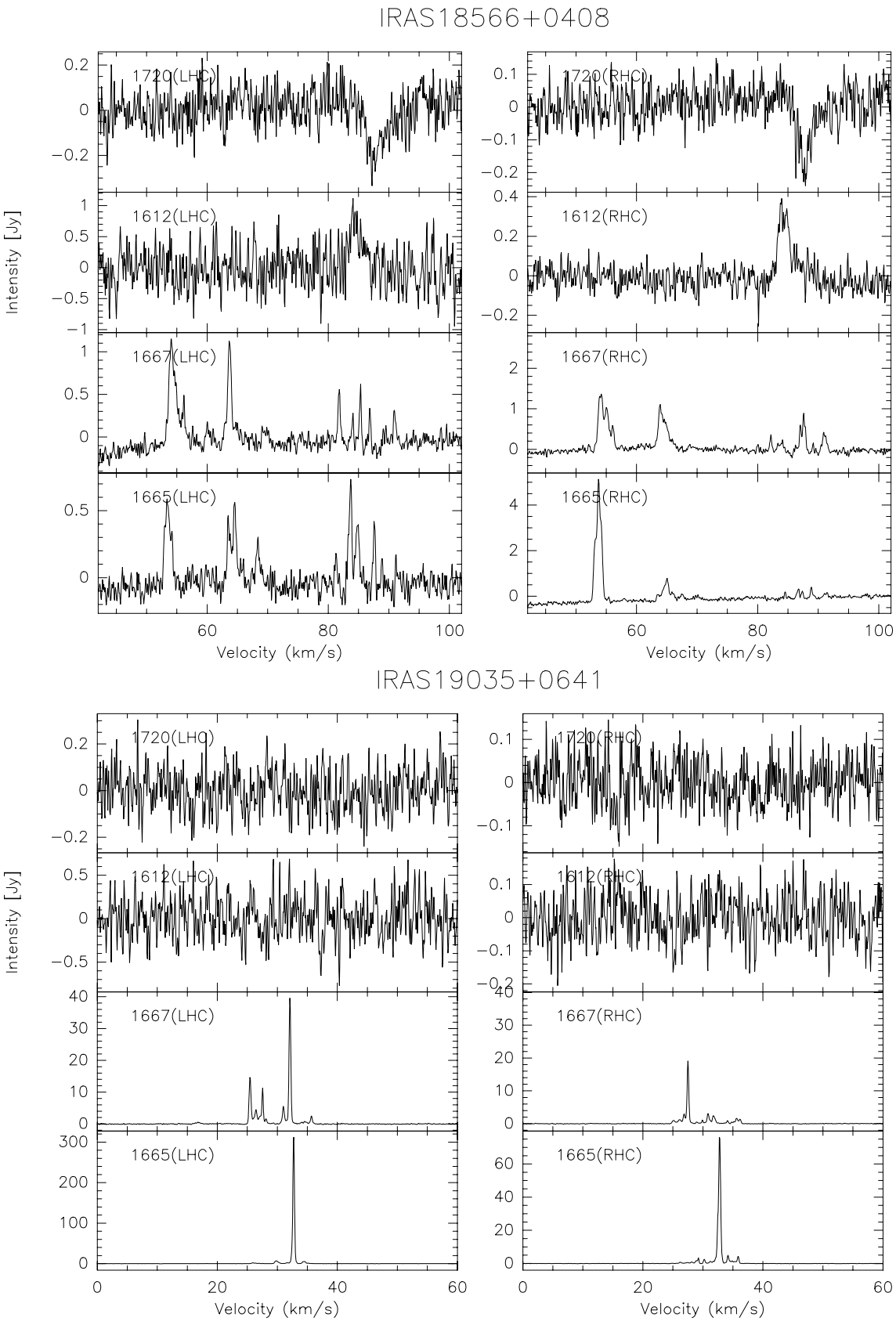

Fig. 19. continued.

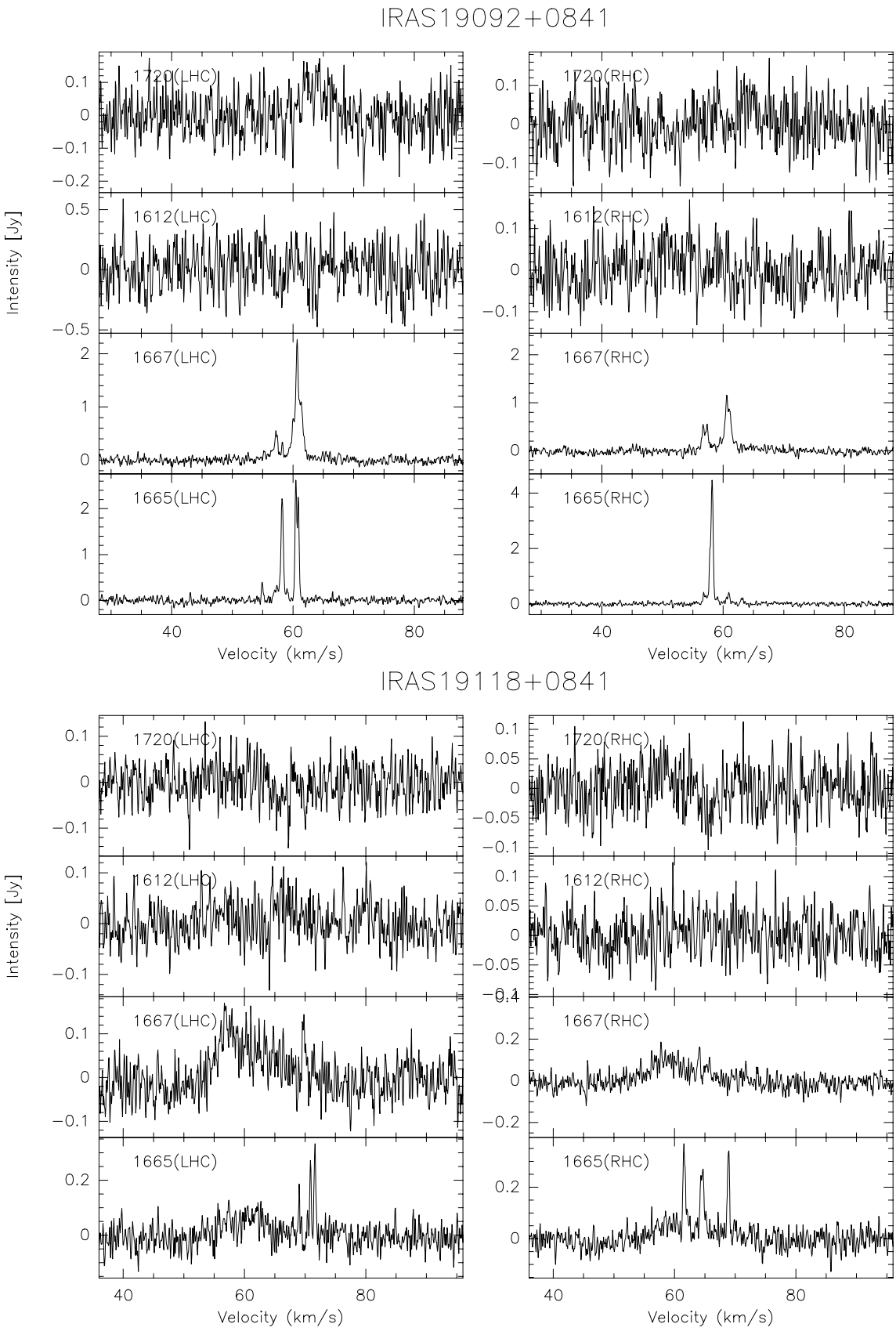

Fig. 19. continued.

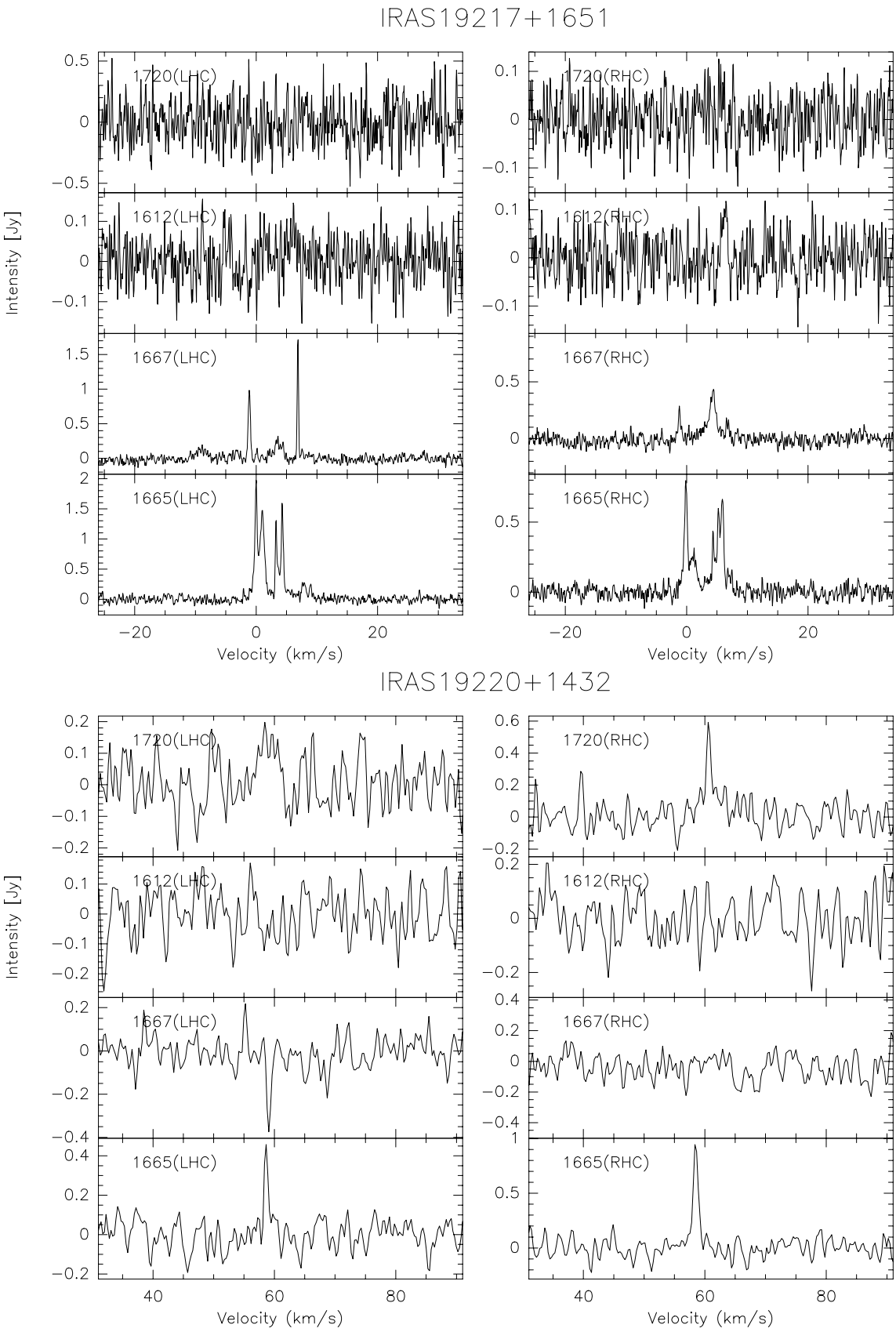

Fig. 19. continued.

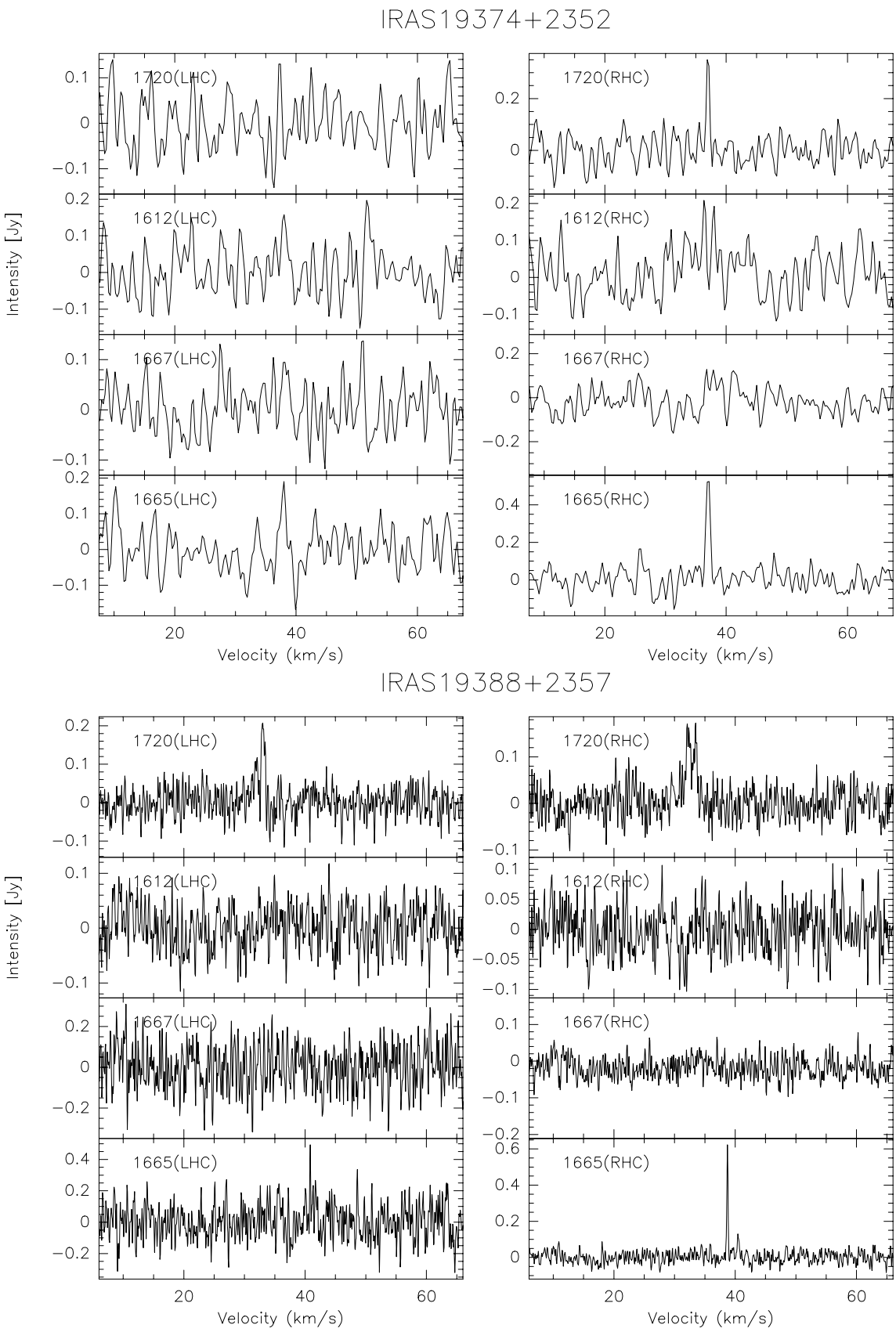

Fig. 19. continued.

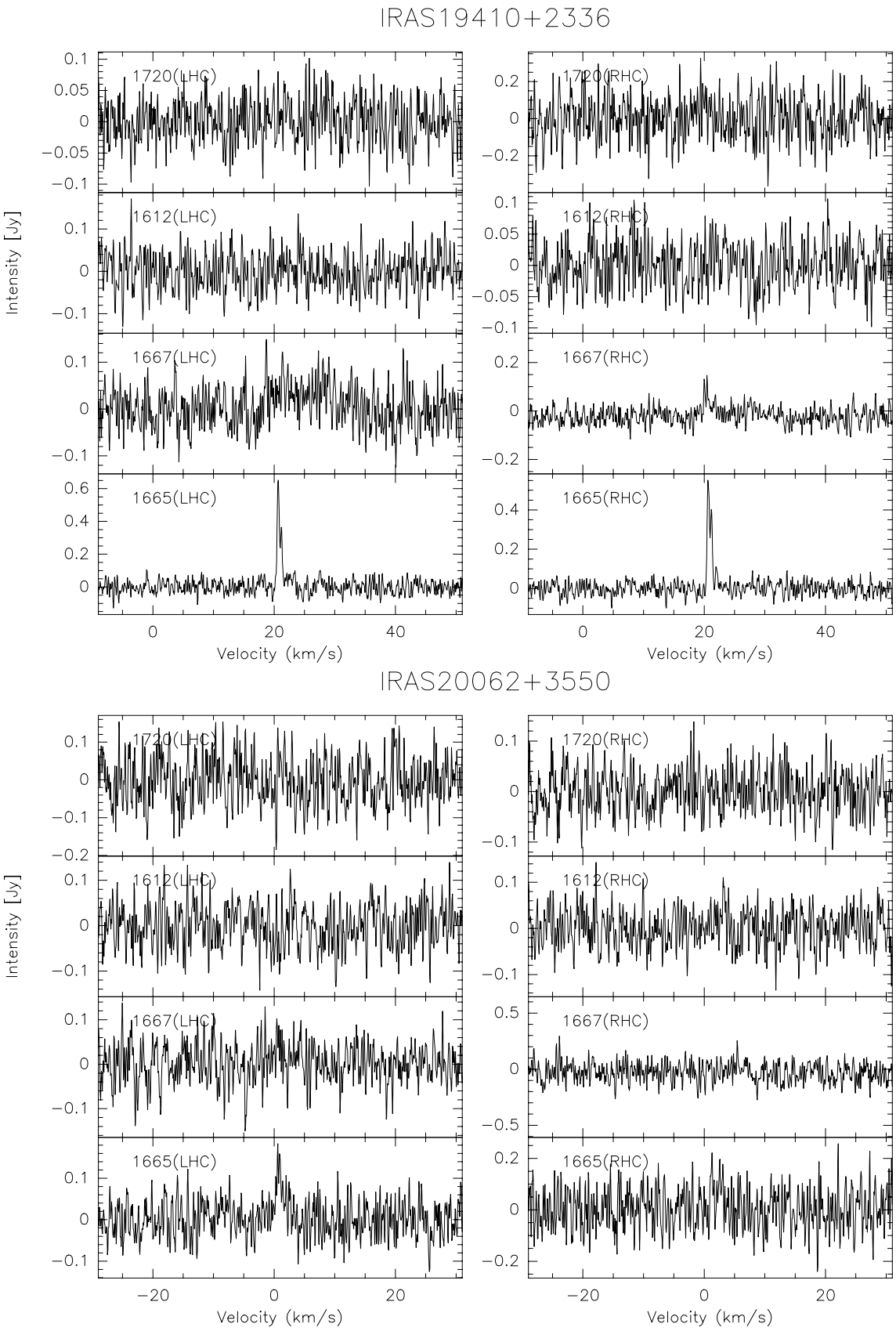

Fig. 19. continued.

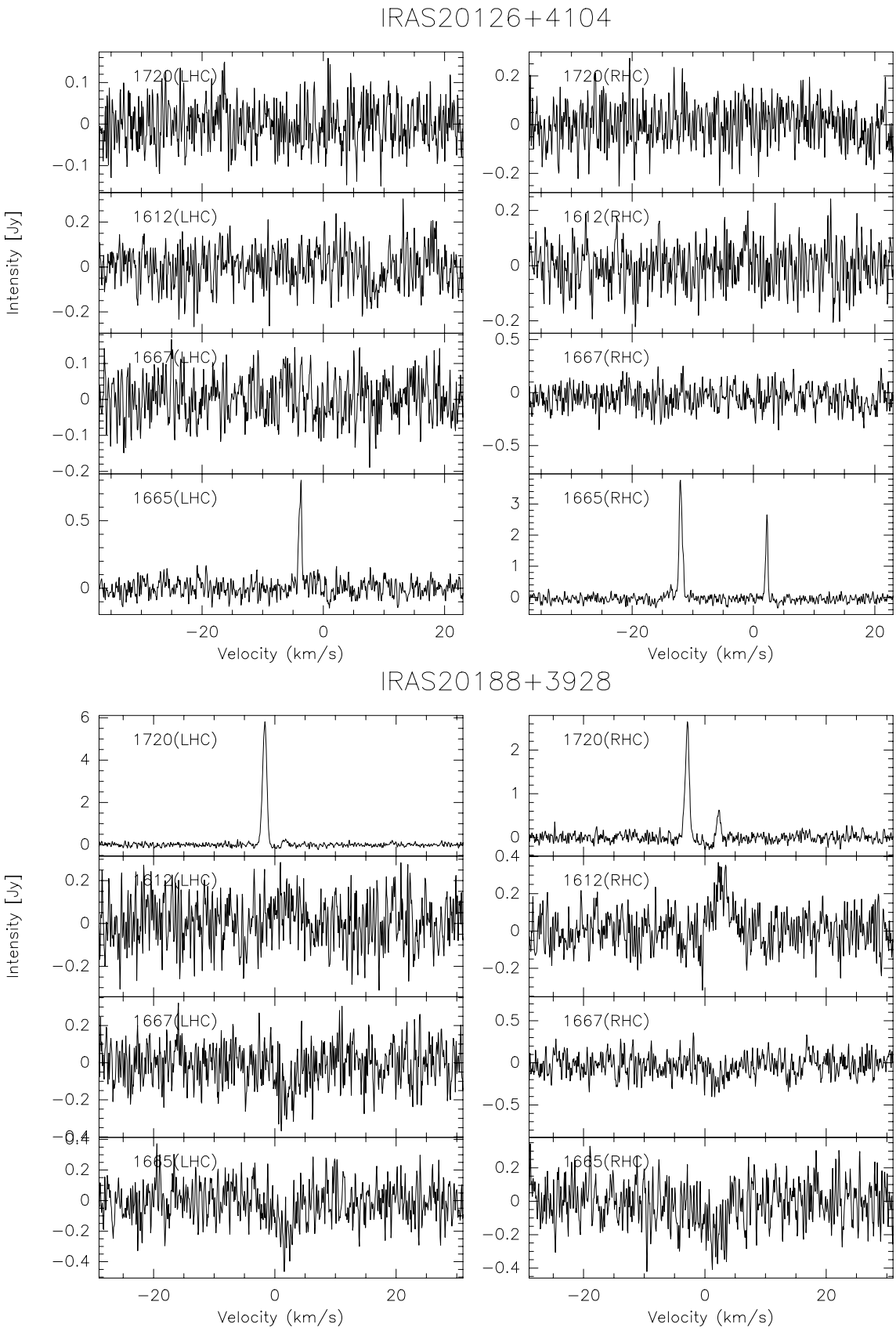

Fig. 19. continued.

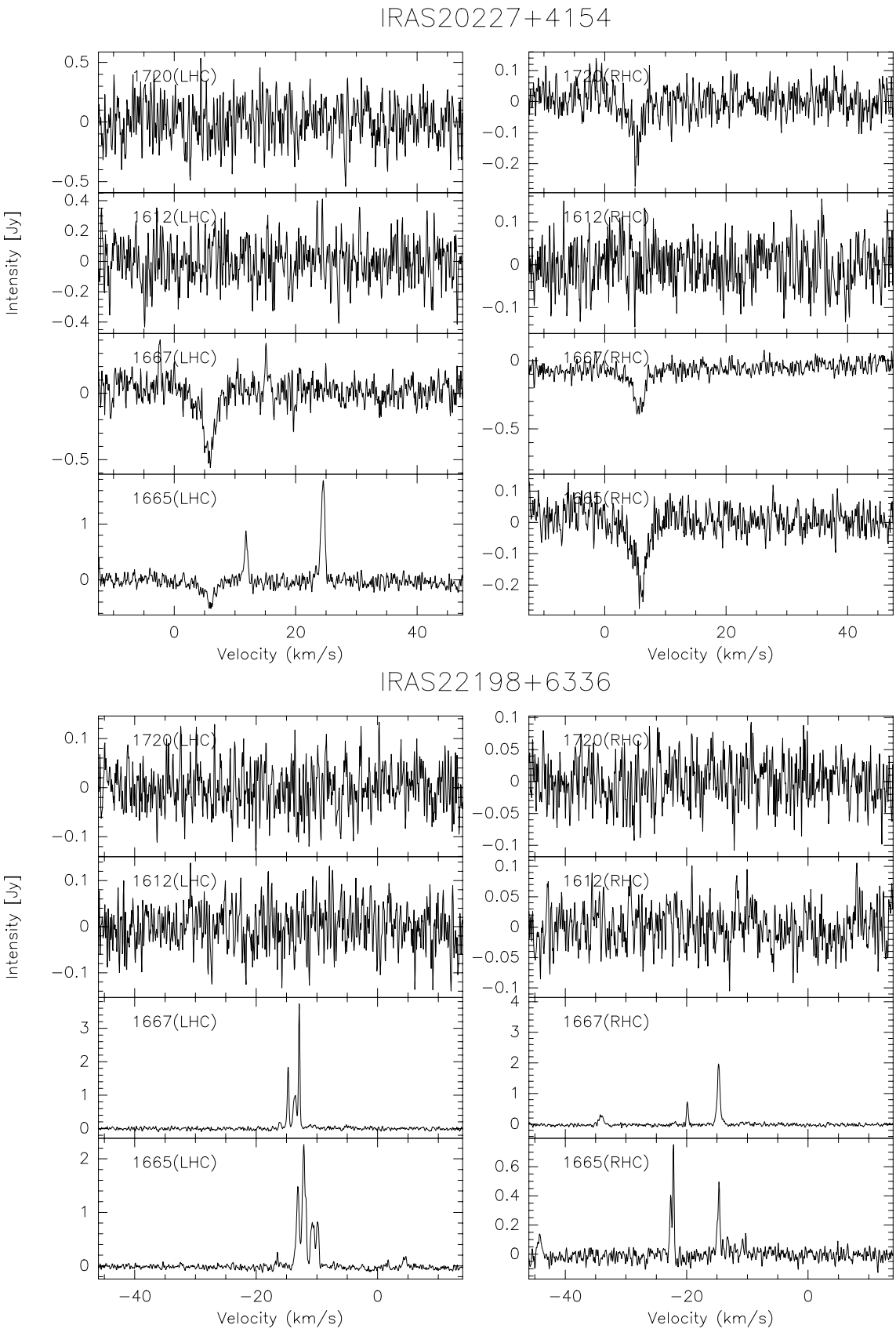

Fig. 19. continued.

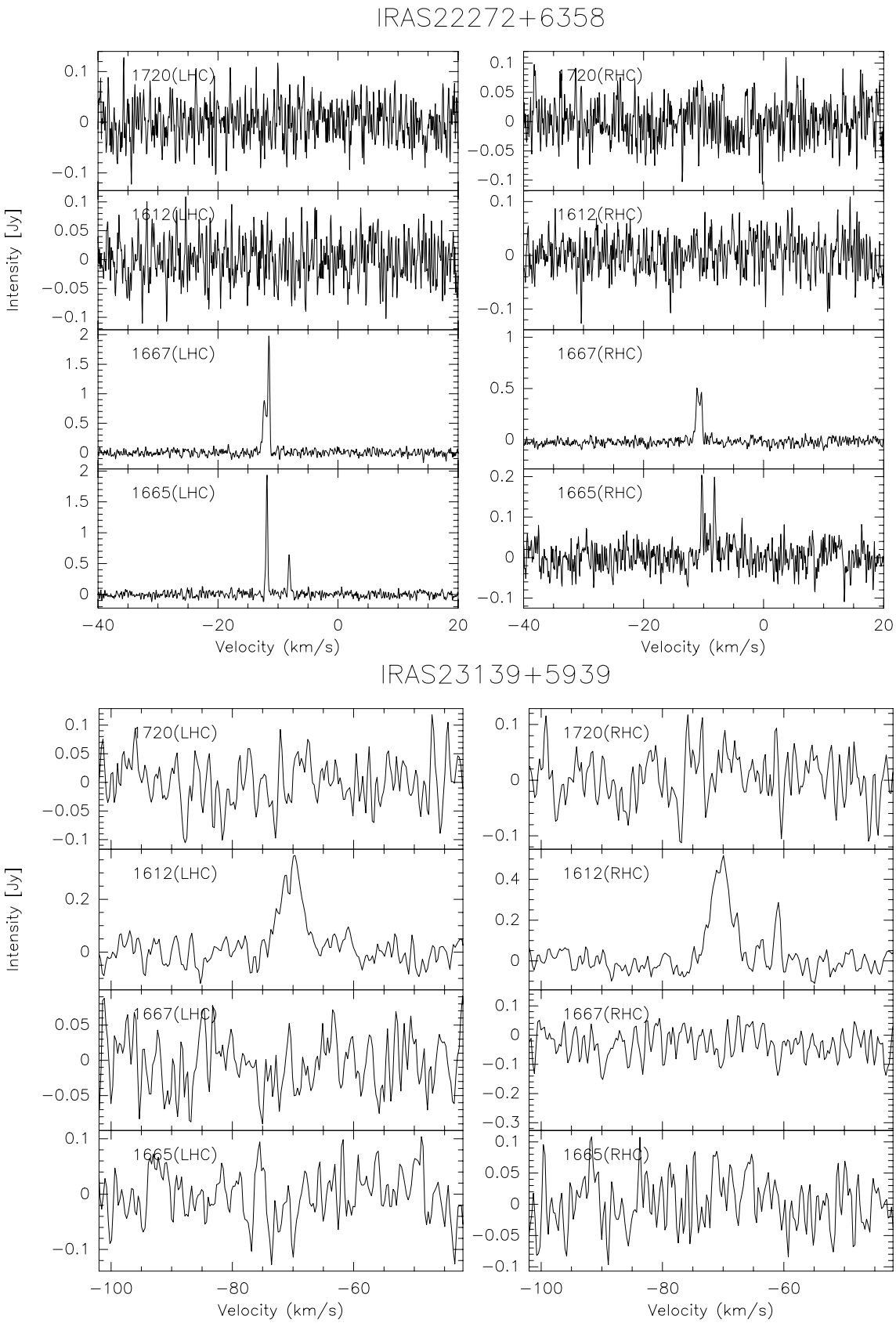

Fig. 19. continued.

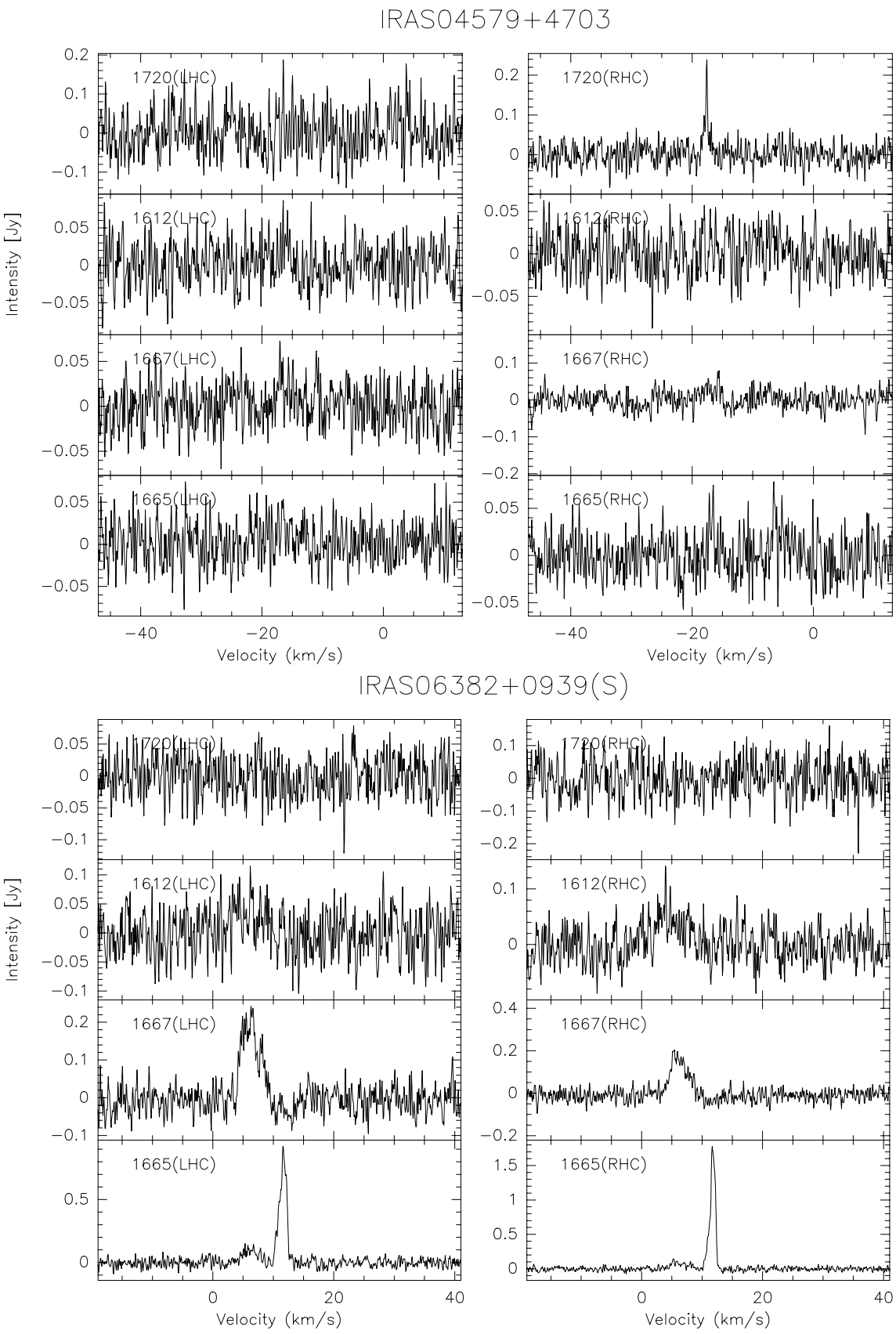

Fig. 20. Same as Fig. 19 but for sources with maser emission offset from the IRAS position by >2′.

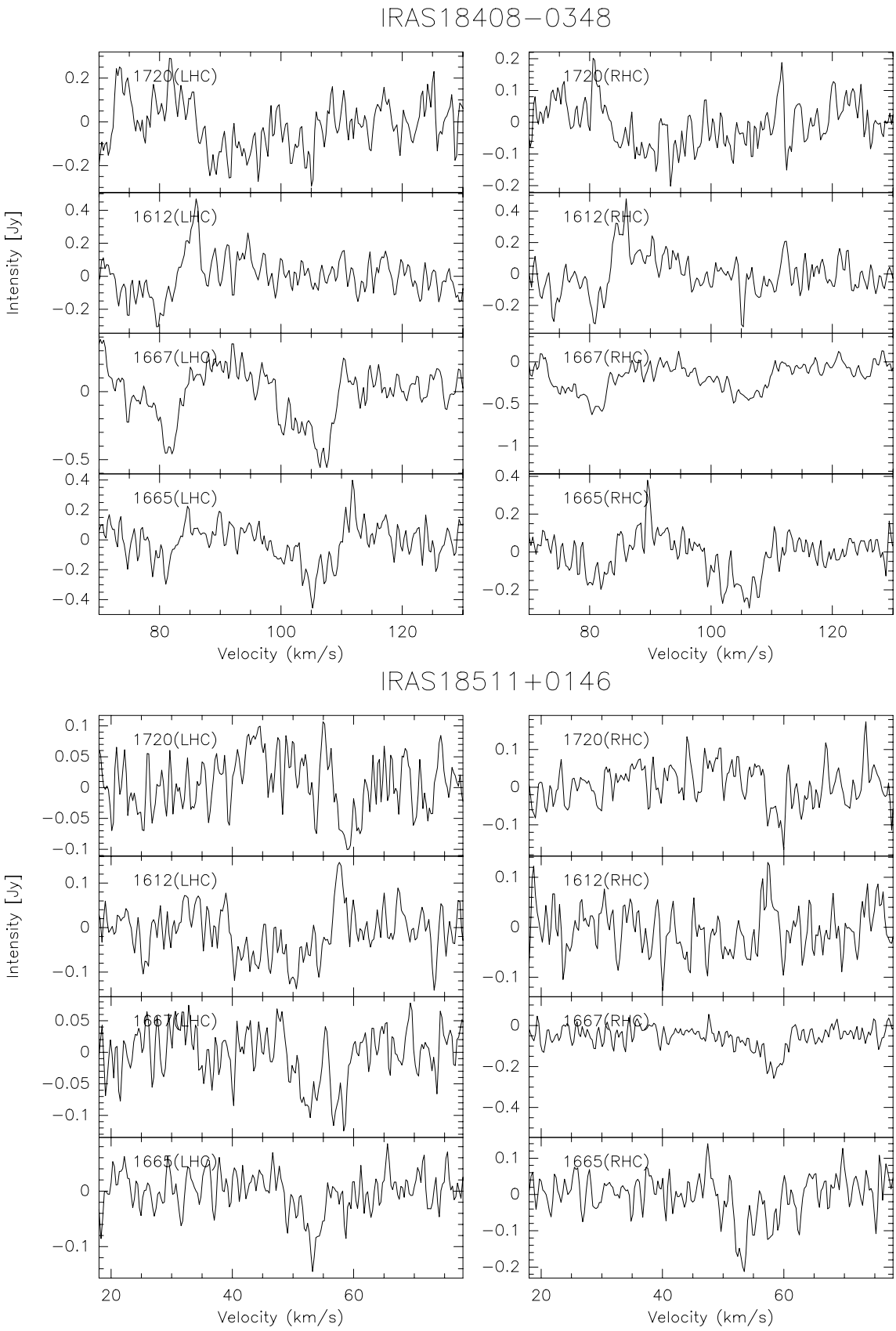

Fig. 20. continued.

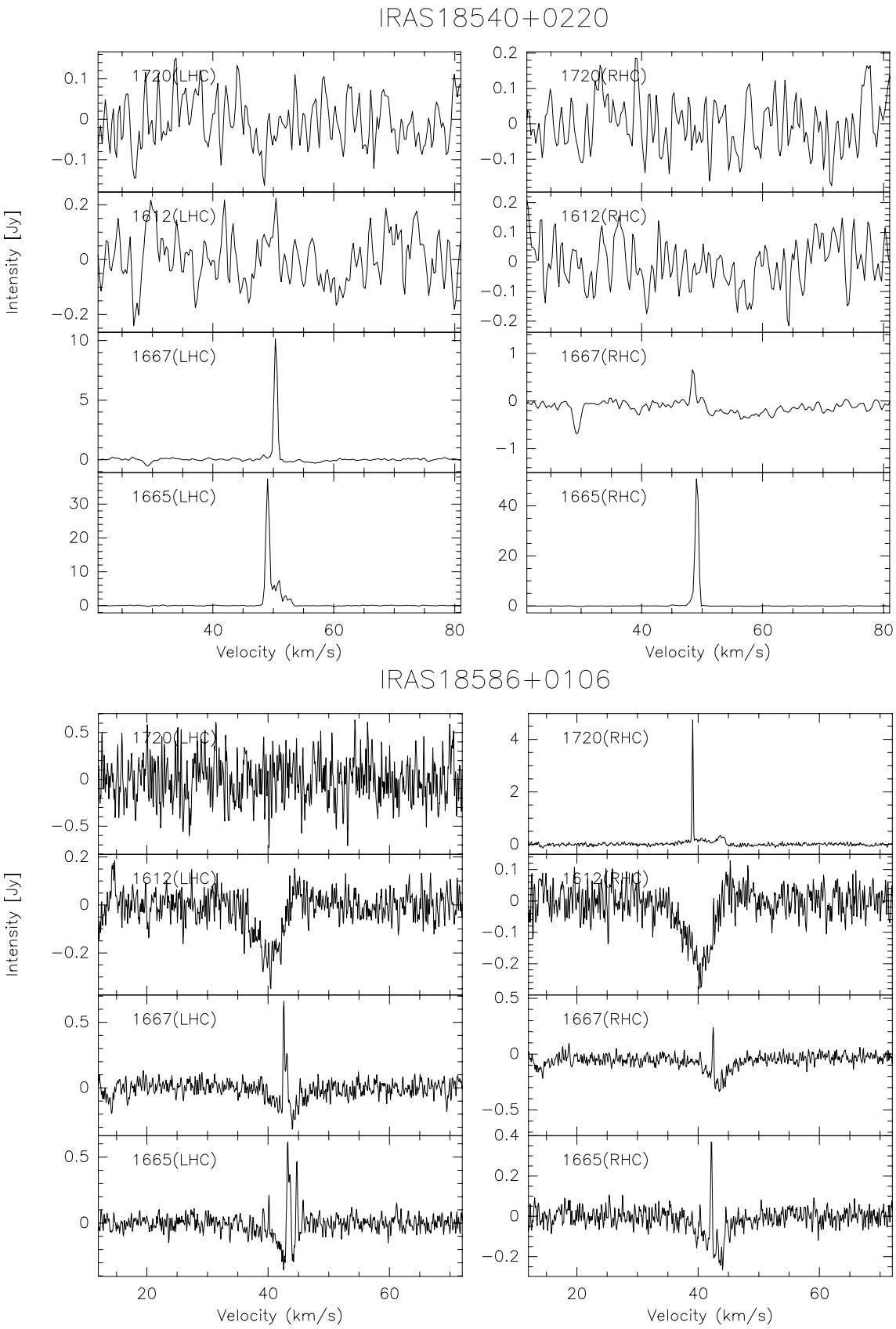

Fig. 20. continued.

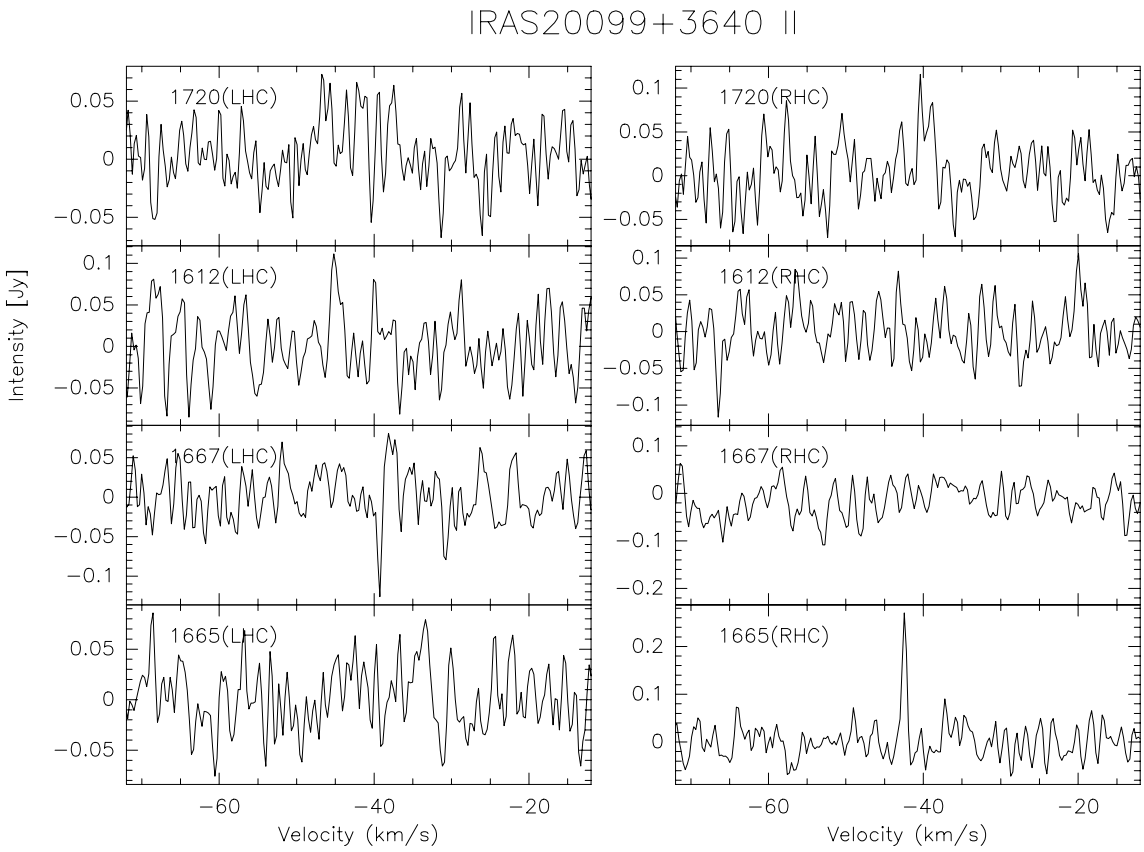

Fig. 20. continued.

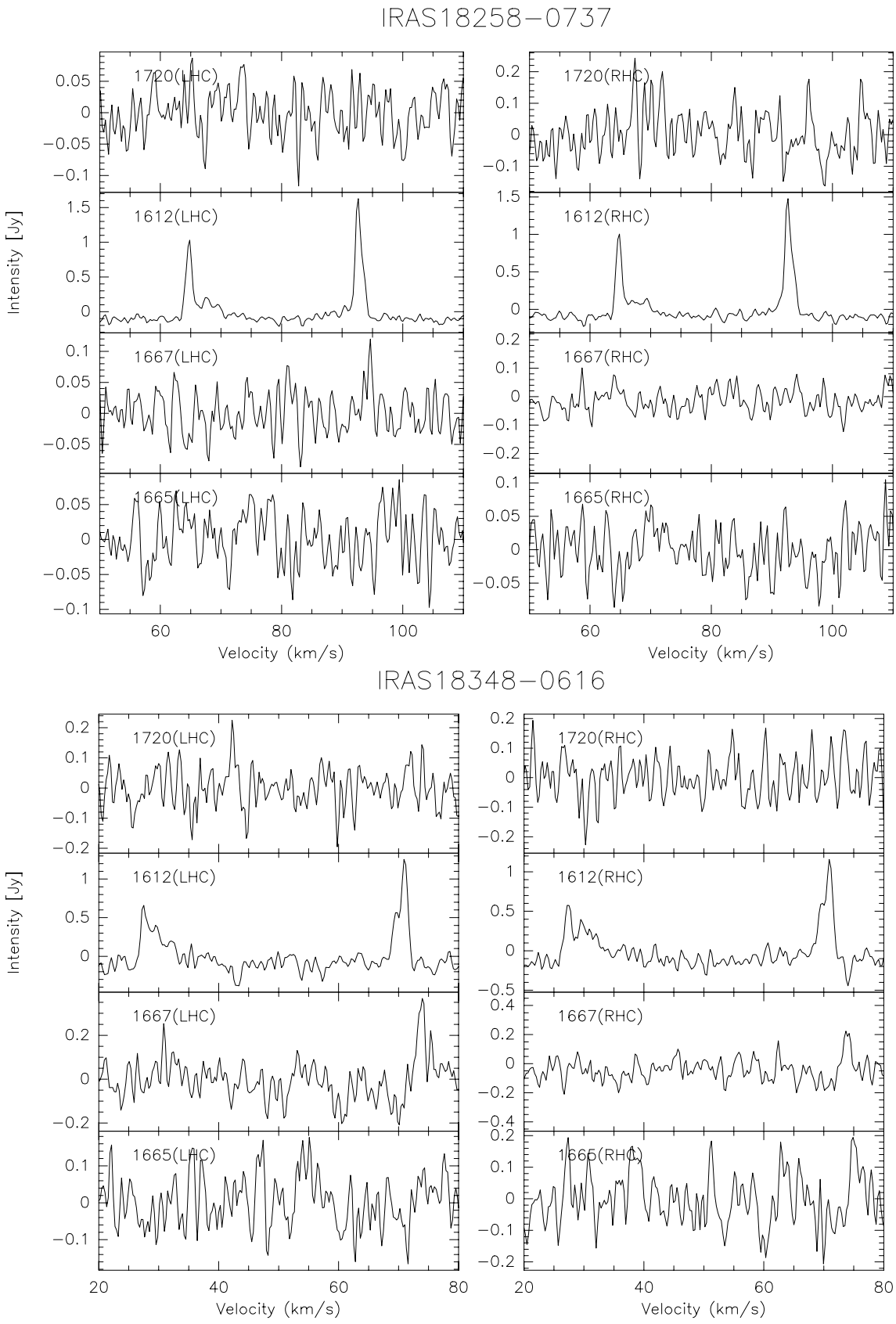

Fig. 20. continued.

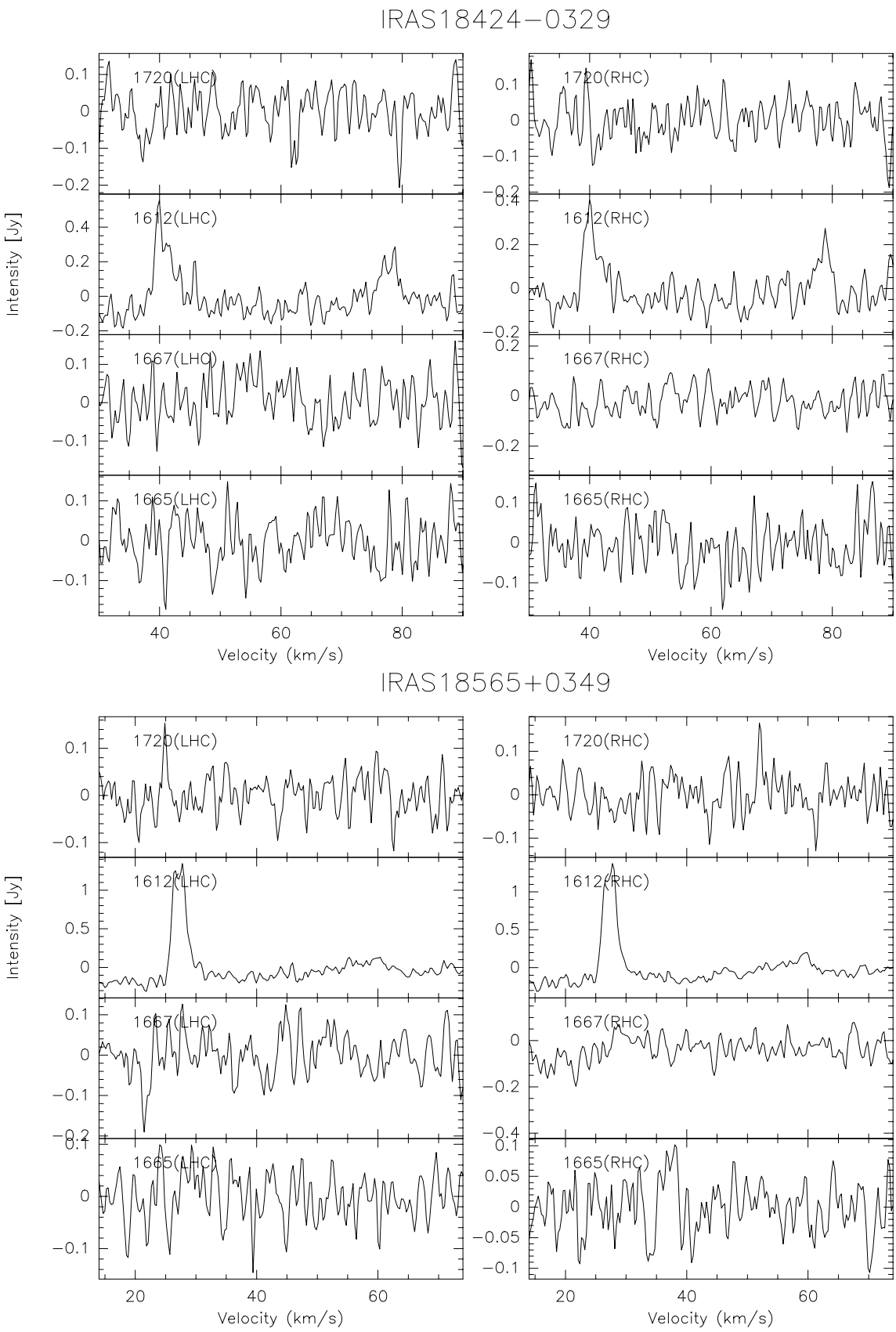

Fig. 20. continued.

Appendix A: Notes on individual sources where OH masers were detected

IRAS 05137+3919. This source also shows water maser emission (P91). This IRAS source is one of the sources studied in detail at high angular resolution by Molinari et al. (2002) at millimeter and centimeter wavelengths in both continuum and spectral lines. There is a core which shows radio continuum emission detected at 3.6 cm wavelength (VLA1) and mm continuum emission detected at 3.4 mm wavelength (Fig. 1 of Molinari et al. 2002). At 2.2 μm the IRAS source is resolved in to a cluster of objects (Molinari et al. 2002).

IRAS 05274+3345 (AFGL5142). This source is also associated with H_2O (Verdes-Montenegro et al. 1989; P91) and CH_3OH (SHK2000) masers. OH maser emission was previously reported towards this source by Braz et al. (1990). The OH lines detected towards this source, namely 1665, 1667 and 1612 MHz, have varied since the Braz et al. observations. While the 1665 MHz line has strengthened, the other two lines have weakened.

IRAS 05358+3543 (G173.481+2.445, S231, S233IR). This source has been mapped at high angular resolution, 1.5″, with the VLA (see Fig. 27 of Argon et al. 2000). The Nançay-GBT observations detected maser components in the two main lines, 1665 and 1667 MHz, in both the left and right circular polarisations, while only four components were reported by Argon et al. in the (LHC) 1665 MHz line. Two components of these four coincide very well with the IRAS source and the others are just ∼0.2″ south. Szymczak et al. (2000b) failed to detect maser emission at the 4765 MHz OH line towards this source. The IRAS source is also associated with H_2O (S02) and a strong CH_3OH masers (Galt 2004, and references therein). No radio continuum detection has been reported towards IRAS 05358+3543 in S02. On the other hand recent sub-millimeter continuum maps revealed a total of four sources (Williams et al. 2004; Minier et al. 2005). One of these sources is coincident with the IRAS source and OH maser and ∼40″ north-east another submm source harbours the CH_3OH maser, exhibits mid-infrared emission and coincides with one of the three 1.2-mm continuum sources detected by Beuther et al. (2002c) (see Fig. 4 of Minier et al. 2005). High angular resolution observations with Plateau de Bure Interferometer by Beuther et al. (2002d) reveal that this region contains at least three molecular outflows.

IRAS 05382+3547. The OH maser towards this source was discovered by Szymczak & Kus (2000), but no position for it was measured. GBT observations show that the 1665-MHz OH maser components detected by Szymczak & Kus centred at velocities −27 and −22 km s^{-1} are offset from the IRAS position by ∼3′. GBT observations found new components centred at velocities −20 and −24.7 km s^{-1} offset ∼30″ northwest of the IRAS source. This source is also associated with a CH_3OH maser (SHK2000) with velocity centred at 24.1 km s^{-1} close to one of the OH maser components.

IRAS 06056+2131. Cohen et al. (1988) detected OH maser emission at 1665 MHz only. The Nançay-GBT observations found emission at 1667 and 1720 MHz as well.

IRAS 17527−2439. This source is also coincident with a H_2O maser (P91).

IRAS 18018−2426 (G6.049−1.447, M8E). This OH maser was first detected by Cohen et al. (1988) and was mapped by Argon et al. (2000). These previous observations detected emission at 1665 MHz only, while Nançay-GBT detected maser emission in the 1667 MHz line as well. The OH maser emission is variable towards this source (Cohen et al. 1988). The water maser was detected towards this source by Lada et al. (1976) but P91 failed to detect any water maser emission. This source is known to be associated with a compact HII region (Simon et al. 1984). Molinari et al. (2002) detected 6.75 and 4.9 mJy continuum radio emission at 2 and 6 cm wavelengths respectively. The maser towards this source is not polarized which is unusual (e.g. Cohen 1989). The disappearance of H_2O masers and the association of OH maser with compact HII region suggest that this may be in a late stage of star formation where the UCHII region has expanded and only the OH maser emission is surviving. No CH_3OH maser towards this source has been reported.

IRAS 18024−2119. The newly detected OH main line maser emission towards this source has a relatively wide velocity range, covering ∼40 km s^{-1}. An H_2O maser was also detected by P91. A relatively strong CH_3OH maser of 100 Jy was recently detected by Galt (2004). No molecular outflow was detected towards this source by Zhang et al. (2005).

IRAS 18048−2019. This source shows very weak OH maser emission in both main lines. Water (P91) and CH_3OH (Schutte et al. 1993) masers are also associated with this source.

IRAS 18089−1732. This source is common in the S02 sample and the *High* sub-sample of M96. The OH maser emission was detected by Cohen et al. (1988) in the 1665 MHz line only. The Argon et al. (2000) VLA map shows several 1665-MHz OH maser components in three different positions. We detected maser emission at 1667 MHz as well. This source is also associated with H_2O (P91) and CH_3OH (SHK2000) masers and is associated with very weak 3.6 cm continuum emission, 0.9 mJy (S02). Recent high angular resolution submillimeter observations in various spectral lines by Beuther et al. (2005) detect a massive rotating structure perpendicular to an emanating outflow which is likely associated with the central accretion disk.

IRAS 18090−1832. This source also shows a relatively strong, 77 Jy, CH_3OH maser (SHK2000) and weak OH maser emission in the two main lines.

IRAS 18102−1800. This source is also associated with radio continuum emission, 44 mJy, at 3.6 cm wavelength (S02).

IRAS 18144−1723. This is a relatively strong OH maser source in the main lines. There is a significant gap, 13 km s^{-1} between the central velocities of strongest components in the 1665 and 1667 MHz lines. The IRAS source is also associated with CH_3OH (SHK2000) and H_2O (P91) masers. Radio continuum emission was also detected towards this source at 2 and 6 cm wavelengths (Molinari et al. 1998).

IRAS 18182−1433. The H_2O and CH_3OH masers associated with this source were mapped in high angular resolution, ∼1″ by Beuther et al. (2002a). Only one CH_3OH maser component was detected, while several H_2O maser components were detected. The H_2O and CH_3OH positions are coincident with the 1.2 mm continuum emission detected by Beuther et al. (2002c). Extremely weak radio continuum emission has been detected by Foster & Caswell (2000) (0.3 mJy at 3.5 cm) and S02 (<1 mJy at 3.6 cm). An outflow was detected towards this source by Beuther et al. (2002b).

IRAS 18236−1205. This IRAS source is also associated with CH_3OH (SHK2000) and H_2O (P91) masers.

IRAS 18264−1152. This source shows maser emission at the 6.7 GHz CH_3OH and 22 GHz H_2O maser lines (SHK2000 and P91 respectively). No radio continuum emission, <1 mJy, is detected at 3.6 cm wavelength (S02). An outflow was detected towards this source by Beuther et al. (2002b).

IRAS 18278−1009. This source is also associated with a CH_3OH maser (SHK2000). No radio continuum emission was detected at 2 and 6 cm wavelengths by Molinari et al. (1998).

IRAS 18290−0924. This source is also associated with H_2O and CH_3OH masers (S02). The mm observations (Beuther et al. 2002c) towards this source show two peaks separated by 12″ with the masers coincident with one of them. This source is also associated with radio continuum emission at 3.6 cm detected by S02.

IRAS 18310−0825. This source is the only source in our sample associated only with the 1667-MHz of OH maser lines. It is also associated with a CH_3OH maser detected by SHK2000 and mapped by Beuther et al. (2002a). The methanol maser is offset from the IRAS source and coincident with one of two mm and cm peaks (see Fig. 1 of Beuther et al. 2002a).

IRAS 18316−0602. This source is also associated with very strong H_2O (725.83 Jy, P91), and CH_3OH (178 Jy, SHK2000) masers. This source is known to be associated with an UCHII region (Jenness et al. 1995) and molecular outflow (Wu et al. 2004). The OH maser emission is detected in the main lines while the satellite lines show conjugate behaviour with thermal emission at 1612 MHz and absorption at 1720 MHz.

IRAS 18345−0641. Towards this star-forming region only the 1612 MHz OH maser line was detected. The IRAS source is associated with strongly, variable CH_3OH masers (SHK2000) which coincide with a mm continuum peak (Beuther et al. 2002a). Also free-free emission at 3.6 cm (S02) and an outflow have been detected towards this IRAS source (Beuther et al. 2002b).

IRAS 18360−0537. In addition to the OH main line masers detected here, this source is also associated with relative strong H_2O maser emission, 92.73 Jy (P91).

IRAS 18385−0512. This source is also associated with a relatively strong H_2O maser emission, 200 Jy (S02). Several H_2O maser components coincide with a mm continuum peak (Beuther et al. 2002a). Radio continuum emission of 29 mJy was measured by S02 at 3.6 cm.

IRAS 18440−0148. This source is also associated with a CH_3OH maser (SHK2000; Walsh et al. 1998). The CH_3OH maser components coincident with a 1.2 mm, 3.6 cm peak and mid-infrared source (Beuther et al. 2002a; S02). A tentative detection of H_2O maser emission is reported by S02.

IRAS 18454−0158. This is one of the sources which has an OH maser but does not have any other known masers. S02 observations did not detect H_2O or CH_3OH maser emission. This source is associated with 1.2 mm continuum emission as well as radio continuum emission (Beuther et al. 2002c and S02 respectively).

IRAS 18463+0052. Only 1612 MHz line OH masers are detected towards this source with a line profile with peaks at 67 and 92 $km\,s^{-1}$, suggesting this source is an OH/IR star rather than a star-forming region. There are no H_2O or CH_3OH masers associated with the IRAS source.

IRAS 18488+0000. This is one of the common sources in the S02 sample and the *High* sub-sample of M96. This source is associated with a variable CH_3OH maser (SHK2000, and references therein). Although not detected by P91, H_2O maser emission has been detected by S02. The water maser is coincident within few arcsecond with a mid-infrared source but offset from a millimetre continuum source (Beuther et al. 2002a). Relatively strong radio continuum emission, 194 mJy, has been detected towards this source (S02). Our Nançay-GBT observations detect OH maser emission in the two main lines which is coincident (within ∼30″) with the 1.2 mm emission source rather than other tracers.

IRAS 18507+0121. This source is roughly 11′ north from G34.257+0.154 (or G34.3+0.2) which shows strong OH maser emission in the main lines as well as 1720 MHz satellite line (Argon et al. 2000). G34.257+0.154 also has H_2O masers and is classified as an HII region (Benson & Johnston 1984; Genzel & Downes 1977). The Nançay-GBT observations detect new (relatively weaker) OH maser emission associated with the IRAS source in the main lines. The IRAS source is also associated with H_2O (P91) and CH_3OH (SHK2000) masers. IRAS 18507+0121 region was studied in detail by Shepherd et al. (2004) at several millimeter and near-infrared (NIR) wavelengths. Shepherd et al. detected two compact molecular cores separated by ∼40″ north-south. The northern molecular core contains a newly discovered, deeply embedded, B2 protostar surrounded by several hundred solar masses of warm gas and dust, G34.4+0.23 MM. Based on the presence of warm dust emission and the lack of detection at NIR wavelengths, Shepherd et al. suggest that G34.4+0.23 MM may represent the relatively rare discovery of a massive protostar (analogous to a low-mass "Class 0" protostar). The southern molecular core is associated with an NIR cluster of young stars and an UCHII region, G34.4+0.23 (detected by Miralles et al. 1994), with a central B0.5 star. Shepherd et al. to suggest an upper limit on the age of the IRAS 18507+0121 star-forming region of 3 Myr. This IRAS source is not associated with molecular outflow (Zhang et al. 2005).

IRAS 18527+0301. This source was searched for OH masers by Szymczak & Kus (2000) to a rms noise level of 0.2 Jy but none were detected. The present observations, with better sensitivity (0.02 Jy), detected weak emission in the two main lines. Methanol maser emission was detected by SHK2000 in the same OH velocity range. No radio continuum emission at 6 cm was detected by Molinari et al. (1998).

IRAS 18553+0414. This source is also associated with H_2O maser emission (S02) which is coincidence with a millimeter continuum source (Beuther et al. 2002c).

IRAS 18566+0408. This common source in the S02 sample and the *High* sub-sample of M96 is also associated with CH_3OH maser emission (S02; SHK2000). The H_2O maser emission was newly detected by S02, while not detected by P91. The H_2O masers are in better agreement with a millimeter continuum (Beuther et al. 2002a). The newly detected OH maser emission also seemingly coincides with the mm source mapped by Beuther et al. (2002c). An outflow was detected by Beuther et al. (2002b) and S02 place an upper limit of 1 mJy on the 3.6 cm radio continuum flux from any source in this region.

IRAS 19035+0641 (G40.622−0.137). This source is one of the OH maser sources mapped with the VLA by Argon et al. (2000). Several components, at different velocities in the range of 25 to 36 $km\,s^{-1}$, were detected in the two main lines and spread over ∼1 arcsec (Fig. 14 of Argon et al. 2000). Our Nançay-GBT observations show similar emission although the flux density of the components has varied since the Argon et al. observations. The flux density of the 1667 MHz RHC compoment centered at velocity 27.39 $km\,s^{-1}$ has rocketed up from 0.44 to 22.3 Jy. The IRAS source is also associated with H_2O and CH_3OH masers (S02, SHK2000 and references therein). The H_2O and CH_3OH masers are coincident with a mid-infrared and 1.2 mm continuum emission sources (see Fig. 1 of Beuther et al. 2002a). The UCHII region, detected at 6-cm by Hughes & Macleod (1993) and 3.6-cm by S02, shows

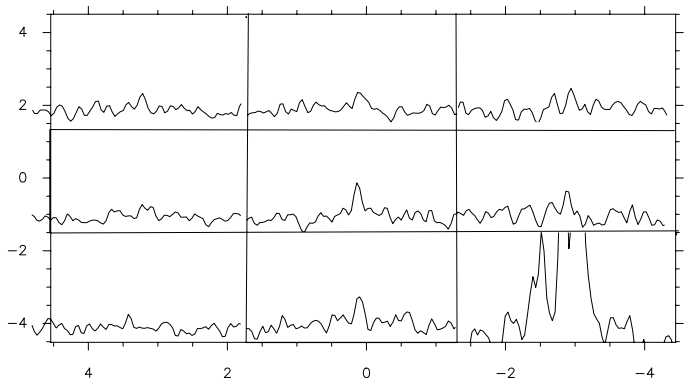

Fig. A.1. The spectra from the IRAS 19220+1432 map in the 1720 MHz OH maser. The OH maser associated with the IRAS position (middle panel) is contaminated by the strong OH maser source W51 which appears in the lower right hand side panel of the map. The axes show offsets in arcminutes from the IRAS position.

weak emission, of 3.8 and 4 mJy respectively. An outflow was detected towards this source by Beuther et al. (2002b).

IRAS 19092+0841. This source, also associated with H_2O (P91) and CH_3OH (SHK2000) masers, is one of the newly detected of OH masers. Radio continuum emission of 2.74 and 1.04 mJy have been detected by Molinari et al. (1998) at the 2- and 6-cm wavelengths respectively.

IRAS 19118+0945. This is one of the sources with only OH masers. No H_2O or CH_3OH masers have been detected towards this source (P91; SHK2000).

IRAS 19217+1651. This source is also associated with CH_3OH masers and recently detected H_2O masers as well as radio continuum emission (S02). One mm source was detected by Beuther et al. (2002c) $\sim 5''$ north of the IRAS source and consistent with the H_2O and CH_3OH masers and a mid-infrared source. The radio continuum source is $\sim 5''$ west of the mm source. The detected OH maser emission seems not consistent with any of the previous sources, being located $\sim 1'$ to the south. Beuther et al. (2004) studied this region in detail with high spatial resolution using Plateau de Bure Interferometer in the CO $J = 2-1$ and SiO $J = 2-1$ transitions. They conclude that the high-mass region IRAS 19217+1651 exhibits a bipolar outflow and the region is dominated by the central driving source.

IRAS 19220+1432. The OH maser towards this source is contaminated by the nearby OH maser source W51. However the GBT map (Fig. 17) shows that there is a maser emission in the 1720-MHz (RHC) line associated with the IRAS position. This is better illustrated in Fig. A.1 where the spectra from the map are plotted. The contamination of W51 maser is clear in the lower right corner of the map, but a component centred on the IRAS source is also visible. There is no other maser types associated with this source (S02). An flux density of 11 mJy in the radio continuum was detected by S02 at 3.6-cm wavelength.

IRAS 19374+2352. This source is also associated with a H_2O maser (P91), but no CH_3OH maser emission was detected by SHK2000. Free-free emission at 64.4 mJy was detected by Molinari et al. (1998).

IRAS 19388+2357. This source was searched by Szymczak & Kus (2000) for OH maser but no emission was found. The observations here detect OH maser emission in the 1665-MHz line spread over velocity range 34 to 39 km s^{-1}. On the other hand, CH_3OH maser emission, although detected by Schutte et al. (1993) in 1992 and Slysh et al. (1999) in 1995, was not detected in later observations by SHK2000 in 1999. This source is also associated with H_2O maser (P91) and free-free emission (Molinari et al. 1998).

IRAS 19410+2336. This source is also associated with H_2O and CH_3OH masers (S02; SHK2000). Near the H_2O maser source, a radio continuum emission of 1 mJy was detected by S02. Beuther et al. (2002c) 1.2-mm continuum observations detect one source consistent with a mid-infrared source. The 1665-MHz OH maser emission detected close to the mid-infrared source. An outflow was detected towards this source by Beuther et al. (2002b).

IRAS 20062+3550. This source was detected by Szymczak & Kus (2000) at the velocity of -2.4 km s^{-1} in the 1665-MHz line. The observations reported here detect a component in the same line over the velocity range -1 to 2.2 km s^{-1}. Water and CH_3OH masers have also been detected towards this source (P91; Slysh et al. 1999; SHK2000). No radio emission has been detected at 6 cm towards this source by Molinari et al. (1998). This source is one of sources studied in detail by Molinari et al. (2002) with the Owens Valley Radio Observatory (OVRO) millimeter wave array. Four distinct cores were identified in the HCO^+ $J = 1-0$. Two of them are also detected in $H^{13}CO^+$ $J = 1-0$. One core also has a 3.4 mm counterpart and is likely the most massive member of this cluster (Molinari et al. 2002).

IRAS 20126+4104. This source has a luminosity of 10^4 $L_\odot$ and is perhaps the best studied example of a massive protostar associated with a Keplerian disk and a jet/outflow system (Cesaroni et al. 1997, 1999; Hofner et al. 1999; Zhang et al. 1998; Cohen et al. 1988; Tofani et al. 1995; Moscadelli et al. 2000). The source is associated with OH, H_2O and CH_3OH masers. Observations of the water masers using the VLA with angular resolution of $0.1''$ identified three emission regions (Tofani et al. 1995). Moscadelli et al. (2000) resolved two of these into 26 unresolved spots using the VLBA. The velocity and spatial structure of these spots were well fitted by a model with the spots arising at the interface between a jet and the surrounding molecular gas. Two features of OH masers were first detected in the 1665-MHz line by Cohen et al. (1988). More recently mapping of the OH and CH_3OH masers at high angular resolution using MERLIN, Edris et al. (2005) showed that OH and methanol masers appear to trace part of the circumstellar disk around the central source.

IRAS 20188+3928. Only the 1720 MHz of four OH lines is detected towards this source. The source is also associated with a H_2O maser (P91) and a 2.86 Jy 6 cm radio continuum source (Molinari et al. 1998).

IRAS 20227+4154. This source is associated with a H_2O maser (P91) but no CH_3OH maser emission was detected by SHK2000. Only the 1665 MHz OH maser line has been detected by our Nançay-GBT observations.

IRAS 22198+6336. This source is also associated with a H_2O maser emission (P91) but no CH_3OH maser emission was detected by SHK2000. No radio emission was detected by Molinari et al. (2002) at 6 cm wavelength. The two main lines of OH maser were detected by our Nançay-GBT observations.

IRAS 22272+6358. Although not detected in 1993 to a 3σ upper limit of about 0.15 Jy (Slysh et al. 1994), OH emission was found in 1999 in both main lines by Szymczak & Kus (2000). This suggests considerable variations of the source. Approximately three years after Szymczak & Kus observations, the Nançay-GBT observations show that the OH masers have varied. At the 1665 MHz (LHC), a new component was detected centred at 8.46 km s^{-1} and the velocity of a bright component has slightly varied by ~ 1.2 km s^{-1} (from -10.9 to -12.12 km s^{-1}). The velocity range of the OH emission is similar to that observed

for the 6.7 GHz methanol maser (SHK2000). No H_2O maser was detected by P91.

IRAS 23139+5939. This sources is very similar to IRAS 18345−0641. Only the 1612 MHz OH maser line has been detected and the source is also associated with 3.6-cm radio continuum emission (S02). It is also associated with a H_2O maser (S02) which coincides with a mm continuum emission and mid-infrared sources (Beuther et al. 2002a). An outflow along the line of sight was detected by Beuther et al. (2002b).